Reliable Vehicle State and Parameter Estimation

by

Mohammad Pirani

A thesis
presented to the University of Waterloo
in fulfillment of the
thesis requirement for the degree of
Doctor of Philosophy
in
Mechanical and Mechatronics Engineering

Waterloo, Ontario, Canada, 2017

Examining Committee Membership The following served on the Examining Committee for this thesis. The decision of the Examining Committee is by majority vote.

External Examiner	NAME: Chun-Yi Su
	TITLE: Professor, Mechanical Engineering
Supervisors	NAME: Amir Khajepour
	TITLE: Professor, Mechanical Engineering
	NAME: Baris Fidan
	TITLE: Associate Professor, Mechanical Engineering
Internal Member	NAME: William M. Melek
	TITLE: Professor, Mechanical Engineering
Internal Member	NAME: Steven Waslander
	TITLE: Associate Professor, Mechanical Engineering
Internal-external member	NAME: David Wang
	TITLE: Professor, Electrical and Computer Engineering

Author's Declaration

I hereby declare that I am the sole author of this thesis. This is a true copy of the thesis, including any required final revisions, as accepted by my examiners.

I understand that my thesis may be made electronically available to the public.

Abstract

Diverse vehicle active safety systems including vehicle electronic stability control (ESC) system, anti-lock braking system (ABS), and traction control system (TCS) are significantly relying on information about the vehicle's states and parameters, as well as the vehicle's surroundings. However, many important states or parameters, such as sideslip angle, tire-road friction coefficient, road gradient and vehicle mass are hard to directly measure, and hence advanced estimation algorithms are needed. Furthermore, enhancements of sensor technologies and the emergence of new concepts such as *Internet of Things* and their automotive version, *Internet of Vehicles*, facilitate reliable and resilient estimation of vehicle states and road conditions. Consequently, developing a resilient estimation structure to operate with the available sensor data in commercial vehicles and be flexible enough to incorporate new information in future cars is the main objective of this thesis.

This thesis presents a reliable corner-based vehicle velocity estimation and a road condition classification algorithm. For vehicle velocity estimation, a combination of vehicle kinematics and the LuGre tire model is introduced in the design of a corner-based velocity observer. Moreover, the observability condition for both cases of time-invariant and parameter varying is studied. The effect of suspension compliance on enhancing the accuracy of the vehicle corner velocity estimation is also investigated and the results are verified via several experimental tests.

The performance and the robustness of the proposed corner-based vehicle velocity estimation to model and road condition uncertainties is analyzed. The stability of the observer is discussed, and analytical expressions for the boundedness of the estimation error in the presence of system uncertainties for the case of fixed observer gains are derived. Furthermore, the stability of the observer under arbitrary and stochastic observer gain switching is studied and the performances of the observer for these two switching scenarios are compared. At the end, the sensitivity of the proposed observer to tire parameter variations is analyzed. These analyses are referred to as offline reliability methods.

In addition to the off-line reliability analysis, an online reliability measure of the proposed velocity estimation is introduced, using vehicle kinematic relations. Moreover, meth-

ods to distinguish measurement faults from estimation faults are presented. Several experimental results are provided to verify the approach.

An algorithm for identifying (classifying) road friction is proposed in this thesis. The analytical foundation of this algorithm, which is based on vehicle response to lateral excitation, is introduced and its performance is discussed and compared to previous approaches. The sensitivity of this algorithm to vehicle/tire parameter variations is also studied. At the end, various experimental results consisting of several maneuvers on different road conditions are presented to verify the performance of the algorithm.

Acknowledgements

Foremost, I would like to express my many thanks to Prof. Amir Khajepour and Prof. Baris Fidan, for their support, encouragement, and supervision of the research presented in this thesis.

I also would like to acknowledge the financial support of Automotive Partnership Canada, Ontario Research Fund and General Motors. I extend my appreciation to Prof. Chun-Yi Su, Prof. Steven Waslander, Prof. William Melek and Prof. David Wang for their role as readers of the thesis.

I want to express my appreciation to Prof. Shreyas Sundaram for the interactions and scientific collaborations that we have had over the years which inspired me in my research. My whole experience would not have been as rewarding without the help of my colleague Ehsan Hashemi. I am also grateful to Ebrahim Moradi Shahrivar, Mohsen Raeis-Zadeh, Mehdi Jalalmaab and all my friend in Waterloo and Toronto for all the hangouts, laughters and travels that we have shared.

I am deeply grateful to my sister Parisa, her husband Abouzar and their lovely daughter Hannah. Most importantly, none of this would have been possible without the patience, love and support of my parents, Fereidoon Pirani and Mahboobeh Heydari, whom I cordially dedicate the honor of all my current and future achievements to.

Table of Contents

List of Tables

List of Figures

Chapter 1

Introduction

1.1 Motivation

Great advancements in vehicular technologies have resulted in increasingly sophisticated vehicles in recent years. While a vehicle's economic performance and ride comfort are developed via optimizing the energy management system and advanced suspension system, vehicle active safety systems are critical to the driving safety of vehicles and are becoming more and more important. The annual report announced by Canada Ministry of Transportation on traffic collisions and crash statistics echoes the necessity of automotive safety and reveals the importance of enhancing active safety based on the todays multifarious urban requirements. Diverse representations of vehicle active safety system include (but are not limited to): vehicle electronic stability control (ESC) system, anti-lock braking system (ABS), and traction control system (TCS). It is commonly recognized that the operation of active safety systems significantly rely on information about the vehicle's states and parameters as well as the vehicle's surroundings. For instance, the control strategies mentioned above are considering the vehicle's time-varying longitudinal and lateral velocities. However, many of the important states or parameters, such as sideslip angle, tire-road friction coefficient, road gradient, and vehicle mass, are hard to directly measure, so advanced estimation algorithms have to be developed. Hence, having a cost efficient vehicle state and road condition estimation is a necessity for active safety systems in current commercial

vehicles, and the ongoing research in this field highlights this importance. Furthermore, enhancements of sensor technologies and the emergence of new concepts such as *Internet of Things* and their automotive version, *Internet of Vehicles*, facilitate reliable and resilient estimation of vehicle states and road condition. Consequently, developing a resilient estimation structure to operate with the available sensor data in commercial vehicles and be flexible to incorporating new information in future cars is a preeminent objective. Two major practical issues that have dominated the vehicle state/parameter estimation field are *vehicle velocity estimation*, in both longitudinal and lateral directions, and *road condition estimation (classification)*. Fig. 1.1 illustrates the roles that a reliable vehicle velocity and road condition estimation play in the overall vehicle estimation/control structure.

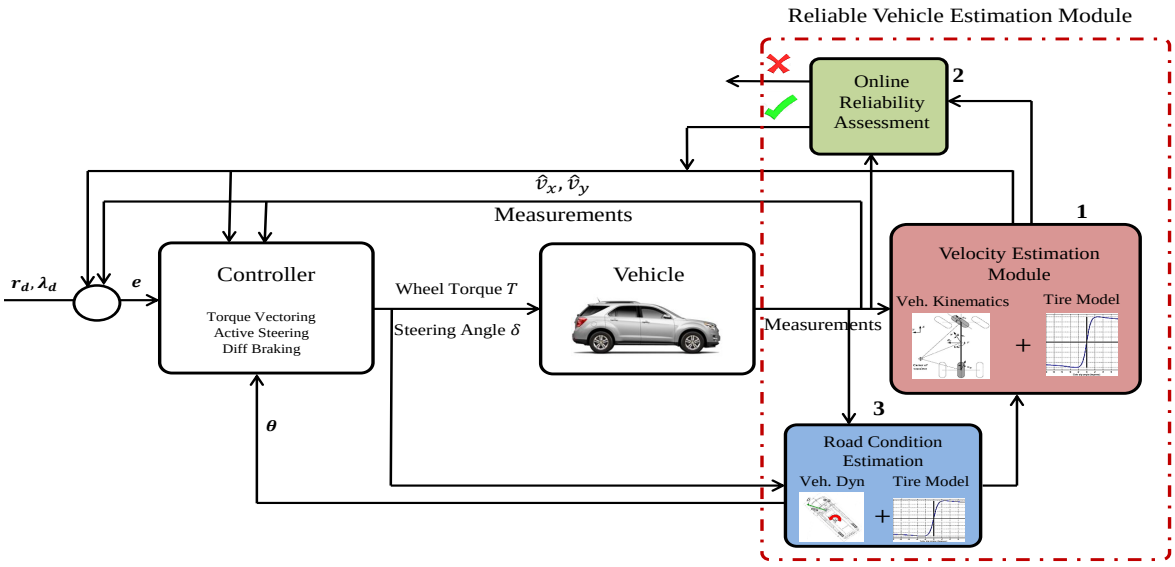

Figure 1.1: Vehicle state estimation in the overall vehicle control scheme.

Vehicle velocities, in both longitudinal and lateral directions, play fundamental roles in traction and stability control systems. They can be directly measured using Global Positioning System (GPS); however, the insufficient precision of conventional GPSs (specifically for the lateral direction) and their occasional signal drop issues are the drawbacks of this method. Moreover, implementing high-accuracy GPSs imposes a high production cost, which makes it infeasible to use. Thus, an alternative approach is to estimate the velocity,

based on available sensor data instead of direct measurement. To this end, the prominence of having a reliable velocity estimation that is resilient to the road condition and vehicle parameter uncertainties, has been amplified in recent research in automotive control and autonomous driving systems. There has been much effort in utilizing the latest theoretical results as well as overcoming technical obstacles to estimate vehicle longitudinal and lateral velocities via using the few available sensor measurements embedded in conventional cars. From a theoretical perspective, the fact is that a more accurate vehicle model results in a more precise vehicle velocity estimation. The imprecision in the vehicle dynamics can be rooted in an inaccurate tire model or the omission of some additional dynamics, such as the effect of the suspension compliance on the wheel speed. Moreover, the effect of the driver's actions is another unmodeled dynamics that should be taken into account as well. Hence, in order to come up with a reliable vehicle velocity estimation, detailed vehicle dynamics obtained from an accurate tire model with a known road condition are needed.

Having knowledge about the road condition will have a great impact on the performance of the vehicle's velocity estimation, as shown in Fig. 1.1, in the blue box. In particular, if the type of the road that the vehicle is driven on is known, the conservative robustness conditions which are imposed on velocity estimators will be relaxed and consequently, the performance of the estimators will increase. Moreover, it also has a considerable effect on the vehicle's slip control for both longitudinal and lateral directions. Hence, identifying (or classifying) the road condition is required to improve the performance of the vehicle velocity estimation and control. Road condition classification can be done independently or performed with a joint estimation scheme with other vehicle/tire states. The latter approach, which has received more attention in the literature, requires a high level of excitation, including harsh steerings as well as accelerations and decelerations. Another approach is to estimate in low-slip regions (Slip-Slope method). However, in the region where the slip-slope condition applies, the road condition (which is proportional to the slope of the line) is very sensitive to the force and slip variations. Therefore, small uncertainties in the tire force or slip measurements may lead to inaccurate identification of the road condition. Hence, a practical and reliable road condition identification method is still an ongoing problem in the automotive industry.

As mentioned earlier, due to the existence of unmodeled dynamics, external distur-

bances and occasional measurement faults, failures in estimation algorithms during real time implementation are unavoidable. To address this issue, it is imperative to design a reliability monitoring module, beside vehicle velocity estimation, as shown in Fig. 1.1, in the green box. Two general approaches can address the reliability of a vehicle velocity estimation:

1. Real time (on-line) approach: In this method, during the estimator operation, the estimated velocity is concurrently translated into parameters that can be measured directly with a desirable accuracy. Finally, by comparing the results, a level of reliability is determined. A simple example of this method is to translate the estimated velocity (in each direction) to the measured acceleration in the corresponding direction, measured from the IMU, and compare them to find a possible failure in the estimation.

2. Offline methods: These methods provide the fundamental limitations that a vehicle velocity estimator faces in terms of its performance and robustness to inaccuracies of parameters and input data such as road conditions and sensor measurements. To yield this, one can utilize robustness and stability theorems available in systems and control literature to come up with analytical descriptions of the reliability of the estimator. Since such analyses show the characteristics of the designed velocity estimator and can be determined offline, they are referred to as *offline methods*.

The advantage of a real time approach is that it can provide information regarding the reliability of the estimator in a concurrent manner. However, the advantage of off-line methods is to propose concrete milestones (in terms of vehicle characteristics and road condition) that should be met in order to reach to a desirable estimation. As mentioned, one of the main sources of unreliability of the vehicle velocity estimation is the uncertainty in road condition. Due to this fact, reliable velocity estimation and road condition identification always coexist in such studies.

1.2 Objectives

The first objective of this thesis is to design a reliable corner-based vehicle velocity estimator using a combination of vehicle kinematics and LuGre tire model. In the proposed vehicle velocity estimation algorithm, there is no need to have knowledge about the road friction condition. Moreover, the estimator is resilient to time-varying and uncertain tire characteristics. The observability of the dynamics as a linear time-varying system, as influenced by the time-varying wheel speed, should be analytically studied prior to designing the observer. The effect of the suspension compliance and the resulting extra degree of freedom on enhancing the accuracy of the proposed vehicle velocity estimation will also be investigated, and the overall velocity estimation algorithm will be tested via several experiments on different road conditions.

The second objective is to analytically investigate the performance and robustness of the proposed corner-based vehicle velocity estimator, from a system theoretic viewpoint. More specifically, fundamental limitations that exist on the proposed estimator to mitigate the effect of tire or road uncertainties should be analytically studied. These results will be presented in the form of bounds on the velocity estimation error using Lyapunov-based methods as well as frequency-based method ($\mathcal{H}_\infty$ analysis). As real-time observer gain switching is inevitable in experiments, in order to change the reliance of the estimator to measurements in different instances, the stability of the velocity estimator in the presence of estimation gain switchings is also studied for two cases of arbitrary and stochastic gain switching scenarios. At the end, the sensitivity of the performance of the designed velocity estimator to tire parameter variations will be investigated. These analyses are referred to as an *offline* reliability assessment of the velocity observer in this thesis.

The third objective is to propose a real-time reliability measure for the vehicle velocity estimation, which differs from the offline analysis mentioned above. The proposed on-line reliability measure is considered to be a milestone that the observer should reach in real time before its outputs (estimated states) are used in the control module. The proposed on-line reliability measure is tested with experiments comprised of several maneuvers on various road conditions.

The fourth objective is to identify (classify) the road friction condition. The proposed

road friction identification algorithm is based on vehicle responses, vehicle lateral dynamics and appropriate tire models. This algorithm can take advantage of receiving information from the road-independent velocity estimation module to enhance its accuracy and performance. The performance of this algorithm will be verified via various experiments on different road conditions and for different maneuvers. The resilience of the proposed algorithm to tire and vehicle parameter uncertainties will be also be discussed.

The objectives of this thesis and the connections between topics discussed above are shown in Fig. 1.2.

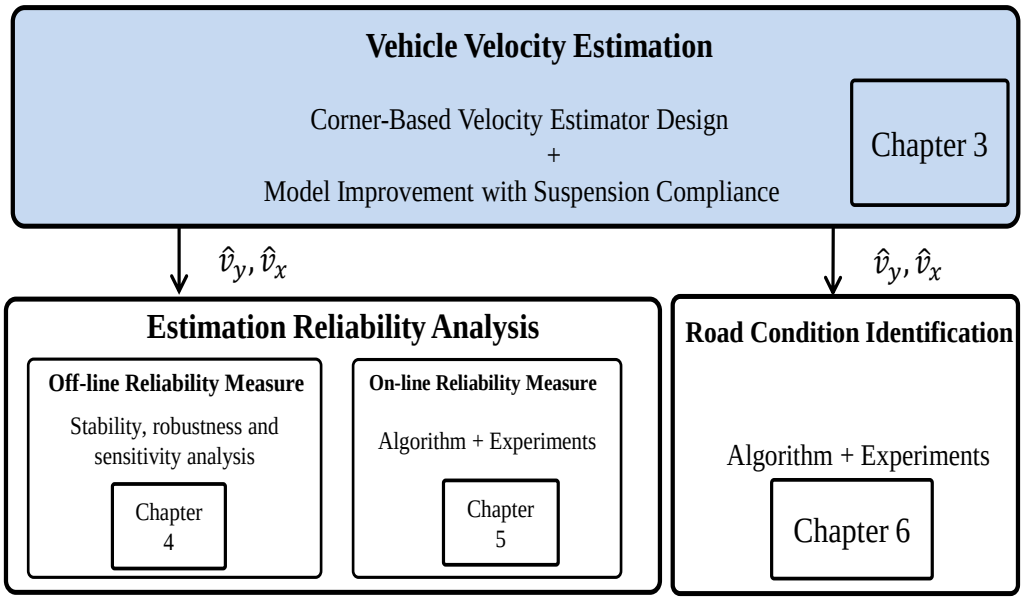

Figure 1.2: The objectives of the thesis in a glimpse.

1.3 Thesis Outline

In the second chapter of this thesis, a literature review on vehicle state and parameter estimation, specifically vehicle velocity and road condition estimation, is presented. Moreover, an overview of studies done in reliable system and controller (estimator) design, for deter-

ministic and stochastic systems, are discussed. Furthermore, a brief background on vehicle tire model as well as vehicle lateral dynamics (known as bicycle model) is introduced.

In the third chapter, the vehicle corner-based velocity estimator is proposed. More specifically, the combination of vehicle kinematics and the LuGre tire model is introduced in the design of the base dynamics for a corner-based velocity observer of the vehicle. Moreover, the observability condition for both cases of time-invariant and parameter varying is studied. At the end, the effect of suspension compliance on enhancing the accuracy of the vehicle corner velocity estimation is also investigated and the results are verified via several experimental tests.

In the fourth chapter, the performance and the robustness of the proposed corner-based vehicle velocity estimation to model and road condition uncertainties is analyzed. The stability of the observer is discussed, and analytical expressions for the boundedness of the estimation error in the presence of system uncertainties for the case of fixed observer gains are derived. Furthermore, the stability of the observer under arbitrary and stochastic observer gain switching is studied and the performances of the observer for these two switching scenarios are compared. At the end, the sensitivity of the proposed observer to tire parameter variations is analyzed.

Chapter five presents an online reliability measure of the proposed velocity estimation, using vehicle kinematic relations. Moreover, methods to distinguish measurement faults from estimation faults are presented. Several experimental results are also provided to verify the approach.

Chapter six pertains to proposing an algorithm for the road condition identification. The analytical foundation of this algorithm, which is based on vehicle response to lateral excitation, is introduced and its performance is discussed and compared to previous approaches. The sensitivity of this algorithm to vehicle/tire parameter variations is also studied. At the end, various experimental results consisting of several maneuvers on different road conditions are presented to verify the performance of the algorithm.

In chapter seven, the conclusions and the contributions of this thesis are presented. Moreover, some possible future avenues for further research are mentioned.

Chapter 2

Background and Literature Review

In this chapter, a comprehensive literature review on the vehicle states, road condition estimation, and reliability of the estimators is presented. Moreover, a brief background on the vehicle tire model as well as vehicle lateral dynamics is presented, both of which will be used later in the thesis.

2.1 Vehicle States and Road Condition Estimation

Advanced vehicle stability control and active safety systems require dependable vehicle states, which may not be accessible by measurements so they should be estimated. Two major practical issues that have dominated the vehicle state estimation field are velocity and tire force estimations that are robust to road friction changes.

Tire forces are one of the main vehicle states that should be estimated and they have a great degree of influence in corner based vehicle velocity estimation. Tire forces can be measured at each corner with sensors mounted on the wheel hub, but their significant cost, required space, and calibration and maintenance make them completely unfeasible for mass production vehicles. Provided that the tire force calculation needs road friction, even accurate slip ratio/angle information from the GPS will not engender forces at each corner. Estimation of longitudinal and lateral forces independent from the road condition

may be classified on the basis of wheel dynamics into the nonlinear and sliding mode observers [2–4], Kalman-based estimation [5–7], and unknown input observers [8–10]. A force estimation method based on the steering torque measurement is introduced in [11], which requires additional measurements.

Vehicle velocity, in both longitudinal and lateral directions, greatly influence traction and stability control systems. Velocity can be measured with the advent of the GPS; however, the insufficient accuracy of the commonly used conventional GPSs (especially for the lateral direction) and their occasional loss of reception are primary impediments. Two major approaches have been developed in the literature for the estimation of longitudinal and lateral velocities:

1. Integrating an automotive grade accelerometer and rate gyro directly; namely, kinematic-based estimation: This method uses acceleration and the yaw rate measurements from an inertial measurement unit (IMU) and estimates the vehicle states by employing Kalman-based [12, 13] or nonlinear [14] observers. This method does not employ a tire model, but instead, the sensors bias and noise should be identified precisely in order to achieve a reliable estimation. In addition, low-excitation cases that lead to erroneous estimation should be handled with this method. To increase the accuracy of the estimated heading and position, Farrell et al. [15] used the carrier-phase differential GPS, which requires a base tower and increases the cost significantly. To remove noises and address the low excitation scenarios, some kinematic-based methodologies [16, 17] employ accurate GPSs, which are susceptible to getting lost and they impose additional costs on commercial vehicles. Yoon and Peng [18] utilize two low-cost GPS receivers for the lateral state estimation and compensate the low update rate issue of conventional GPS receivers by combining the IMU and GPS data using an extended Kalman Filter (EKF).

2. Combination of integration (kinematic-based) and vehicle tire model observers: This method integrates measured longitudinal/lateral accelerations and uses a tire model to correct the estimation [19], [20]. This approach requires a good perception of the road friction and a precise tire model. However, there are some studies which focused on the state estimation using tire model robust to the road condition, but

they implemented additional measurements that are not common for conventional cars or require identification of tire parameters. Hsu et al. proposed a method in [11] and [21] to estimate the side slip angle and road friction limits using the known road friction and steering torque sensor, which may not be applicable for all production vehicles. Nam et al. [22] presents a sideslip angle estimation method with a recursive least squares algorithm to improve vehicle stability of in-wheel-motor-driven electric vehicles, but their approach uses force measurements from the multisensing hub units, which are not available for all electric and conventional cars.[1]

The real time knowledge of the road condition is important for many vehicle estimation and control systems, particularly, in active safety control systems such as adaptive cruise control, anti-lock braking systems (ABS), electronic stability control, and rollover prevention [23], [24], [25]. Several different approaches were thus developed to estimate this coefficient in real time [26], [27], [4], [28]. However, a reliable estimation of the road condition often requires that the regression vector satisfies the persistence of excitation (PE) conditions. Consequently, the aforementioned road condition estimation approaches demand specific vehicle maneuvers or motion excitation (e.g., extensive steering action, accelerating and decelerating), which could be unrealistic/impossible in certain situations/constraints, such as constant speed cruising, surveillance, and military operations, and/or it may violate vehicle desired motion control and trajectory tracking objectives.

On the other hand, some literature attempted to identify the road condition and estimated vehicle states simultaneously. Grip et al. suggest a nonlinear side slip observer in [29, 30] that incorporates time-varying gains and estimates the vehicle states as well as the road condition using a tire model. Their method should cope with the noises and uncertainties imposed by road identification errors due to the lack of excitation. You et al. [31] introduces an adaptive least square approach to jointly estimate the lateral velocities and tires' cornering stiffness (road friction terms). The road bank angle is also identified in their approach. However, the measured lateral accelerations are assumed as accurate signals and

[1] This thesis is concerned with the second method and it aims to develop an observer-based vehicle state estimator using conventional sensor measurements (wheel speed, steering angle, and IMU) that are ideally robust to road friction.

measurement noises have not been addressed. A sliding-mode observer is provided by Magallan et al. in [32] based on the LuGre tire model [33] to estimate the longitudinal velocity and the surface friction. Zhang et al. propose a sliding-mode observer in [34] to estimate velocities using wheel speed sensors, braking torque, and longitudinal/lateral acceleration measurements. Their approach utilizes a sliding-mode observer for the velocity estimation and an EKF for estimation of the Burckhardt tire model's friction parameter. However, this method needs accurate tire parameters in presence of tire wear, inflation pressure, and road uncertainties. A switched nonlinear observer based on a simplified Pacejka tire model is introduced by Sun et al. [35] to provide estimates of longitudinal and lateral vehicle velocities and the tire-road friction coefficient during anti-lock braking. Their approach benefits from switching in specific cases because of unreliability of the measurements, but it relies on a predefined zero slip ratio for the longitudinal velocity measurement.

Based on what is mentioned above and as shown in the literature review on vehicle states and road condition estimation, reliable velocity estimation resilient to tire and road condition uncertainties and model parameter variations have been underlined in recent stability control methods. In the following section, a brief background on the vehicle tire model and vehicle lateral dynamics will be presented.

2.2 Literature Review and Background on Vehicle Tire Modeling

Tire models play a vital role in recent progress in vehicle state estimation and control. Numerous studies have documented the tire model for the vehicle's velocity estimation for both longitudinal and lateral directions. The tire model is a relation between the forces exerted on the tire to the tire slip. These forces are represented by a group of curves, among which the most commonly used are those of algebraic force-slip relationships [36], [37]. The most widely used static model, known as the Magic Formula was proposed by Pacejka et al. [38] and Uil [39] and provides a semi-experimental approach for tire force calculation. Kinematic tire models such as Brush and dynamic models seem more reliable for considering the transient phases as examined in [40], [41]. Canudas-de-Wit et

al. proposed a dynamic tire - road friction model, known as the LuGre model, in [33], [42] and introduced tire deflection as a state in the system dynamics. A subsequent transient LuGre model is presented in [43], [44] to meet the physical characteristics of tires during high frequency excitations.

A common assumption in most tire friction models is that the normalized tire force, defined as[2]

$$\mu \triangleq \frac{F_x}{F_z}, \tag{2.1}$$

where F_x and F_z are longitudinal and normal tire forces, defined in Table 3.1. The normalized tire force is a nonlinear function of the normalized relative velocity between the road and the tire slip ratio, which is defined as

$$\lambda \triangleq |\frac{R_e|\omega| - V_{xt}}{\max\{R_e|\omega|, V_{xt}\}}|, \tag{2.2}$$

with a distinct maximum as shown in Fig. 2.1 (a). The slip ratio λ which is a positive number in the interval $\lambda \in [0, 1]$ represents how much the actual vehicle's corner velocity V_{xt} differs from $R_e\omega$. The tire's effective radius R_e, its angular speed ω, and center velocity V_{xt} are schematically shown in Fig. 2.1 (b). All of these tire parameters and states are also defined in Table 3.1. The parameter $0 \leq \theta \leq 1$ represents the road friction condition. The larger value of θ represents a less slippery road. In particular, the value of the road friction θ is the maximum normalized tire force μ over all values of the slip ratio λ. When the value of the slip ratio λ exceeds a certain level, the slip-force relation in the tire model exits from the linear region (which is shown by purple dashed lines). In this case, it is said that the tire is saturated since the force on the tire will no longer increase by increasing the tire slip.

In the following sections, different forms of the tire model will be introduced.

[2]Normalized tire forces are denoted by μ in the literature. However, in the observer design algorithm discussed in the next chapter, it will be denoted by f_n, instead of μ.

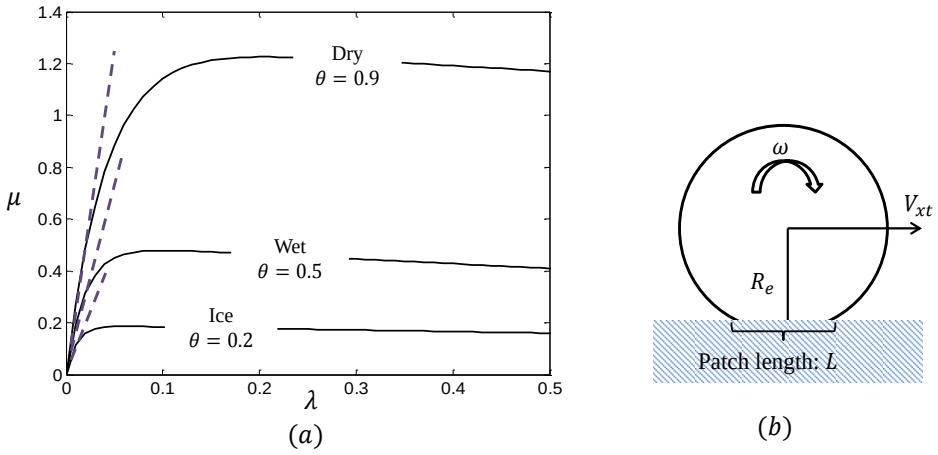

Figure 2.1: (a) The nonlinear tire force-slip relation for longitudinal motion and various road conditions. (b) Tire geometric characteristics.

2.2.1 Static Tire Model

The most commonly used static tire friction models in the literature are those of algebraic slip/force relationships. They are defined as one-to-one maps between the normalized tire force μ, and the longitudinal slip ratio λ. One of the most well-known static tire models is the Pacejka model [38], also known as the Magic Formula. This model has been shown to suitably match experimental data obtained under particular conditions of constant linear and angular velocity. The Pacejka model has the form:

$$\mu = D\sin[C\arctan\{B\lambda - E(B\lambda - \arctan(B\lambda))\}], \tag{2.3}$$

Here, B is the stiffness factor of the tire, C is the shape factor, D is the peak value, and E is the curvature factor, as shown in Fig. 2.2. The parameters B, C, D, and E are defined in order to get an appearance similar to the experimental curve.

2.2.2 Dynamic Tire Model

The static friction models discussed in the previous subsection are appropriate when there are steady-state conditions for the linear and angular velocities. This steady-state situation

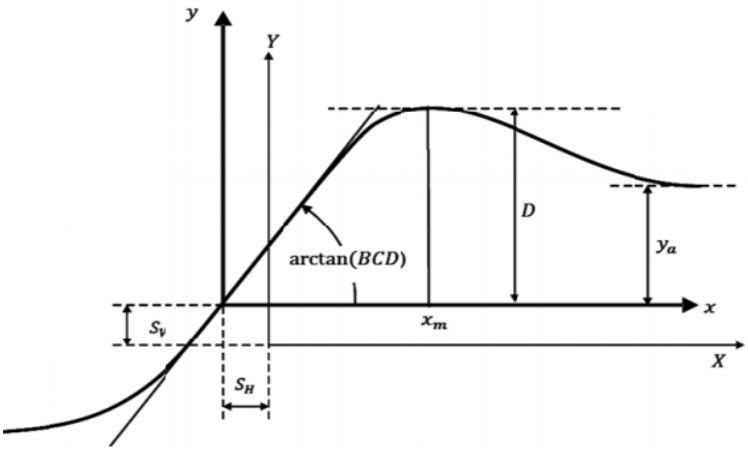

Figure 2.2: The curve obtained from the Magic formula [1].

is rarely true in reality, especially when the vehicle goes through continuous successive phases between acceleration and braking in harsh maneuvers. The dynamic friction models attempt to capture the transient behavior of the tire - road contact forces under time-varying velocity conditions. A number of dynamic models have been proposed in the literature that can be classified under the term "dynamic friction models". One of the most recent dynamic tire models is LuGre model, which is discussed in the following subsection.

2.2.3 LuGre Tire Model

One of the most well-known dynamic models that can be used to accurately predict the friction forces during transience is the LuGre friction model [45]. Pre-sliding and hysteresis loops are considered in this model along with the tire deflections for various maneuvers. Compared to the other conventional approaches, e.g. Pacejka, the LuGre model utilizes relative velocity rather than slip ratio and slip angle. Passivity of the transient LuGre makes it a bounded and stable model and prohibits the divergence of both internal tire states and consequent forces [46]. The LuGre model symbolizes the distributed model with the tire deflection and some simplifications on the normal force distribution with an

averaged representation of z_x for the longitudinal direction as:

$$\dot{z}_x(t) = V_{rx} - (\frac{\sigma_0|V_{rx}|}{\theta g(V_{rx})} + \kappa R_e|\omega|)z_x(t),$$
$$\mu = \sigma_0 z_x(t) + \sigma_1 \dot{z}_x(t) + \sigma_2 V_{rx}, \tag{2.4}$$

where $V_{rx} = R_e\omega - V_{xt}$ is the tire relative velocity, and all parameters are defined in Table 3.1. The function $g(V_{rx})$ is defined as

$$g(V_{rx}) = \mu_c + (\mu_s - \mu_c)\, e^{-|\frac{V_{rx}}{V_s}|^{\frac{1}{2}}} \tag{2.5}$$

In the LuGre model, the tire relative velocity V_{rx} plays the role of tire slip λ in the static tire models. The tuning of LuGre tire parameters can be done with experimental curves of the tire and by utilizing an error cost function and least square techniques. In (2.4), parameter θ represents the road friction condition. The force distribution along the patch line is represented by parameter κ in the model (2.4) and can be a function of time, a constant, or may be approximated by an asymmetric trapezoidal scheme. The suggested value for κ in [33] is $\kappa = \frac{7}{6L}$ where L is the tire patch length, shown in Fig. 2.1, (b). It can also be obtained from an acceptable range of $\frac{1.1}{L} \leq \kappa \leq \frac{1.4}{L}$.

In the following section, a brief overview of the vehicle's lateral dynamics is presented.

2.3 Vehicle Lateral Dynamics

In this section, vehicle lateral dynamics is described for both linear and non-linear (using LuGre tire model) tire model cases. Hence, to develop these dynamics, the knowledge from the previous section on tire models will be used. The discussion in this section will be used in the subsequent chapters.

2.3.1 Linear Lateral Dynamics Model

The 2DOF bicycle model, a well-known vehicle lateral model, provides vehicle lateral velocity and yaw rate based on longitudinal and lateral tire forces, F_x and F_y. The lateral

dynamic is in the following form with the vehicle mass m and moment of inertia I_z:

$$\begin{aligned} m\left(\dot{v}_y + r v_x\right) &= F_{xf} sin\delta + F_{yf} cos\delta + F_{yr} \\ I_z \dot{r} &= a\left(F_{xf} sin\delta + F_{yf} cos\delta\right) - b F_{yr}, \end{aligned} \tag{2.6}$$

where v_x is the speed, subscripts f and r symbolize front and rear tracks, a and b represent the distance of the front and rear tracks from CG, δ is the steering angle on the front wheels, and v and r denote the lateral velocity at CG and the yaw rate, respectively. A linear tire model suggests lateral forces at each track $F_{yf} = C_{\alpha_f}\alpha_f, F_{yr} = C_{\alpha_r}\alpha_r$, in which α_f and α_r are the front and rear slip angles, respectively, and C_{α_f} and C_{α_r} are the cornering stiffness values, which are functions of the road condition θ. These quantities are schematically shown in Fig. 2.3.

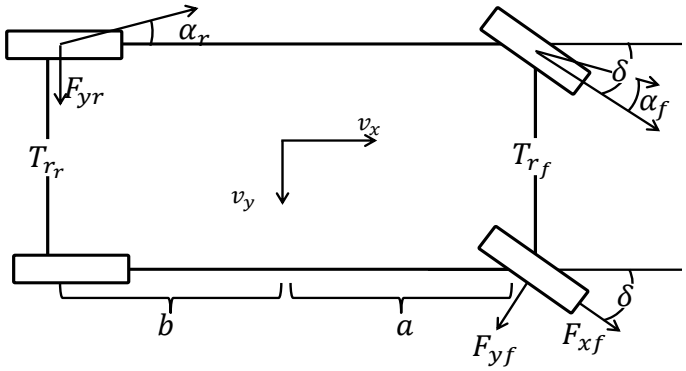

Figure 2.3: The tire forces and side slip angles in each track.

The front and rear slip angles are related to the lateral states v_y, r as $\alpha_f = \delta - \frac{v_y + ar}{v_x}, \alpha_r = \frac{rb - v_y}{v_x}$. The steering angle effect on the longitudinal/lateral forces can be ignored, and the lateral dynamic equations can be simplified as follows:

$$\begin{aligned} m\left(\dot{v}_y + r v_x\right) &= F_{yf} + F_{yr} \\ I_z \dot{r} &= a F_{yf} - b F_{yr}. \end{aligned} \tag{2.7}$$

Consequently, the linear tire-vehicle handling model can be represented by

$$\underbrace{\begin{bmatrix}\dot{v}_y(t)\\ \dot{r}(t)\end{bmatrix}}_{\dot{x}} = \underbrace{\begin{bmatrix}-\frac{C_{\alpha_f}+C_{\alpha_r}}{v_x m} & -(\frac{aC_{\alpha_f}-bC_{\alpha_r}}{v_x m}+v_x)\\ -\frac{aC_{\alpha_f}-bC_{\alpha_r}}{v_x I_z} & -\frac{a^2C_{\alpha_f}+b^2C_{\alpha_r}}{v_x I_z}\end{bmatrix}}_{A}\begin{bmatrix}v_y(t)\\ r(t)\end{bmatrix} + \underbrace{\begin{bmatrix}\frac{C_{\alpha_f}}{m}\\ a\frac{C_{\alpha_f}}{I_z}\end{bmatrix}}_{B}\delta \tag{2.8}$$

As pointed out above, the bicycle model is obtained under the assumption that the relation between the lateral force and slip angle is linear. However, this assumption is not always realistic. More specifically, the relation between the kinematic variables (e.g., slip ratio or slip angle) and the forces of the tire is generally nonlinear, as pointed out in the previous section.

2.3.2 Nonlinear Lateral Dynamics Model

In the previous subsection, a *linear* tire model is assumed and used to derive the lateral dynamic equation (2.8). However, this assumption is not realistic due to the nonlinear nature of tire-road interactions. After discussing the LuGre model in Section 2.2, we incorporate it into the vehicle lateral dynamics (2.7) in this section. For simplicity, here we use a steady-state LuGre model to derive the lateral dynamics. It is discussed by detail in [47] that using steady-state and transient LuGre models provide similar results in lateral dynamics (due to the passivity if the tire model).

If we assume the steady state LuGre model for the lateral direction ($\dot{z}_y = 0$) by defining new variables

$$\rho = \theta g(V_{ry}), \quad \gamma = \kappa R_e \omega/\sigma_{0y}, \tag{2.9}$$

the normalized lateral force μ_y will be as follows with α as the slip angle at each tire/axle. (Details of this derivation is provided in [47])

$$\mu_y = \left(\frac{\rho}{v_x|\alpha| + \gamma\rho} + \sigma_{2y}\right) v_x \alpha. \tag{2.10}$$

To be able to write the state-space form of the lateral dynamics based on the LuGre model, we need to analyze the effect of the slip angle as discussed in the following sections. For

the case where $|\alpha| \ll \gamma\rho/v_x$, the normalized lateral force (2.10) will be

$$\mu_y = \theta \left(\frac{1}{\gamma} + \sigma_{2y} \right) v_x \alpha. \tag{2.11}$$

Here, θ is employed with direct multiplication as an implication of the effect of road conditions. It helps in making the suggested pure-slip formulation compatible with the real tire model since the slope of the linear region of the force-slip curve is a function of the road condition as studied in the slip-slope method [4, 48].

The lateral dynamics with the tire model can be expressed as follows after putting the tire forces of each track $F_{yi} = \mu_{yi} F_{zi}$ in (2.7)

$$\begin{aligned} m\left(\dot{v}_y + r v_x\right) &= \mu_{yf} F_{zf} + \mu_{yr} F_{zr} \\ I_z \dot{r} &= a\mu_{yf} F_{zf} - b\mu_{yr} F_{zr}, \end{aligned} \tag{2.12}$$

Several studies focus on the normal force calculation on each axle using load transfer and acceleration measurements [49, 50]. The calculated normal forces on the front and rear axles F_{zf} and F_{zr} can then be utilized in (2.12) whenever lateral/longitudinal acceleration measurements are available. A static normal load distribution is used, which results in the following vehicle state form after substituting the corresponding lateral forces from (2.11)

$$\begin{aligned} \dot{v}_y &= -\frac{g}{l}\left(bk_f + ak_r\right) v_y - \left(\frac{abg}{l}\left(k_f - k_r\right) + v_x \right) r + \frac{bg}{l} k_f v_x \delta, \\ \dot{r} &= \frac{mabg}{I_z l}\left(k_r - k_f\right) v_y - \frac{mabg}{I_z l}\left(bk_r + ak_f\right) r + \frac{mabg}{I_z l} k_f v_x \delta, \end{aligned} \tag{2.13}$$

where $k_f = \theta \left(\frac{1}{\gamma_f} + \sigma_{2f} \right)$ and $k_r = \theta \left(\frac{1}{\gamma_r} + \sigma_{2r} \right)$. Equation (2.13) represents a linear time-varying system for the lateral dynamics with states $x = [v_y(t) \quad r(t)]^T$ and front steering; it is based on the LuGre linearized model for small slip angles. To consider the nonlinear part, disregarding the $|\alpha| \ll \gamma\rho/v_x$ condition, one can rewrite the normalized lateral force (2.10) at each corner

$$\mu_{yi} = k_i v_x \alpha_i - \frac{1}{\gamma_i \left(1 + \frac{\gamma_i \rho_i}{v_x |\alpha_i|} \right)} v_x \alpha_i, \tag{2.14}$$

where $i \in \{f, r\}$ can be front or rear tires, ρ_i and γ_i are defined in (2.9), v_x is the vehicle speed, and α_i is the slip angle at each track. The term $k_i v_x \alpha$ represents the linear part (2.11), and the second term shows the nonlinear behavior of the lateral force with respect to the slip angle. By substituting (2.14) in the lateral dynamics (2.12), one will get:

$$\underbrace{\begin{bmatrix} \dot{v}_y(t) \\ \dot{r}(t) \end{bmatrix}}_{\dot{x}} = \underbrace{\begin{bmatrix} \frac{-g}{l}(bk_f + ak_r) & -(\frac{abg}{l}(k_f - k_r) + v_x) \\ \frac{mabg}{I_z l}(k_r - k_f) & -\frac{mabg}{I_z l}(bk_r + ak_f) \end{bmatrix}}_{A} \begin{bmatrix} v_y(t) \\ r(t) \end{bmatrix} + \underbrace{\begin{bmatrix} \frac{bg}{l} k_f v_x \\ \frac{mabg}{I_z l} k_f v_x \end{bmatrix}}_{B} \delta_f + \underbrace{\begin{bmatrix} \frac{gv_x}{l}(b\phi_f \alpha_f + a\phi_r \alpha_r) \\ \frac{mabgv_x}{I_z l}(\phi_f \alpha_f - \phi_r \alpha_r) \end{bmatrix}}_{H}, \tag{2.15}$$

in which ϕ_f and ϕ_r are obtained as follows for the front and rear tires, respectively

$$\phi_i = \left(\frac{\rho_i}{v_x |\alpha_i| + \gamma_i \rho_i} - \frac{\theta}{\gamma_i} \right). \tag{2.16}$$

The linear part, $A(t)$, of system (2.15) is parameter-varying due to the varying wheel speed $\omega(t)$ in γ_f and γ_r and in k_f and k_r consequently.

Remark 1 *The linear part of the state-space* (2.15) *can be directly compared with the bicycle model* (2.8).

2.4 Estimation Reliability

It is imperative that design systems be resilient[3] to unexpected uncertainties, errors, and sensor failures. Much work has been done over the past few decades on developing mechanisms for obtaining desired reliability in different types of systems. These mechanisms

[3] *Resilience* in this thesis is referred to the robustness of the estimator to external disturbances and its flexibility of operation towards vehicle parameter variations. This terminology has been recently used in the control literature, e.g., see [51].

range from conceptually simple modular redundancy schemes to more advanced model-based fault-diagnosis techniques.

The need for a rigorous theory of reliability and fault diagnostics in control systems has only recently been recognized as a fertile and important area of research. The report in [52] highlights several key differences in reliability requirements for control systems and traditional information technology systems. One particularly important differentiating factor is that control systems involve the regulation of physical processes. This fact imposes hard real-time constraints on the system since a delay in processing could lead to instabilities or cascading failures in the control loop, potentially cause severe physical and economic damage. Papers [53, 54] echo a call for the development of a rigorous theory of reliability in control systems, and it details several open challenges for research.

To evaluate the performance of a reliable estimator (or controller), one compares the actual behavior of the estimator to the expected behavior and raises an alarm if the two deviate. The expected behavior is usually determined from a model of the plant; when there are disturbances or the model is uncertain, the expected and actual outputs will not coincide exactly. In such cases, the control system's designer must determine how different the two signals are allowed to be before raising an alarm. There is a trade-off here: if the threshold is set too low, there will be many false alarms, and if the threshold is too high, some legitimate faults might be missed. The relative weighting of these two factors will depend on the application at hand. It is important to note that this scheme is called the *real-time fault diagnostics* in that it runs concurrently with the system. This is in contrast to a scheduled fault-diagnosis, where the system is checked at regular intervals according to some maintenance schedule to ensure that it is operating correctly. Real-time monitoring is important for safety-critical systems so that a fault does not cause the system to become unstable or progress to a state where it cannot be repaired.

There are a variety of methods to perform fault-detection. The most straightforward method is to use *physical redundancy*: the fault-prone components are replicated, and a comparison mechanism (e.g., majority voter [55]) is used to determine which components are operating correctly. This scheme has the benefit of being simple to understand and implement, but it has the potential to be costly due to the replication of components. An alternative (or perhaps complementary) approach to diagnose faults is to analyze the

behavior of the component over time using a model of how the component is supposed to behave. This is known as *analytical redundancy* or *temporal redundancy* [56]. The goal of the fault-tolerant and reliable estimator (control) system is to allow the system to gracefully degrade or continue functioning under failures, and prevent faults from propagating to other parts of the system. A reliable system design can broadly be broken down into two objectives [57, 58]

1. Fault detection and identification (FDI): determine whether a fault has occurred, and isolate the component that has failed.

2. Fault accommodation: take steps to correct for the fault, or reconfigure the system to avoid the faulty component.

Fig. 2.4 shows a block diagram that illustrates the structure of a fault-tolerant control system. It is a complete version of what is discussed in [57], and the estimation fault diagnosis is also added to the block diagram. According to this figure, the detected fault in the estimation module is either compensated for and corrected or the existence of such fault is reported to the controller module to change the reliance of the controller to the estimated signal.

As one of the approaches adopted in this thesis to tackle the reliability of estimators is the probabilistic and stochastic approach, a literature review of these methods is presented in the following subsection.

2.4.1 Probabilistic methods in reliable estimator design

The problem of how to deal with uncertainties and unmodeled dynamics in the stability and performance analysis of dynamical systems has been investigated deeply in the past decades. Most of the efforts are towards an analysis of robust controller design under unmodeled dynamics. The main trend in those analyses is to show the exponential (robust) stability of the nominal system (the system disregarding the unmodeled part) and then find a (tight) bound for the states of the system in the presence of the unmodeled dynamics [59, 60]. However, there are times when the system operates in multiple modes. Even if

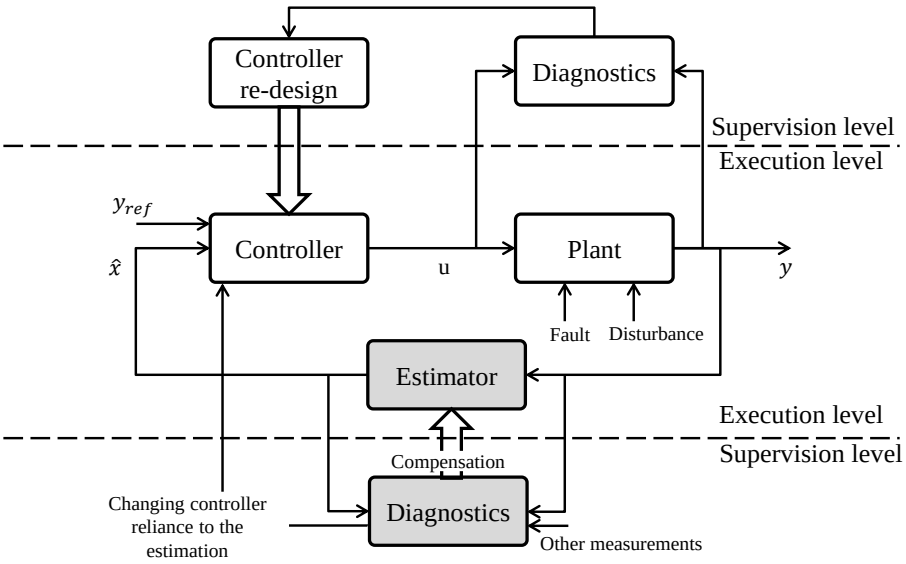

Figure 2.4: Reliable estimator or controller design.

each of the individual modes is linear and can be easily analyzed, analyzing the switching system is challenging. Analyzing the stability of switching systems has been an interesting field of study in the past two decades [61], [62]. Switching in dynamical systems introduces a hybrid system (a coupled continuous and discrete time system). However, tighter results can be developed if further assumptions hold, where the mode switches are governed by a *stochastic process* that is statistically independent from the state values. In the case when the stochastic process can be described by a Markov chain, the resulting hybrid system is called a Markovian jump linear system.

Markovian jump systems (MJS) have been widely investigated and many useful results have been obtained [63], [64]. The motivation of the study of this class of systems is the fact that many dynamical systems subject to random abrupt variations can be modeled by MJS such as manufacturing systems, networked control systems, and automotive systems (as discussed in this thesis). Typically, MJS are described by a set of continuous-time systems, described by classical differential equations, and a Markov stochastic process (or Markov chain) governing the jumps among those continuous-time systems. As a dominant factor, the transition probabilities in the jumping process determine the system's behavior to a

large extent, and so far, many analysis and synthesis results have been reported assuming the complete knowledge of the transition probabilities. Recently, an interesting extension to this research is in considering the uncertain transition probabilities, which aims to utilize robust methodologies to deal with the norm-bounded or polytopic uncertainties presumed in the transition probabilities, see for example [65], [66]. Ideal knowledge of the transition probabilities are definitely expected to simplify the system analysis and design, however, the likelihood of obtaining such available knowledge is actually questionable and probably expensive. A typical example can be found in network control systems, where the packet dropouts and channel delays are well-known to be modeled by Markov Chains with the usual assumption that all the transition probabilities are completely accessible [67], [68], [69]. In this thesis, much attention is focused on using this methodology in designing a reliable estimator in the presence of faulty measurements as well as analyzing the robustness of the observer toward unknown changes in the system parameters. The faulty measurements are equivalent to the dropped packets in network control systems, and the stability of the resulting hybrid system is analyzed.

2.5 Summary

A comprehensive literature review on vehicle estimation, including vehicle tire forces and velocities, was discussed in this chapter. Moreover, a detailed review of the works done in the field of road friction identification was done and the problems in each approach was also discussed. Beyond introducing recent research on vehicle state and road condition estimation, a brief overview of the vehicle tire model as well as vehicle handling dynamics was also introduced, which will be used in the subsequent chapters. Lastly, recent approaches to reliability and fault detection and identification algorithms for estimation and control of dynamical systems were discussed.

Chapter 3

Vehicle Corner Velocity Estimation

In Chapter 1, the necessity and importance of having a reliable estimation of vehicle velocity was discussed and the efforts done in studying this subject and challenges that should be overcome were reviewed. To this end, an algorithm for estimating vehicle corner velocity is introduced in this chapter. In this algorithm, a vehicle kinematics (tire-free) approach is coupled with the tire's internal states at each corner to estimate relative velocities of the tires as in [70–73]. The selected tire model is the average lumped LuGre [43] because of the dynamics in the internal deflection state as described briefly in the following subsection. The vehicle and tire parameters (with their actual values used for experiments) are presented in Table 3.1.

3.1 Longitudinal Velocity Estimation

The LuGre tire model was introduced in detail in Chapter 2 and here, we briefly review the dynamics that are used for the velocity estimator design. The internal longitudinal and lateral states z_q ($q \in \{x, y\}$)[1] and the normalized tire forces f_{nq} (i.e. $f_{nx} = F_x/F_z, f_{ny} =$

[1]From now, an index q for tire states or parameters indicates the direction of interest, i.e. $q \in \{x, y\}$. Tire forces and velocities in tire coordinates are shown in Fig. 3.3 (b).

F_y/F_z) in the pure-slip case are described as follows in the LuGre model:

$$\dot{z}_q = V_{rq} - (\kappa_q R_e|\omega| + \frac{\sigma_{0q}|V_{rq}|}{\theta g(V_{rq})})z_q, \tag{3.1}$$

$$f_{nq} = \sigma_{0q} z_q + \sigma_{1q}\dot{z}_q + \sigma_{2q} V_{rq}, \tag{3.2}$$

in which ω is the wheel speed and $V_{rx} = R_e\omega - V_{xt}$, $V_{ry} = -V_{yt}$ are the longitudinal/lateral relative velocities. The tires' center velocities in the tire coordinates are denoted by V_{xt}, V_{yt}. The function, $g(V_{rq})$ in the pure-slip model is defined as $g(V_{rq}) = \mu_c + (\mu_s - \mu_c)e^{-|\frac{V_{rq}}{V_s}|^{0.5}}$. The effect of pure and combined-slip LuGre tire models in the vehicle stability is explored in [47]. The parameter $\theta \in [0, 1]$ in (3.1) represents the road condition; this value is small when the road is slippery and it is close to 1 otherwise. In the following subsection, θ is assumed to be unknown resulting in the unknown term $\frac{\sigma_{0q}|V_{rq}|}{\theta g(V_{rq})} z_q$ in (3.1).

Assuming the unknown road friction term $\varrho_{zx} = \frac{\sigma_{0q}|V_{rq}|}{\theta g(V_{rq})} z_q$ as the bounded uncertainty, one can write the LuGre model (3.1) as follows at each corner for the longitudinal direction:

$$\dot{z}_x = V_{rx} - \kappa_x R_e|\omega| z_x + \varrho_{zx}. \tag{3.3}$$

The time derivative of the longitudinal relative velocity is described as:

$$\dot{V}_{rx} = R_e\dot{\omega} - \dot{V}_{xt}. \tag{3.4}$$

However, the measured signals[2] $\dot{V}_{xt}$ and ω (and particularly its derivative $\dot{\omega}$) are corrupted due to the sensor noises and bias. The deviation of the measured relative acceleration $R_e\dot{\omega} - \dot{V}_{xt}$ from $\dot{V}_{rx}$ at each corner due to the sensor noises is denoted by ϱ_{ax} and we have

$$\dot{V}_{rx} = R_e\dot{\omega} - \dot{V}_{xt} + \varrho_{ax}. \tag{3.5}$$

Dynamics of the tires' internal states (3.3) together with relative velocities (3.5) are used to develop the following dynamics:

$$\dot{\mathbf{x}} = \underbrace{\begin{bmatrix} -\kappa_x R_e|\omega| & 1 \\ 0 & 0 \end{bmatrix}}_{\mathbf{A}_x(\omega)} \mathbf{x} + \mathbf{B}_x u_x + \boldsymbol{\varrho}_x, \tag{3.6}$$

[2]The value of the longitudinal acceleration at CG (measured by IMU) is projected into the tires' center $\dot{V}_{xt}$.

in which $\mathbf{B}_x = [0 \quad 1]^T$, uncertainties are denoted by $\boldsymbol{\varrho}_x = [\varrho_{zx} \quad \varrho_{ax}]^T$, the states are $\mathbf{x} = [z_x \quad V_{rx}]^T$, and $u_x = R_e\dot{\omega} - \dot{V}_{xt}$. By substituting $\dot{z}_x$ from (3.3) into the normalized longitudinal force of the pure-slip case (3.2), one can rewrite the output equation as:

$$\begin{aligned} f_{nx} &= [(\sigma_{0x} - \sigma_{1x}\kappa_x R_e|\omega|) \quad (\sigma_{1x} + \sigma_{2x})]\mathbf{x} + \sigma_{1x}\varrho_{zx} \\ &= \mathbf{C}_x(\omega)\mathbf{x} + \sigma_{1x}\varrho_{zx}. \end{aligned} \tag{3.7}$$

By employing the normalized longitudinal force (3.7) and the system (3.6), the following observer is obtained for a longitudinal velocity estimation with the estimated output $\hat{y} = \hat{f}_{nx} = \mathbf{C}_x(\omega)\hat{\mathbf{x}}$ and observer gains $\mathbf{L}_x = [L_{1x} \quad L_{2x}]^T$:

$$\dot{\hat{\mathbf{x}}} = \mathbf{A}_x(\omega)\hat{\mathbf{x}} + \mathbf{B}_x u_x + \mathbf{L}_x(f_{nx} - \hat{f}_{nx}), \tag{3.8}$$

where $f_{nx} = F_x/F_z$ is the normalized longitudinal tire force. The bounded time-varying parameter in (3.8) is the wheel speed and the parameter varying state transition matrix is $\mathbf{A}_x(\omega) \in \mathbb{R}^{2\times 2}$. The error dynamics $\mathbf{e}_x = \mathbf{x} - \hat{\mathbf{x}}$ from (3.6) and (3.8) yields:

$$\begin{aligned} \dot{\mathbf{e}}_x &= [\mathbf{A}_x(\omega) - \mathbf{L}_x\mathbf{C}_x]\mathbf{e}_x - \mathbf{L}_x\sigma_{1x}\varrho_{zx} + \boldsymbol{\varrho}_x \\ &= \mathbf{A}_{e_x}(\omega)\mathbf{e}_x + \begin{bmatrix} 1 - L_{1x}\sigma_{1x} & 0 \\ -L_{2x}\sigma_{1x} & 1 \end{bmatrix} \boldsymbol{\varrho}_x \\ &= \mathbf{A}_{e_x}(\omega)\mathbf{e}_x + \mathbf{B}_{e_x}\boldsymbol{\varrho}_x. \end{aligned} \tag{3.9}$$

The system matrix $\mathbf{A}_x(\omega)$ in (3.8) is physically bounded; thus, a conventional observability test is performed. The observability matrix for parameter-varying systems like (3.6) with output (3.7) is given by [74] as:

$$\begin{aligned} \mathcal{O}_n &= [\epsilon_1 \quad \epsilon_2 ... \quad \epsilon_n]^T, \\ \epsilon_1 = \mathbf{C}_x, &\quad \epsilon_{i+1} = \epsilon_i\mathbf{A}_x(\omega) + \dot{\epsilon}_i. \end{aligned} \tag{3.10}$$

Observability is confirmed by holding the full rank condition $rank(\mathcal{O}_2) = 2$ at each fixed time span for the operating regions of the wheel speed and its time derivatives. Thus, the parameter-varying system (3.6) with output (3.7) is observable, and it is feasible to estimate the tires' longitudinal internal states $\hat{z}_x$ and the relative velocity $\hat{V}_{rx}$ by employing the longitudinal force as the output.

Remark 2 *For implementation and road experiments, discretization of the continuous-time system (3.6) with the output* $y = \mathbf{C}_x\mathbf{x} + \mathbf{D}_x u_x$ *is done by the Step-Invariance method because of its precision and response characteristics. The step-invariance discretization is the zero-order hold method and includes a constant input signal* $u_x(t)$ *during integration. It has good accuracy with the platform sampling frequency of* $200[Hz]$*. Moreover, the richness of the step signal, in terms of the frequencies that it carries, makes the step invariance method very suitable for automotive applications as there exist a large amount of uncertainties and disturbances. The input of the continuous-time system is the hold signal* $u_x[k] = u_x[t_k]$ *for a period between* $t_k \leq t < t_{k+1}$ *with the sample time* T_s*. Then, the discrete-time system* $\mathbf{x}[k+1] = \mathbf{A}_x^d[k]\mathbf{x}[k] + \mathbf{B}_x^d u_x[k], y[k] = \mathbf{C}_x^d\mathbf{x}[k] + \mathbf{D}_x^d u_x[k]$ *has the output matrices* $\mathbf{C}_x^d = \mathbf{C}_x, \mathbf{D}_x^d = \mathbf{D}_x$ *and state/input matrices:*

$$\mathbf{A}_x^d = e^{\mathbf{A}_x(t)T_s}, \quad \mathbf{B}_x^d = \int_0^{T_s} e^{\mathbf{A}_x(t)\tau}\mathbf{B}_x(t)d\tau. \tag{3.11}$$

The discretized from of the error dynamics (3.9), can now be written as $\mathbf{e}_x[k+1] = \mathbf{A}_{e_x}^d[k]\mathbf{e}_x[k] + \mathbf{B}_{e_x}^d\boldsymbol{\varrho}_x[k]$*. The following subsection focuses on the corner-based velocity observer for the lateral direction.*

3.2 Lateral Velocity Estimation

The LuGre output equation (3.2) for the lateral direction can be expressed as follows:

$$\begin{aligned} f_{ny} &= [(\sigma_{0y} - \sigma_{1y}\kappa_y R_e|\omega|) \quad (\sigma_{1y} + \sigma_{2y})]\bar{\mathbf{x}} + \sigma_{1y}\varrho_{zy} \\ &= \mathbf{C}_y(\omega)\bar{\mathbf{x}} + \sigma_{1y}\varrho_{zy}, \end{aligned} \tag{3.12}$$

where the states are $\bar{\mathbf{x}} = [z_y \quad V_{ry}]^T$. The relative lateral acceleration $\dot{V}_{ry} = -\dot{V}_{yt} + \varrho_{ay}$ (the projected lateral acceleration in the tire coordinate system is denoted by $\dot{V}_{yt}$, compensated by road angles from a real-time road angle estiamtor [75]) is combined with the lateral LuGre internal state to form the lateral velocity estimator. Equation (3.6) can be rewritten

for the lateral direction as

$$\dot{\bar{\mathbf{x}}} = \underbrace{\begin{bmatrix} -\kappa_y R_e|\omega| & 1 \\ 0 & 0 \end{bmatrix}}_{\mathbf{A}_y(\omega)} \bar{\mathbf{x}} + \mathbf{B}_y u_y + \boldsymbol{\varrho}_x, \tag{3.13}$$

where $\mathbf{B}_y = \mathbf{B}_x$, and $u_y = -\dot{v}_{yt}$. Uncertainties in the lateral states are denoted by $\boldsymbol{\varrho}_y = [\varrho_{zy} \quad \varrho_{ay}]^T$. The state estimator can be expressed as follows for the lateral direction with the output $\hat{y}_l = \hat{f}_{ny} = \mathbf{C}_y(\omega)\hat{\mathbf{x}}_l$:

$$\dot{\hat{\bar{\mathbf{x}}}} = \mathbf{A}_y(\omega)\hat{\bar{\mathbf{x}}} + \mathbf{B}_y u_y + \mathbf{L}_y(f_{ny} - \hat{f}_{ny}), \tag{3.14}$$

in which $\mathbf{L}_y = [L_{1y} \quad L_{2y}]^T$.

Remark 3 *Similar to the longitudinal direction, the observability of the lateral direction dynamics can be verified by the observability criterion (3.10) for the parameter-varying system with* $\mathbf{A}_y(\omega), \mathbf{C}_y(\omega)$.

The error dynamics is then derived as follows for the lateral velocity estimator and represents a linear parameter varying system:

$$\dot{\mathbf{e}}_y = \mathbf{A}_{e_y}(\omega)\mathbf{e}_y + \underbrace{\begin{bmatrix} 1 - L_{1y}\sigma_{1y} & 0 \\ -L_{2y}\sigma_{1y} & 1 \end{bmatrix}}_{\mathbf{B}_{ey}} \boldsymbol{\varrho}_y, \tag{3.15}$$

where $\mathbf{A}_{e_y} = [\mathbf{A}_y(\omega) - \mathbf{L}_y\mathbf{C}_y]$. The error dynamics in discrete-time yields $\mathbf{e}_y[k+1] = \mathbf{A}^d_{e_y}[k]\mathbf{e}_y[k] + \mathbf{B}^d_{e_y}\boldsymbol{\varrho}_y[k]$. In order to increase the accuracy of the velocity estimation at each corner, the effect of the suspension compliance is considered on the estimators and is discussed in the following section.

In the above analysis, we assumed the vehicle as a solid (rigid) body and there is no relative motion between its parts. However, in estimating the slip of the tire, it is important to consider the extra degree of freedom that exists between the chassis and the wheel due to the suspension compliance. Modeling and analyzing the effect of the suspension compliance on the vehicle corner velocity estimation is the subject of the following section.

3.3 Model improvement by Inclusion of Suspension Compliance

As discussed in Chapter 1, one of the sources of inaccuracy in vehicle velocity estimation are unmodeled dynamics which are not included in the design of the observer. One of the examples of such inaccuracies in the dynamics is the effect of extra dynamics (relative motion) between the wheel and the vehicle chassis due to the existence of suspension compliance. In this chapter, the effect of the suspension compliance on the vehicle's corner velocity estimation is analyzed. It is worth noting that this effect is not captured by GPS measurements as GPS only provides the vehicle's velocity at CG. Thus, analyzing the effect of the suspension dynamics in both longitudinal and lateral directions is vital for having a more accurate estimation of the tire slip.

3.3.1 Suspension Model

The extra degree of freedom between the chassis and the tire due to the suspension compliance follows specific dynamics. This dynamics can be represented by a second-order system as:

$$\begin{aligned} M_u\ddot{\psi}_x(t) + C_x\dot{\psi}_x(t) + K_x\psi_x(t) &= F_x \\ M_u\ddot{\psi}_y(t) + C_y\dot{\psi}_y(t) + K_y\psi_y(t) &= F_y, \end{aligned} \tag{3.16}$$

where F_x and F_y are longitudinal and lateral forces on each tire, K_x and K_y are the equivalent stiffness of the suspension compliance in each direction, C_x and C_y are the equivalent damping of the suspension compliance in each direction and M_u is the quarter car unsprung mass. Displacements due to the suspension in each direction, are denoted by $\psi_x(t)$ and $\psi_y(t)$. The suspension dynamics at each corner can be written in the following state space form:

$$\begin{bmatrix} \dot{\psi}_q(t) \\ \ddot{\psi}_q(t) \end{bmatrix} = \begin{bmatrix} 0 & 1 \\ \frac{-K_q}{M_u} & \frac{-C_q}{M_u} \end{bmatrix} \begin{bmatrix} \psi_q(t) \\ \dot{\psi}_q(t) \end{bmatrix} + \begin{bmatrix} 0 \\ 1 \end{bmatrix} \frac{F_q}{M_u}, \tag{3.17}$$

where $q \in \{x, y\}$ is used for brevity. The velocity term $\dot{\psi}_q(t)$ should be directly added to the estimated velocity at each corner due to the dynamics (3.17). This procedure is discussed in detail bellow:

The estimated relative velocities $\hat{V}_{rx}$ and $\hat{V}_{ry}$ by (3.8), (3.14) are used for the longitudinal velocity estimation at the tire coordinates as $\hat{V}_{xt} = R_e\omega - \hat{V}_{rx}$ and $\hat{V}_{yt} = -\hat{V}_{ry}$. Afterwards, utilizing the steering angle δ at the front and rear tracks (i.e. $\delta = 0$ for the rear track of front-steering vehicles) and each corner's velocity in the vehicle coordinates yields $\hat{\tilde{V}}_{xc} = \hat{V}_{xt}\cos\delta - \hat{V}_{yt}\sin\delta$ for the longitudinal direction and $\hat{\tilde{V}}_{yc} = \hat{V}_{xt}\sin\delta + \hat{V}_{yt}\cos\delta$ for the lateral direction. To account for suspension compliance, the velocities (3.17) are then added to the estimated velocities in the vehicle coordinates as:

$$\hat{V}_{xc} = \hat{\tilde{V}}_{xc} + \dot{\psi}_x, \quad \hat{V}_{yc} = \hat{\tilde{V}}_{yc} + \dot{\psi}_y. \tag{3.18}$$

The above procedure is schematically shown in Fig. 3.1. Estimated corner velocities, $\hat{V}_{xc}$

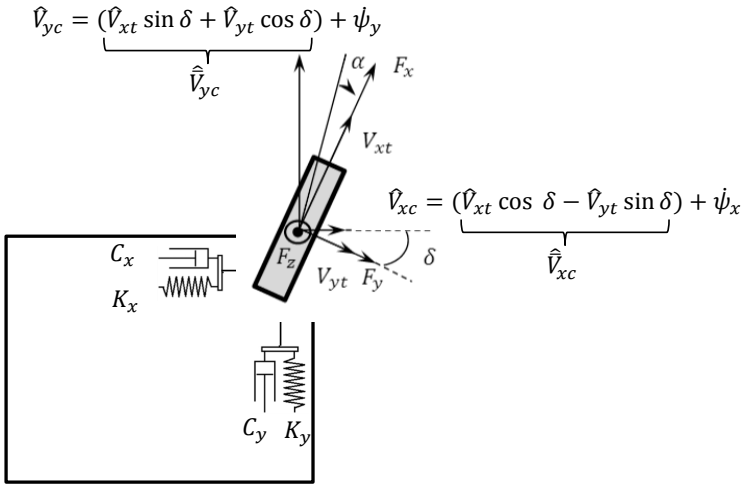

Figure 3.1: The effect of the suspension compliance on the vehicle corner velocities are schematically represented by spring and dampers.

and $\hat{V}_{yc}$, are then used for calculation of the vehicle's velocity at CG. The longitudinal velocity of the vehicle at its CG, called $\hat{v}_x$, is calculated by the front or the rear axle speed via

$$\hat{v}_x = 0.5(\hat{V}_{xc_{fL}} + \hat{V}_{xc_{fR}}), \quad \text{or} \quad \hat{v}_x = 0.5(\hat{V}_{xc_{rL}} + \hat{V}_{xc_{rR}}), \tag{3.19}$$

where fL, fR, rL, rR represent the front-left, front-right, rear-left, and rear-right tires, respectively. Similarly, the lateral velocity at the vehicle's CG, $\hat{v}_y$, can be calculated from the front or rear axle's lateral speed as

$$\hat{v}_y = -ra + 0.5(\hat{V}_{yc_{fL}} + \hat{V}_{yc_{fR}}), \quad \text{or} \quad \hat{v}_y = rb + 0.5(\hat{V}_{yc_{rL}} + \hat{V}_{yc_{rR}}), \tag{3.20}$$

in which r is the yaw rate and a and b are the distances from the front and rear axles to CG, as defined in Table 3.1.

In order to assess the performance of the estimators with the suspension compliance, we revisit the tire model. In particular, the relative velocities (i.e. slip ratio/angle) corrected by the suspension dynamics are employed in a tire model to calculate the normalized tire forces. The calculated tire forces are then compared to the measured ones to determine Δf_n, which represents the difference between the measured and estimated tire forces with (and without) consideration of the suspension compliance. The quantity Δf_n is supposed to be less if we consider the effect of the suspension compliance in estimating the tire slip. This validation approach is schematically shown in Fig. 3.2.

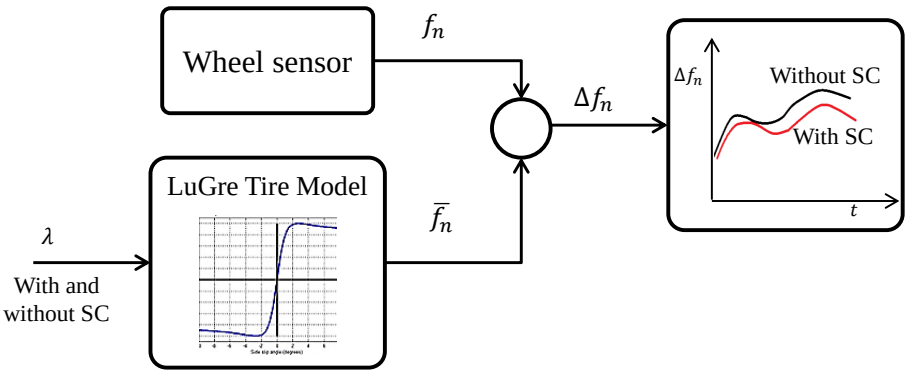

Figure 3.2: Assessment of the effect of the suspension compliance via tire model.

The structure of the augmented velocity estimators with the Suspension Compliance (SC) effect is depicted in Fig. 3.3. Considering road friction and measurement noises as uncertainties, the kinematics-based velocity estimation is combined with the internal tire states in *Long. Velocity Est.* and *Lat. Velocity Est.* Measured accelerations by the IMU attached to the sprung mass are corrected with the vehicle's body pitch and roll angles

to include only the kinematics of the motion. These corrected values are then used in the velocity estimators. A high-slip detection algorithm is used for appropriate observer gain switch to tackle the slippery cases, which will be discussed in the next chapter. Estimated corner velocities are augmented with the suspension effect and mapped onto the vehicle's CG in the *SC and Mapping* module.

Remark 4 *Tire forces can be measured by wheel sensors. However, because of high cost impact on mass production vehicles, installation problems, and maintenance issues, tire force estimation has extensively been tried only in the literature. Longitudinal and lateral tire forces at each corner can be estimated using nonlinear and sliding mode observers [3], unknown input observers [8, 10], or Kalman Filter based estimators [5–7]. Normalized longitudinal and lateral forces f_{nx}, f_{ny} are assumed to be known from the Kalman Filter based estimation on wheel and lateral dynamics [7, 50]. Due to the fact that the vehicle's normal force has a significant impact on the normalized longitudinal and lateral tire forces, a detailed study on tire normal force calculation is done in [50]. Since tire forces are used as measurements for the velocity estimation in this thesis, they are referred to as force measurement and force estimation interchangeably.*

The experimental validation of the proposed corner-based vehicle velocity observer together with consideration of the effect of the suspension compliance are discussed in the following section. The estimated vehicle velocities are compared with those of GPS measurements for various maneuvers on different road conditions. Moreover, it will be shown that the effect of the suspension compliance is during harsh traction and braking maneuvers where the applied tire forces are considerable. Such effect in a tiny time interval plays an important role in detecting tire slip more accurately and consequently, on vehicle traction and stability control.

3.4 Experimental Validation

This section demonstrates various experimental results to validate the corner-based vehicle velocity estimation introduced in the beginning of the chapter. Moreover, the effect of

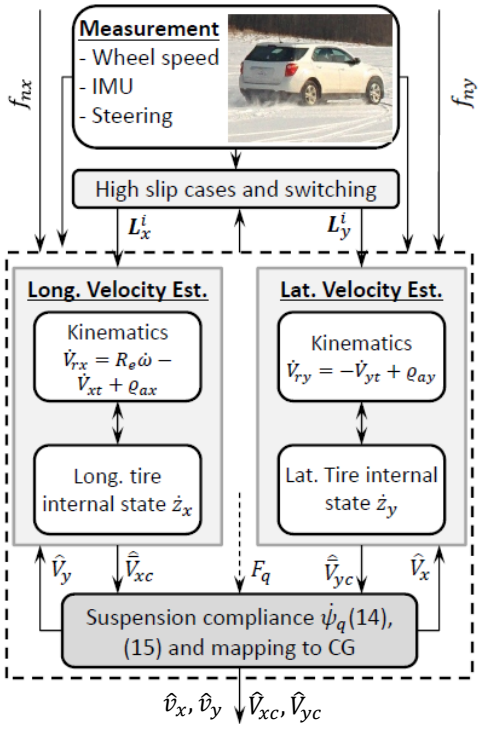

Figure 3.3: Overall vehicle velocity estimation structure with SC.

considering the suspension compliance on the accuracy of the resulting velocity estimation is experimentally examined. The estimated vehicle velocities are compared with those of GPS measurements for various maneuvers on different road conditions. Moreover, it will be shown that the effect of the suspension compliance is considerable during harsh traction and braking maneuvers, where the applied tire forces are considerable. Such effect in a tiny time interval plays an important role in detecting tire slip more accurately and consequently, on vehicle traction and stability control. Before we start showing the experimental results, in the following subsection, we introduce the test facilities which are used together with the empirical approach taken to test the proposed velocity estimation algorithm.

3.4.1 Experimental Setup

The vehicle velocity estimation algorithm is developed in MATLAB Simulink environment and is compiled and implemented on the dSpace micro-Autobox. The micro-Autobox communicates with the Anti-Block System (ABS) encoders, electric motors, GPS unit and vehicle Inertial Measurement Unit (IMU) through the Controlled Area Network (CAN). Stuck IMU sensors used for the production vehicles are also used for these experimental tests. Hence, the proposed algorithms, mentioned in this thesis, are considering their inherent characteristics, e.g., signal to noise ratio and biases. The experimental setup is shown in Figure 3.4. The stock vehicle IMU sensor measures the vehicle's longitudinal and

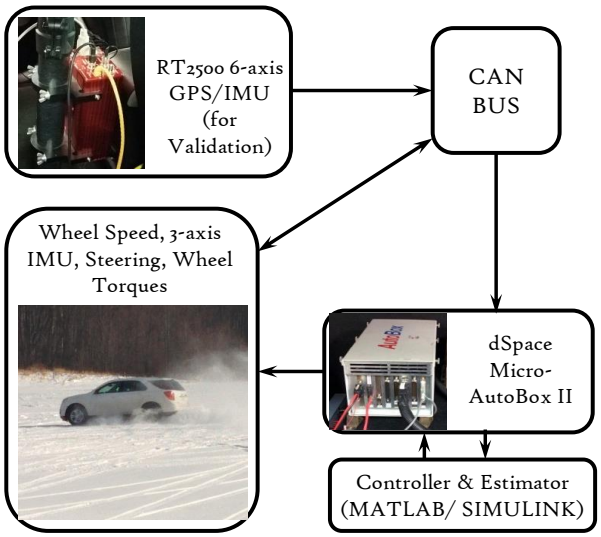

Figure 3.4: Experimental setup for vehicle Estimation.

lateral accelerations, a_x and a_y, and the vehicle yaw rate r. The RT2500 inertial and GPS navigation systems from the OxTS company is installed on the vehicle to provide accurate measures of the vehicle's longitudinal and lateral velocities. The wheel encoders in the ABS module provide each wheel's angular speed, ω_{ij}, and the hydraulic brake system can regulate the brake pressure and brake torque according to the received command (control) signal. Similarly, the electric motors receive the torque command through the CAN bus and deliver the requested drive torque. These command signals (both torque and brake)

are based on the estimated velocities provided to the control module.

Two electric Chevrolet Equinox vehicles have been used in the experiments. These test vehicles are maintained, modified and driven by the technicians of Mechatronic Vehicle Systems Laboratory. Vehicle A is an all-wheel drive (AWD) vehicle with four electric motors installed, one on each corner of the vehicle. The method of actuation is torque vectoring across both front and rear axles. Sport tires are installed on this vehicle. Vehicle B is rear-wheel drive (RWD) and has only two electric motors installed on the rear axle. It uses differential braking as the method of actuation and has all season tires. Figure 3.5 shows both test vehicles used in experimental tests. The main geometric and inertial

(a) Vehicle A (b) Vehicle B

Figure 3.5: Test vehicles used in experimental verifications.

properties of the two vehicles are listed in Table 3.2.

Several critical maneuvers are performed with the test vehicles A and B. The performance of the velocity estimator developed in the previous section is evaluated in these maneuvers and compared to the GPS measurements. These maneuvers are preformed on various road surfaces such as dry pavement, wet sealer, and snow. The tuning parameters of the estimator are the same as those listed in Table 3.1, except for some fine tunings.

3.4.2 Maneuvers with longitudinal excitations

The outcome of the longitudinal velocity estimator modified by the suspension compliance (SC) with all-wheel-drive AWD powertrain configuration (vehicle A) is provided in Fig. 3.6

for a maneuver with successive acceleration and brake on a dry surface. It demonstrates good performance of the estimator validated by the measurement from an accurate GPS at the vehicle's CG. Figure 3.6 also compares the measured velocities and the estimated

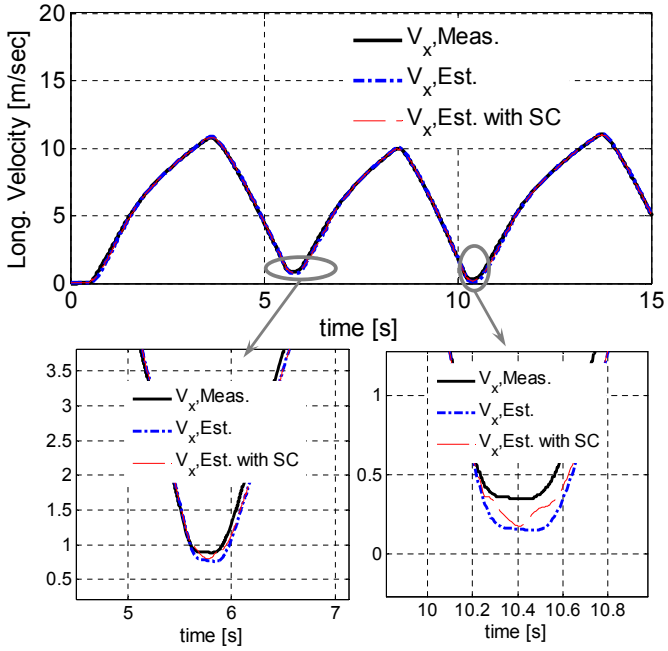

Figure 3.6: Effect of the SC on corner longitudinal velocity estimation in acceleration and brake, AWD.

ones with incorporation of the suspension kinematics which leads to a decrease in the longitudinal error RMS from 5.3% to 3.1%. Although this amount of difference seems to be small, it has considerable effects on the tire slip. Given known road condition, the forces by the augmented estimated slip ratio due to the suspension kinematics are compared to the forces produced by the slip ratio without the suspension compliance in Fig. 3.7 to study the performance of the added kinematics to the augmented estimators. As discussed in the previous section and shown schematically in Fig. 3.2, the difference between the measured and estimated tire forces with (and without) the SC is denoted by Δf_n and is depicted in Fig. 3.7 at a corner. As shown in Fig. 3.7, in the beginning of the maneuver, when there exists a traction, the effect of suspension compliance is to decrease the value of Δf_n.

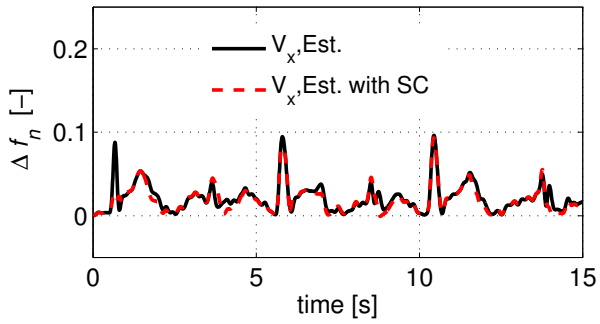

Figure 3.7: *SC* verification with longitudinal forces in acceleration and brake, AWD.

In another test, the augmented longitudinal velocity estimator with the suspension compliance is examined in a harsh launch maneuver on a surface, which has two different friction conditions (this is called a split-μ maneuver), and the results are shown in Fig. 3.8. The left wheels are on ice with $\mu \approx 0.25$, the right wheels are on a dry asphalt, and the powertrain configuration is *AWD*. When the vehicle enters this road, the left side wheels start to slip (their wheel speed ω increase significantly) but the right side wheels do not have major slip. The blue dashed lines depict the pure wheel speed $R_e\omega$, the red lines are the estimated corner velocities of the vehicle, and the black lines represent the GPS measurement of the actual corner velocities. As can be seen from Fig. 3.8, the developed speed estimator at each corner exhibits results with good accuracy and has correspondence with the measured GPS velocity data.

Similar to the previous test, the tire force errors Δf_n at each corner are depicted in Fig. 3.9 for this split-μ maneuver. As can be seen from Fig. 3.9, incorporation of *SC* decreases Δf_n for almost all acceleration and deceleration parts of the maneuver.

Proper observer gain allocation and *SC* incorporation lead to the observed smooth and accurate velocity estimation at the CG as well as each corner for such maneuvers with longitudinal excitations. In the following subsection, some more complicated maneuvers, comprised of both longitudinal and lateral excitations, are discussed.

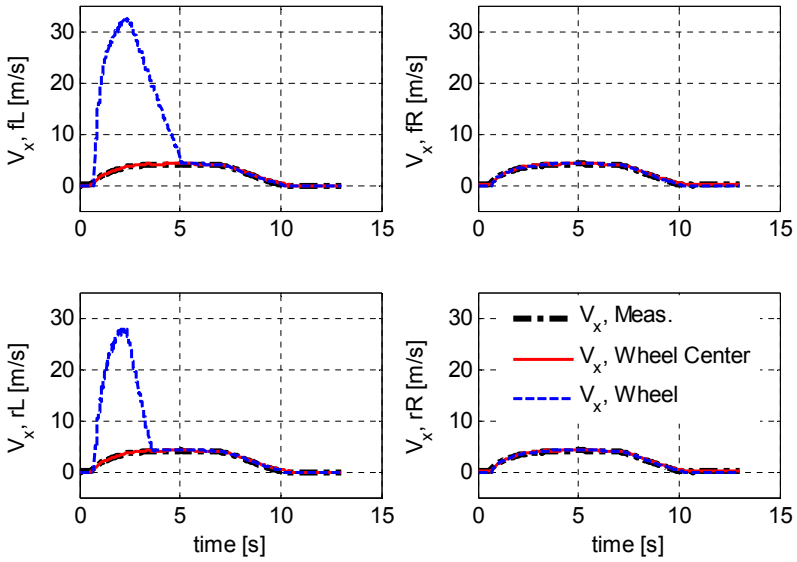

Figure 3.8: Launch on split-μ, ice/dry, and AWD.

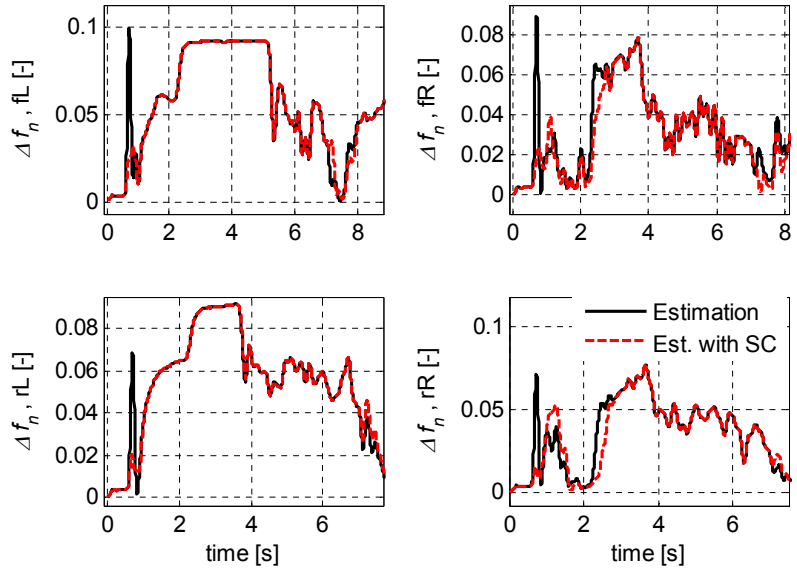

Figure 3.9: *SC* verification with longitudinal forces, split-μ and AWD.

3.4.3 Maneuvers with lateral and combined lateral/longitudinal excitations

In order to assess the corner based approach in combined-slip conditions, where the tire capacities are reduced due to a high slip ratio as well as the high slip angles in each longitudinal/lateral direction, a harsh acceleration-in-turn (AiT) maneuver with *AWD* configuration is done on a dry surface. The results of the longitudinal velocity estimator at each corner are then provided in Fig. 3.10. The measured wheel speeds and the estimated velocities at wheel centers in Fig. 3.10 confirm a large slip condition with oscillations for the front right (fR) tire. High slip ratio regions exist between $t = 4.1$ and $t = 7[s]$, but proper gain switching results in accurate estimation.

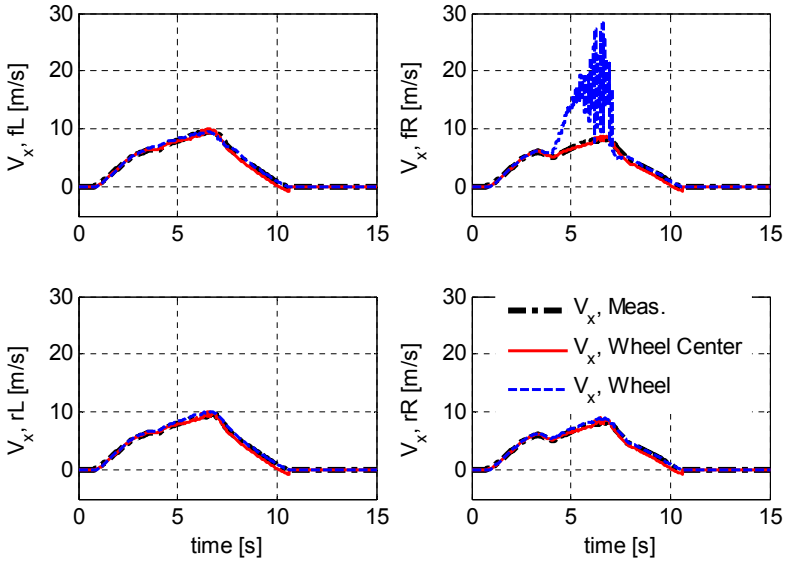

Figure 3.10: Acceleration in turn on a dry road, AWD.

The developed longitudinal observer provides dependable estimates even in such maneuvers with harsh longitudinal/lateral excitation and consequently, high slip ratio regions. Experimental results of Δf_n at the front tires are illustrated in Fig. 3.11, which shows lower force errors for estimation with *SC* and substantiates improvement in accuracy of the estimators.

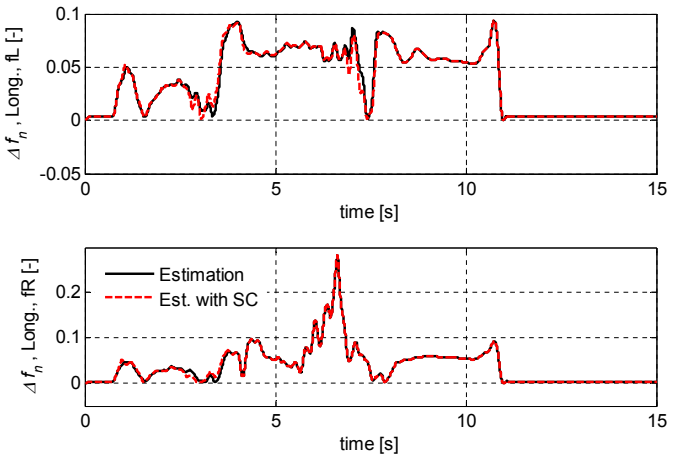

Figure 3.11: *SC* verification with longitudinal forces, acceleration in turn and AWD.

Results of the lateral velocity estimator together with the measured accelerations and the yaw rate are also provided in Fig. 3.12 for the same AiT scenario on dry asphalt. Figure 3.12 reveals that high oscillations exist in both lateral and longitudinal accelerations,

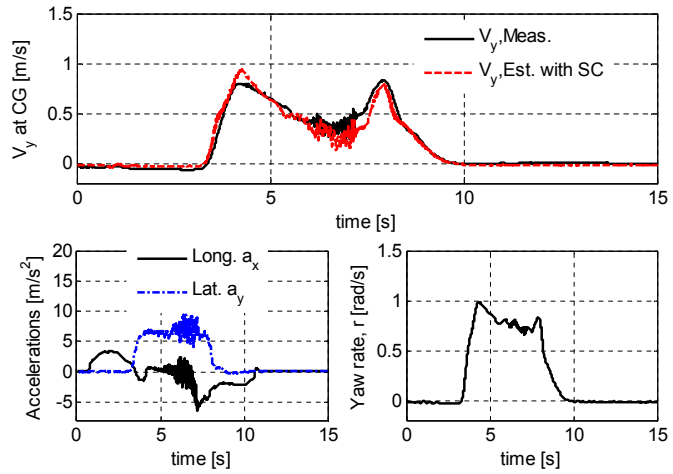

Figure 3.12: Lateral velocity estimation for acceleration in turn on a dry road.

but the lateral state estimation methodology handles these situations and exhibits smooth and accurate outcomes.

The augmented lateral estimation (by the suspension compliance) and the pure lateral

observer are compared with the lateral force measurement and the difference Δf_n at the front tires are shown in Fig. 3.13.

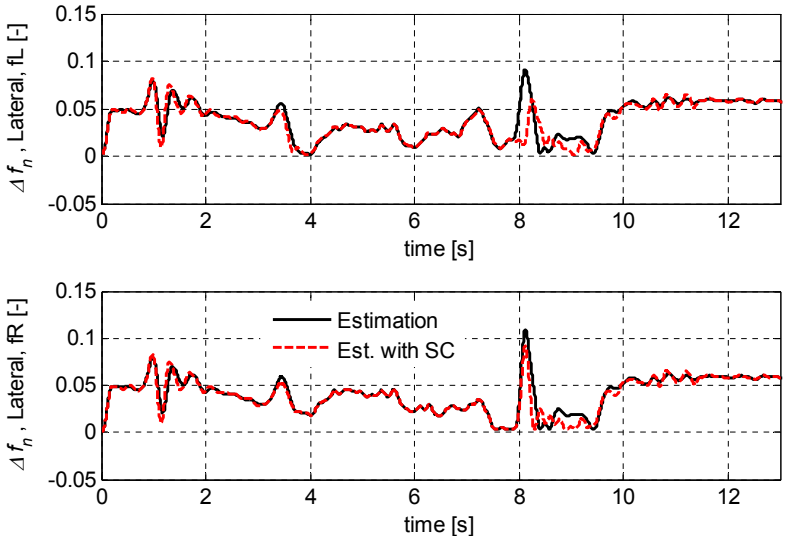

Figure 3.13: *SC* verification with longitudinal forces, acceleration in turn, and AWD.

In another test, the augmented velocity estimators are examined in the vehicle with *AWD* configuration in a harsh lane change (LC) scenario with acceleration and deceleration on snow. Results of the longitudinal velocity estimation are compared to the measured wheel speeds and wheel centers' velocities in Fig. 3.14.

Figure 3.14 shows high slip ratio conditions at all tires, but the developed longitudinal velocity estimator provides reliable and accurate outcomes. The experimental results of the lateral velocity estimator as well as the measured accelerations and the yaw rate are also depicted in Fig. 3.15 for this maneuver. Fluctuations of the measured lateral acceleration and sudden changes of the vehicle yaw rate in Fig. 3.15 substantiate the arduous characteristics of the driving scenario.

As confirmed via the above experimental results, the suggested longitudinal and lateral state estimators with the suspension compliance provide appropriate correspondence with GPS measurements and those estimations can be reliably used for traction and stability control systems.

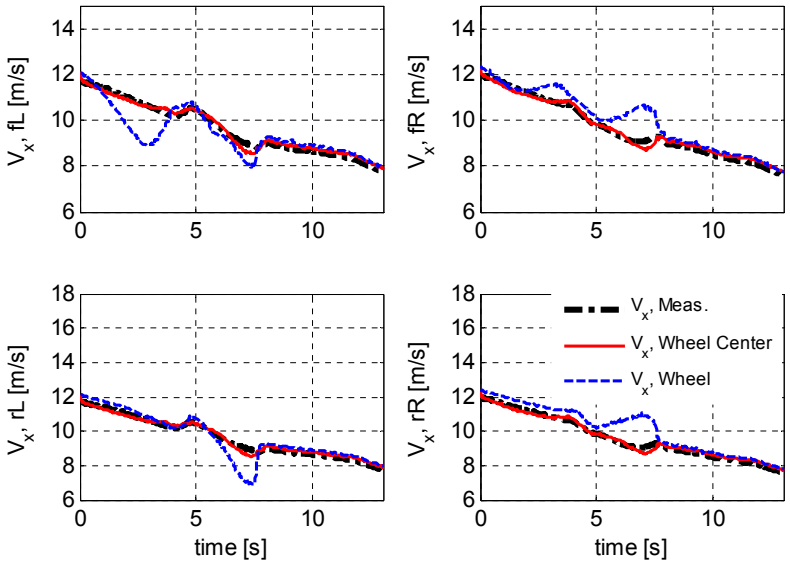

Figure 3.14: Lane change and steering on a snow road.

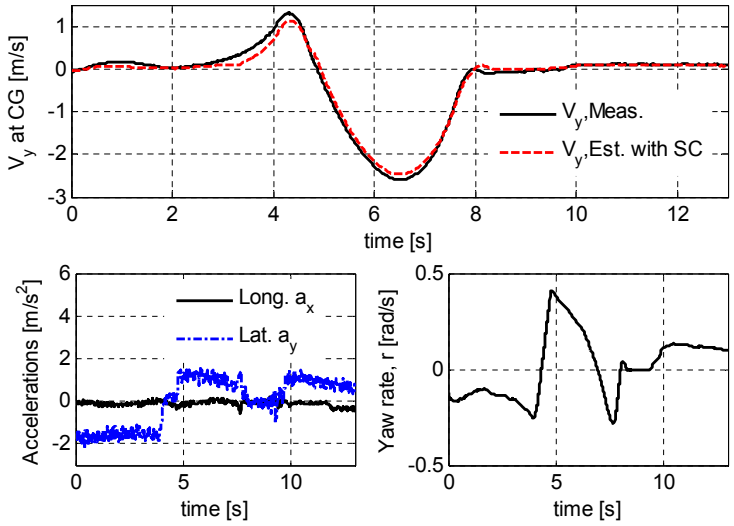

Figure 3.15: Lateral velocity estimates for a lane change (LC) on a snow road.

3.5 Summary

A reliable and resilient corner-based vehicle velocity estimation algorithm was presented in this chapter. This estimator was in the form of a combination of vehicle kinematics and a LuGre tire model. The passivity of the LuGre tire model could help the velocity estimator to improve its performance compared to the previous kinematic based methods. The designed vehicle velocity estimation algorithm is proven to be resilient to the time-varying tire parameters, the road friction condition, as well as sensor measurements uncertainties. The observability of the dynamics as a linear time-varying system, due to the time-varying wheel speed, was analytically studied prior to designing the observer. In order to further increase the performance of the designed velocity estimation algorithm, the effect of the suspension compliance and the resulting extra degree of freedom was directly added to the estimated vehicle corner velocity. The performance of the proposed velocity estimation algorithm was verified via several experimental tests, which were comprised of various standard vehicle maneuvers performed on different road conditions, and the results showed appropriate correspondence with measurements.

Table 3.1: Vehicle Specifications and Tire Parameters/states

Description	Parameter/State	Unit	Sample Values
Rubber stiffness	σ_{0x}, σ_{0y}	$[1/m]$	641, 131.5
Rubber damping	σ_{1x}, σ_{1y}	$[s/m]$	0.85, 0.82
Relative viscous damping	σ_{2x}, σ_{2y}	$[s/m]$	0.0016, 0.001
Load distribution factor	κ_x, κ_y	$[s/m]$	8.1, 13.4
Vehicle mass	m	$[kg]$	2270
Vehicle moment of inertia	I_z	$[kg.m^2]$	4650
Wheel moment of inertia	I_w	$[kg.m^2]$	1.7
Distance from front and rear axles to CG	a, b	$[m]$	1.42, 1.43
Effective radius	R_e	$[m]$	0.33
Vehicle tire center velocity	V_{xt}, V_{yt}	$[m/s]$	
Vehicle corner velocity	V_{xc}, V_{yc}	$[m/s]$	
Tire relative velocity	V_{rx}, V_{ry}	$[m/s]$	
Vehicle longitudinal/lateral velocities at CG	v_x, v_y	$[m/s]$	
Wheel angular speed	ω	$[rad/s]$	
LuGre friction state	z_x, z_y	$[-]$	
Long/Lat/Normal tire force	F_x, F_y, F_x	$[N]$	
Normalized Coulomb friction	μ_c	$[-]$	0.85
Normalized static friction	μ_s	$[-]$	1.1
Stribeck velocity	V_s	$[m/s]$	5
Vehicle yaw rate	r	$[rad/s]$	
Vehicle long/lat acceleration	a_x, a_y	$[m/s^2]$	
Suspension stiffness	K_x, K_y	$[N/m]$	3×10^5, 7×10^5
Suspension damping	C_x, C_y	$[Ns/m]$	3730
Quarter car unsprung mass	M_u	$[kg]$	46
Front/Rear track length	T_{r_f}, T_{r_r}	$[m]$	1.62, 1.56
CG height	h_{CG}	$[m]$	0.65
Height of the roll center	h_{RC}	$[m]$	0.54

Table 3.2: Properties of the two electric vehicles used in experiments.

Vehicle Name	**Vehicle A**	**Vehicle B**	**Parameter (Unit)**
Appearance	Black Equinox	White Equinox	–
Driveline	All Wheel Drive	Rear Wheel Drive	–
Tires	Sport Tires	All-season Tires	–
Vehicle mass	2270	2043	m(kg)
Wheel moment of inertia	1.7	1.7	I_w(kg.m^2)
Wheel base	2.858	2.858	L(m)
Track width	1.589	1.585	W(m)
Wheel effective radius	0.339	0.328	$R_e(m)$

Chapter 4

Reliability of the Vehicle Corner Velocity Estimation

In the previous chapter, a corner-based vehicle velocity estimation algorithm was introduced in the form of a combination of vehicle kinematic relations and LuGre tire model. Moreover, the effect of the suspension compliance on the accuracy of the resulting estimator was discussed. Furthermore, several experimental results validated the performance of the designed velocity estimator. In this chapter, a closer look is taken to the proposed velocity estimator. In particular, using system-theoretic concepts and techniques, rigorous stability, performance, and robustness analyses of the proposed velocity estimator to uncertainties and external disturbances is performed. The performance metrics that will be introduced for the velocity estimator can be considered as fundamental limitations that one can expect from the estimator to meet in terms of performance and resilience to uncertainties. Because of that, this chapter's analysis is referred to as the *off-line reliability analysis* of the vehicle velocity estimation [70]. An on-line approach to the estiamtor's reliability analysis will be discussed in the subsequent chapter.

4.1 Estimator's Stability, Robustness and Sensitivity Analysis

The stability and resilience of the vehicle velocity estimator is investigated in this section. More particularly, the stability of the observer error dynamics (3.9) and (3.15) is analyzed as a linear time-varying system. Moreover, the robustness of the observer dynamics to model uncertainties will be investigated, and the sensitivity of the stability margin and $\mathcal{H}_\infty$ robustness of the error dynamics (3.9) and (3.15) to sensor measurements noises and road condition uncertainties will be discussed.

4.1.1 Stability and $\mathcal{H}_\infty$ Performance

The following proposition introduces a bound on the estimation error in (3.9) and (3.15). A conventional approach is to study the stability of the symmetric part of the matrices $\mathbf{A}_{e_x}$ and $\mathbf{A}_{e_y}$, which usually results in conservative results [76]. In order to tackle such conservativeness, a similarity transformation is utilized in the following proposition to show the boundedness of the estimation error.

Proposition 1 *Estimation errors in linear time-varying error dynamics* (3.9) *and* (3.15) *are bounded.*

Proof 1 *A similarity transformation in the form of* $\bar{\mathbf{e}}_q(t) = \mathbf{T}\mathbf{e}_q(t)$*, where* $q \in \{x, y\}$*, is employed on the longitudinal/lateral estimation error states* (3.9) *and* (3.15)*, which results in* $\bar{\mathbf{A}}_{e_q} = \mathbf{T}\mathbf{A}_{e_q}\mathbf{T}^{-1}$ *and* $\bar{\mathbf{B}}_{e_q} = \mathbf{T}\mathbf{B}_{e_q}$*. Choosing* $\mathbf{T} = \mathrm{diag}(\gamma, 1)$ *with a design parameter* $\gamma > 0$*, leads to* $\bar{\mathbf{A}}_{e_q}$ *whose stability margin,* $\mathcal{SM}_q \triangleq \max_i \lambda_i(\bar{\mathbf{A}}_{e_q})$*, is close to the stability margin of its symmetric part (which will be discussed in Example 1 later). Moreover, due to the fact that* $||\mathbf{T}||$ *and* $||\mathbf{T}^{-1}||$ *are bounded, the transformation matrix* $\mathbf{T}$ *preserves the exponential stability and the exponent (rate) of the convergence [77, 78]. The Lyapunov candidate* $\mathcal{V}(\bar{\mathbf{e}}_q(t)) = \frac{1}{2}\bar{\mathbf{e}}_q(t)^T\bar{\mathbf{e}}_q(t)$ *is then introduced to investigate the stability of the error dynamics* (3.9) *and* (3.15)[1]*. The time derivative of the Lyapunov function along the state*

[1] $\mathcal{V}(\bar{\mathbf{e}}_q(t))$ and $\mathcal{V}$ are used interchangeably.

trajectories leads to

$$\begin{aligned}
\dot{\mathcal{V}} &= \frac{1}{2}\dot{\bar{\mathbf{e}}}_q(t)^T\bar{\mathbf{e}}_q(t) + \frac{1}{2}\bar{\mathbf{e}}_q^T(t)\dot{\bar{\mathbf{e}}}_q(t),\\
&= \bar{\mathbf{e}}_q^T(t)\underbrace{\left(\frac{1}{2}\left(\bar{\mathbf{A}}_{e_q}^T + \bar{\mathbf{A}}_{e_q}\right)\right)}_{\bar{\mathbf{A}}_s}\bar{\mathbf{e}}_q(t)\\
&+ \frac{1}{2}\left(\boldsymbol{\varrho}_q^T\bar{\mathbf{B}}_{e_q}^T\bar{\mathbf{e}}_q(t) + \bar{\mathbf{e}}_q^T(t)\bar{\mathbf{B}}_{e_q}\boldsymbol{\varrho}_q\right)\\
&\leq \lambda_{\max}(\bar{\mathbf{A}}_s)||\bar{\mathbf{e}}_q(t)||^2 + \frac{1}{2}\left(\frac{1}{2\epsilon}\boldsymbol{\varrho}_q^T\bar{\mathbf{B}}_{e_q}^T\bar{\mathbf{B}}_{e_q}\boldsymbol{\varrho}_q + \frac{\epsilon}{2}||\bar{\mathbf{e}}_q(t)||^2\right)\\
&\leq \left(\lambda_{\max}(\bar{\mathbf{A}}_s) + \frac{\epsilon}{4}\right)||\bar{\mathbf{e}}_q(t)||^2 + \lambda_{\max}(\bar{\mathbf{B}}_{e_q}^T\bar{\mathbf{B}}_{e_q})||\boldsymbol{\varrho}_q||^2\\
&= 2\left(\lambda_{\max}(\bar{\mathbf{A}}_s) + \frac{\epsilon}{4}\right)\mathcal{V} + \lambda_{\max}(\bar{\mathbf{B}}_{e_q}^T\bar{\mathbf{B}}_{e_q})||\boldsymbol{\varrho}_q||^2\\
&\leq \eta_1\mathcal{V} + \eta_2,
\end{aligned} \tag{4.1}$$

for some $\eta_1 < 0$ *and* $\eta_2 > 0$. *Here* ϵ *is chosen such that* $0 < \epsilon \ll |\lambda_{\max}(\bar{\mathbf{A}}_s)|$ *to have* $\lambda_{\max}(\bar{\mathbf{A}}_s)+\frac{\epsilon}{4} < 0$*; thus,* $\eta_1 < 0$. *The fourth line is due to Young's inequality and the fifth line is due to the fact that* $\bar{\mathbf{B}}_{e_q}^T\bar{\mathbf{B}}_{e_q}$ *is a symmetric matrix. Introducing* $\mathcal{U}(\bar{\mathbf{e}}_q(t)) = \mathcal{V}(\bar{\mathbf{e}}_q(t)) + \frac{\eta_2}{\eta_1}$*, based on* (4.1) *and the Bellman-Gronwall lemma [59], we have* $\mathcal{U}(\bar{\mathbf{e}}_q(t)) \leq e^{\eta_1 t}\mathcal{U}(\bar{\mathbf{e}}_q(0))$*, which yields:*

$$0 \leq \mathcal{V}(\bar{\mathbf{e}}_q(t)) \leq e^{\eta_1 t}\left(\mathcal{V}(\bar{\mathbf{e}}_q(0)) + \frac{\eta_2}{\eta_1}\right) - \frac{\eta_2}{\eta_1}, \tag{4.2}$$

which results in;

$$0 \leq ||\bar{\mathbf{e}}_q(t)||^2 \leq e^{\eta_1 t}\left(||\bar{\mathbf{e}}_q(0)||^2 + \frac{2\eta_2}{\eta_1}\right) - \frac{2\eta_2}{\eta_1}. \tag{4.3}$$

$\frac{\eta_2}{\eta_1} < 0$ *proves the exponential stability of the nominal part of the error dynamics* (3.9) *and* (3.15) *(without term* $\boldsymbol{\varrho}_q$*) and the boundedness of the estimation error* $\mathbf{e}_q(t)$.

As mentioned in Proposition 1, the transformation matrix $\mathbf{T}$ yields a less conservative stability condition for the symmetric part of $\bar{\mathbf{A}}_{e_q}$ compared to the symmetric part of $\mathbf{A}_{e_q}$. The following example confirms this claim.

Example 1 *Consider error dynamics (3.9) with the observer gains* $\mathbf{L}_x = [1.18, \quad 387]^T$. *For a particular angular velocity, e.g.* $\omega = 40$, *the largest eigenvalue of matrix* $\mathbf{A}_{e_x}$ *and its symmetric parts are* $\lambda_{\max}(\mathbf{A}_{ex}) = -327.1$ *and* $\lambda_{\max}(0.5(\mathbf{A}_{ex} + \mathbf{A}_{ex}^T)) = 108750$, *respectively. Thus, the symmetric part is unstable while matrix* $\mathbf{A}_{e_x}$ *is Hurwitz. However if we use the similarity transformation mentioned in Proposition 1 with* $\mathbf{T} = diag(9000, 1)$, *the largest eigenvalue of the symmetric part of* $\bar{\mathbf{A}}_{e_x}$ *is* $\lambda_{\max}(\bar{\mathbf{A}}_s) = -326.8$, *which is very close to* $\lambda_{max}(\bar{\mathbf{A}}_{e_x})$. *This shows how much the stability of the symmetric part of a matrix can be conservative and how much an appropriate choice of a similarity transformation can help in overcoming this conservativeness.*

Proposition 1 shows the boundedness of the estimation errors. The tightness of this bound is directly related to the magnitude of $\frac{\eta_2}{\eta_1}$ as it can be concluded from (4.3). Moreover, the magnitude of this function, and in particular, η_2, depends on the magnitude of the uncertainty $\boldsymbol{\varrho}_q$. This parameter is a function of the (unknown) road friction. If the value of the road friction is known, the term $\frac{-\sigma_{0q}|V_{rq}|}{\theta g(V_{rq})} z_q$ which is a stabilizing term in the LuGre model (and hence in the observer) would make the observer stability condition less conservative.

In order to come up with some bounds on the performance of the proposed observer from the input-output approach, system $\mathcal{H}_\infty$ norm of error dynamics (3.9) and (3.15) defined as $\mathcal{H}_\infty \triangleq \sup_{\omega \in \mathbb{R}} ||\mathbf{G}(j\omega)||_\infty$, where $\mathbf{G}(.)$ is the transfer function from uncertainty $\boldsymbol{\varrho}_q$ to error $\mathbf{e}_q$, and they are shown in Figure 4.1. It should be noted that the $\mathcal{H}_\infty$ norm is a conservative system norm and Fig. 4.1 reveals that even conservative $\mathcal{H}_\infty$ norms of error dynamics[2] are non-expansive ($||G||_\infty \leq 1$) for the suggested observers.

In the following, we extend the above $\mathcal{H}_\infty$ analysis for the case of the time-varying case, which is to find a set of (time-varying) gains to minimize the $\mathcal{L}_2$ gain from the disturbances to the estimation error.

[2] We should note that the $\mathcal{H}_\infty$ norm is attainable for the proposed estimator in certain cases.

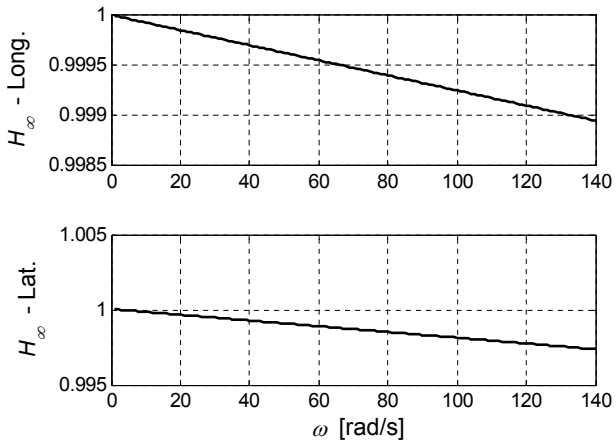

Figure 4.1: System $\mathcal{H}_\infty$ norm for longitudinal and lateral estimators.

Optimal Observer Gains

The objective is to find a range for the observer gains for different values of the angular velocity ω such that the ratio of the estimation error to the disturbance energy is minimized considering the fact that the process disturbance ϱ_{zx} and the measurement disturbance ϱ_{ax} are bounded. Given a compact set $\omega \in [\omega_l, \omega_u]$ for some $\omega_l, \omega_u > 0$ and a bounded rate of variation of $|\dot{\omega}| < \Omega_\omega$, for some $\Omega_\omega > 0$ the error dynamics (3.9) is robustly and exponentially stable if there exists a continuously differentiable positive definite matrix $\mathcal{P}(\omega)$ and a matrix $\phi(\omega)$ such that the following LMI holds [71]:

$$\begin{bmatrix} \Lambda(\omega) & \mathcal{P}(\omega) + \phi(\omega)B_{e1} & I \\ * & -\gamma I & 0 \\ * & * & -\gamma I \end{bmatrix} \prec 0, \tag{4.4}$$

where the symmetric terms are denoted by $*$ and Λ is:

$$\begin{aligned} \Lambda(\omega) = {} & [A_x^T(\omega) - C_x^T(\omega)\mathbf{L}_x^T]\mathcal{P}(\omega) \\ & + \mathcal{P}(\omega)[A_x(\omega) - \mathbf{L}_x C_x(\omega)] + \frac{\partial \mathcal{P}(\omega)}{\partial \omega}\dot{\omega}. \end{aligned} \tag{4.5}$$

In order to isolate the observer gain effect, B_{e_x} can be written as $B_{e_x} = I_{2\times 2} + \mathbf{L}_x B_{e1}$, in which $B_{e1} = [-\sigma_{1x} \quad 0]$. The induced $\mathcal{L}_2$ gain from the input disturbance to the output error

is less than the performance level $\gamma > 0$. The LMI (4.4) is obtained by taking derivative of the Lyapunov function $V(e_x, \omega) = e_x^T \mathcal{P}(\omega) e_x$, imposing the condition $\Lambda(\omega) < 0$, and using the Bounded Real Lemma. Employing $\phi(\omega) = \mathcal{P}(\omega)\mathbf{L}_x$, one can rewrite:

$$\Lambda(\omega) = A_x^T \mathcal{P} + \mathcal{P} A_x - \phi C_x - C_x^T \phi^T + \frac{\partial \mathcal{P}}{\partial \omega}\dot{\omega} \tag{4.6}$$

The LMI (4.4) guarantees that $\dot{V} + \mathbf{e}_x^T \mathbf{e}_x - \gamma^2 \boldsymbol{\varrho}_x^T \boldsymbol{\varrho}_x < 0$. The set of gains will be calculated by $\mathbf{L}_x = \mathcal{P}(\omega)^{-1}\phi(\omega)$. The infinite dimensional parameter-varying LMI (4.4) with $\Lambda(\omega)$ from (4.6) can explicitly be expressed in a finite dimensional problem with the parametric matrices and using appropriate basis functions. The positive definite matrix $\mathcal{P}$ and matrix Λ are defined as $\mathcal{P}(\omega) := \sum_{i=0}^{f} \mathcal{P}_i \omega^i$ and $\Lambda(\omega) := \sum_{i=0}^{f} \Lambda_i \omega^i$, respectively, and the set $\omega = [0 \quad 140]$ is gridded to $\mathcal{N}_{gr} = 140$ points. The time-varying observer gains L_1, L_2 are depicted in Fig. 4.2 for the longitudinal observer and the vehicle parameters provided in Table 3.1.

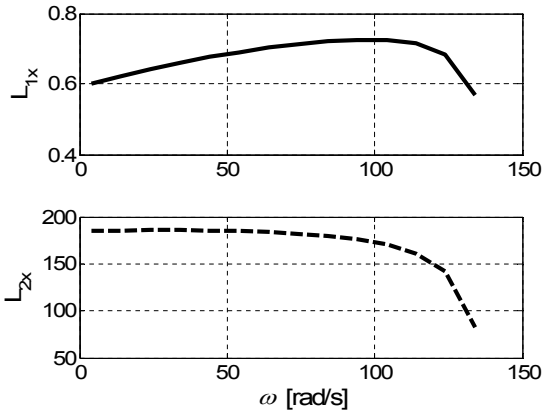

Figure 4.2: Time-varying observer gains for the longitudinal estimator.

A similar procedure can be done for the lateral error dynamics (3.15) and parameter-varying observer gains that are obtained using LMI (4.4) for the lateral direction are illustrated in Fig. 4.3.

It should be noted that in real-time implementation of the proposed velocity estimators, the observer gains do not change over time and some values inside the set of optimal values shown in Fig. 4.2 are chosen. Instead, the observer gains are sometimes switched

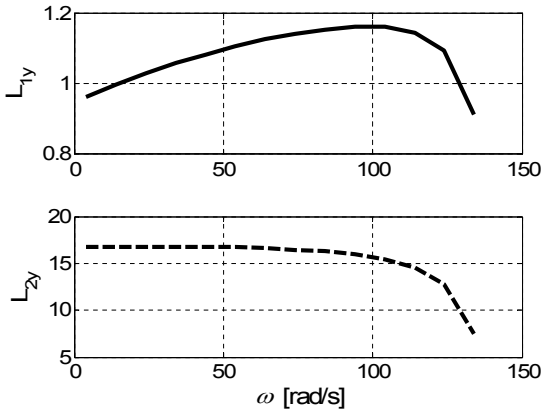

Figure 4.3: Time-varying observer gains for the lateral estimator.

between different values in order to change the reliance of the observer to the tire force measurements. The performance of the velocity estimator in the presence of switching observer gains will be discussed in next section.

4.1.2 Sensitivity of the Stability Margin and $\mathcal{H}_\infty$ Performance to Tire Parameters

Lastly, the sensitivity of the error dynamics stability margin $\mathcal{SM}_q \triangleq \max_i \lambda_i(\bar{\mathbf{A}}_{e_q})$ and system $\mathcal{H}_\infty$ norms to model parameter uncertainties is investigated. Figs. 4.4 and 4.5 show the deviation of the stability margin of the error dynamics (3.9) and (3.15) from their nominal values due to model parameter deviation of up to 20%.[3] Fig. 4.6 shows the sensitivity of the system $\mathcal{H}_\infty$ norm of the error dynamics to the same parameter variations. This figure shows that the performance of the observer is not very sensitive to the tire parameter variations.

[3]Each model parameter $\mathcal{X}$ is perturbed as $\mathcal{X} \pm 0.2\mathcal{X}$.

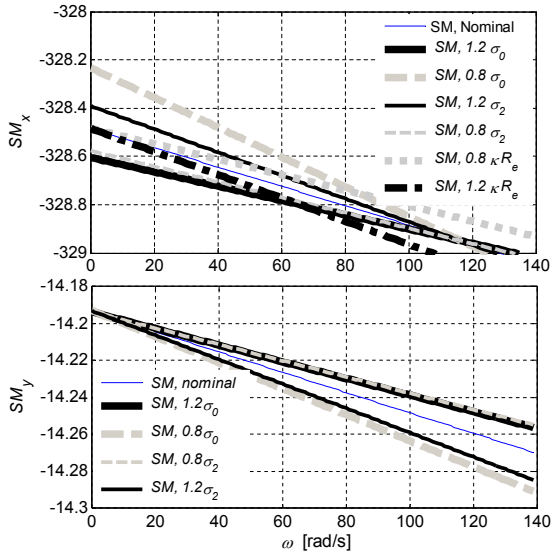

Figure 4.4: Sensitivity of $\mathcal{SM}$ of (3.9) and (3.15).

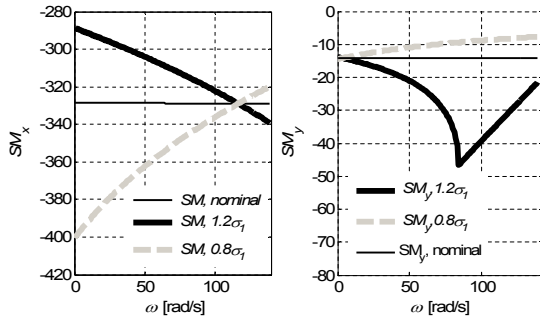

Figure 4.5: Sensitivity of $\mathcal{SM}$ of (3.9) and (3.15) to σ_{1q}.

4.2 Stability of the Estimator Under Gain Switching

To address the high-slip condition, observer gains are switched to change the level of reliance on the output measurements (longitudinal/lateral forces and their uncertainties) and process (road friction uncertainties and acceleration noises). The following figure, which is the simplified version of Fig. 1.1 schematically shows this fact. Hence, analyzing the stability of the resulting velocity observer in the presence of gain switchings is important. The stability of the switched systems have been analyzed extensively under arbitrary [79, 80]

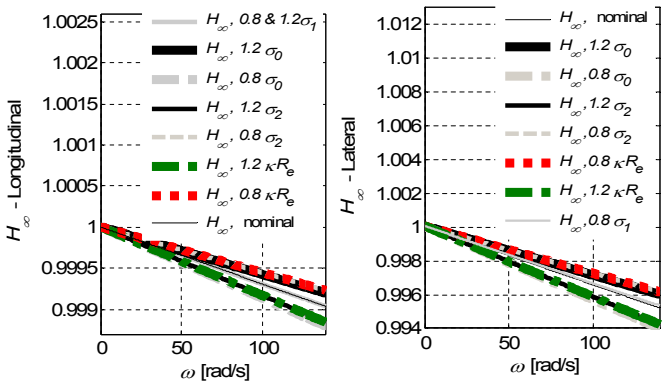

Figure 4.6: Sensitivity of $\mathcal{H}_\infty$ norm of (3.9) and (3.15).

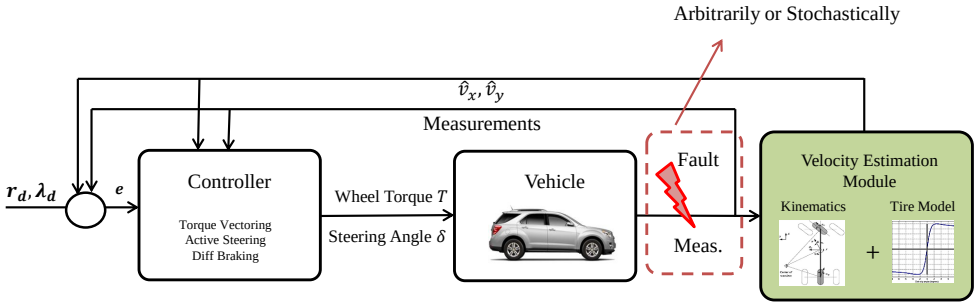

Figure 4.7: Tire forces (which are fed into the estimators) can be faulty.

and stochastic switching [63]. Switched observers are also used in vehicle state or parameter estimation [81]. In this section, the stability of the nominal parts of error dynamics, in the form of (4.7), is analyzed when the observer gains switch between different modes. In this case, the longitudinal and lateral observer gains can attain each of the two modes to result in:

$$\dot{\mathbf{e}}_q = \mathbf{A}^i_{e_q}(\omega)\mathbf{e}_q, \tag{4.7}$$

where $\mathbf{A}^i_{e_q}$ belongs to the i-th set of observer gains $\mathbf{L}^i_q$, and $i = 1, 2$ represents switching modes. Since the stability of (4.7) is a necessary condition for the stability of (3.9) and (3.15), it is analyzed in the presence of arbitrary gain switching.

4.2.1 Stability of the observer under arbitrarily switching gains

A sufficient condition for the quadratic stability of a switched linear system under arbitrary switching is to have a common quadratic Lyapunov function for all switching modes [79]. Similar to the analysis done in Proposition 1, we introduce the transformed matrix $\bar{\mathbf{A}}^i_{e_q} = \mathbf{T}\mathbf{A}^i_{e_q}\mathbf{T}^{-1}$ with the same transformation matrix $\mathbf{T}$ used in Proposition 1. By choosing the Lyapunov function $\mathcal{V}(\bar{\mathbf{e}}_q) = \frac{1}{2}\bar{\mathbf{e}}_q^T\bar{\mathbf{e}}_q$, one can write:

$$\begin{aligned}\dot{\mathcal{V}} &= \frac{1}{2}\dot{\bar{\mathbf{e}}}_q(t)^T\bar{\mathbf{e}}_q(t) + \frac{1}{2}\bar{\mathbf{e}}_q^T(t)\dot{\bar{\mathbf{e}}}_q(t) \\ &= \bar{\mathbf{e}}_q^T(t)\underbrace{\left(\frac{1}{2}\left(\bar{\mathbf{A}}^{i^T}_{e_q} + \bar{\mathbf{A}}^i_{e_q}\right)\right)}_{\bar{\mathbf{A}}^i_s}\bar{\mathbf{e}}_q(t) \leq \lambda_{\max}(\bar{\mathbf{A}}^i_s)||\bar{\mathbf{e}}_q||^2 \\ &= 2\lambda_{\max}(\bar{\mathbf{A}}^i_s)\mathcal{V} \leq \bar{\lambda}\mathcal{V}, \end{aligned} \tag{4.8}$$

where $\bar{\lambda} = \max_{i=1,2}\{\max_{t\geq 0}\{2\lambda_{max}(\bar{\mathbf{A}}^i_s)\}\}$. This shows that the decaying rate of the switched system is based on the worst case decaying rate over time and over switching modes. This is due to the lack of knowledge about the switching policy. In the following subsection, the stability of the suggested observers under stochastic gain switching is analyzed, and the results will be compared to the case of arbitrary switching.

4.2.2 Stability of the observer under stochastically switching gains

In this subsection, switching between the observer gains is assumed to happen in the form of a particular stochastic process represented by a Markov chain. The stability of the Markov jump linear systems has been analyzed in depth [63], [69], [64]. Similar to the arbitrary switching case mentioned in the previous section, stochastic switching will introduce dynamics that is comprised of two sub-dynamics[4]. The switching mechanism is

[4]Since the switching forms a Markov jump linear system and theoretical results (e.g. Theorem 1) for such systems are derived for discrete time case, the discrete version of the estimator with the sampling time $T = 5$ms is used in the experiment setup.

modeled using a Markov chain with the probability transition matrix:

$$\mathbf{P} = \begin{bmatrix} p_{11} & p_{12} \\ p_{21} & p_{22} \end{bmatrix}, \tag{4.9}$$

where $p_{ij} = \mathbf{Pr}(\mathcal{L}[k+1] = \mathbf{L}_q^j | \mathcal{L}[k] = \mathbf{L}_q^i)$. Here, $\mathcal{L}$ is a random vector that takes its values from the sample space $\mathcal{S} = \{\mathbf{L}_q^1, \mathbf{L}_q^2\}$, which are the two sets of observer gains. The following definition is required to investigate the stability of such a switched system.

Definition 1 *[68] The linear system* $\mathbf{e}_q[k+1] = \mathbf{A}_{e_q}^{d_i}\mathbf{e}_q[k]$ *(matrix* $\mathbf{A}_{e_q}^{d_i}$ *is the discrete version of* $\mathbf{A}_{e_q}^{i}$ *in the error dynamics (4.7), as discussed in Remark 2) is called mean square stable (MSS) if* $\lim_{k\to\infty} \mathbb{E}(\mathbf{e}_q[k]^T\mathbf{e}_q[k]) = 0$.

Based on Definition 1, the following theorem is used for the mean square stability of the error dynamics.

Theorem 1 *[82] The linear system* $\mathbf{e}_q[k+1] = \mathbf{A}_{e_q}^{d_i}\mathbf{e}_q[k]$ *is MSS if and only if the following condition holds.*

$$\rho\left[(\mathbf{P}^T \otimes \mathbf{I})diag(\mathbf{A}_{e_q}^{d_i} \otimes \mathbf{A}_{e_q}^{d_i})\right] < 1, \tag{4.10}$$

where $\otimes$ *is the matrix Kronecker product,* $\mathbf{P}$ *is the probability transition matrix between different modes and* $\rho[.]$ *is the spectral radius of a matrix.*

The spectral radius result provides a necessary and sufficient condition for stability under Markovian jumps as well as a measure for the robustness of such stability. In this direction, the stability margin of the linear Markov jump system is given by $1-\rho$. In the following example, the stability margin of the observer when the observer gains are switching with a pre-specified Markovian jump policy is discussed, and it is shown how that stochastic switching policy between the observer gains provides tighter results when compared to the arbitrary switching.

Example 2 *Given two high-slip and low-slip cases with the slip ratio* $\lambda = \frac{R_e|\omega| - V_{xt}}{\max\{R_e|\omega|, V_{xt}\}}$ *and subsequent switching actions, a probability transition matrix represents switching policies*

between two slip conditions. The observer gains attain either mode $\mathbf{L}_x^1 = [1.18, 387]$ *or* $\mathbf{L}_x^2 = [0.22, 0.1]$*, corresponding to two sets of slip ratios* $0 \leq |\lambda| < 0.15$*,* $0.15 \leq |\lambda|$*, respectively. The probability transition matrix is in the following form:*

$$\mathbf{P}_{dry} = \begin{bmatrix} 0.9 & 0.1 \\ 1-\bar{\gamma} & \bar{\gamma} \end{bmatrix}, \tag{4.11}$$

where $\bar{\gamma}$ *is the probability that the observer stays within the high slip mode at time step* $k+1$ *when it is at high slip mode at time step* k*. The stability margin of the switched system with stochastic gain switching for different values of the angular velocity is shown in Fig. 4.8. In this case, the spectral radius obtained from the arbitrary switching, which*

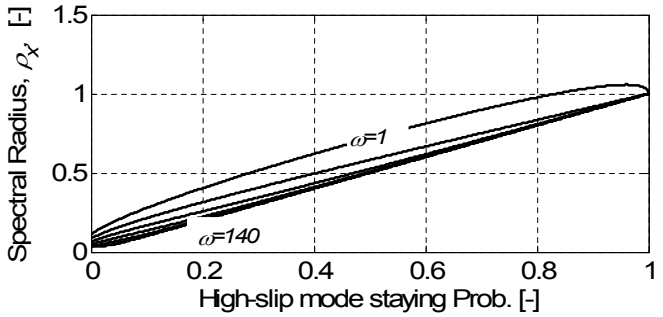

Figure 4.8: Spectral radius ρ with respect to $\bar{\gamma}$.

is based on the worst case gain, is 0.9960*, (close to 1). It can be compared to the values plotted for stochastic switching. This substantiates that having knowledge on the policy of the switching can help us improve the stability margin (robustness) for the switched linear system.*

4.3 Reliable Velocity Estimator in the Presence of Faulty Measurements

Switching in observer gains is performed in order to change the level of the reliance of the observer to the force measurements. In this section, a robustness measure for velocity

observers to the force measurement (estimation) failure, which acts in a cascading scheme, is proposed. Taking advantage of the newly proposed stochastic approach in the previous section, a metric (namely p_{cr}) is introduced that represents the robustness of the velocity observer to the unreliable force estimation.

Suppose that the measurement signal is faulty and does not reach the observer correctly with some probability p, so it can not be utilized (it is dropped) by the longitudinal/lateral observers. It is equivalent to the condition where the observer gain is $\mathbf{L}_q = \mathbf{0}$ with probability p and nonzero (active observer gain $\mathbf{L}_q$) with probability $1-p$. More formally:

$$\mathbf{e}_q[k+1] = \begin{cases} \mathbf{A}_q^d \mathbf{e}_q[k] & \text{with probability} \quad p \\ \mathbf{A}_{e_q}^d \mathbf{e}_q[k] & \text{with probability} \quad 1-p \end{cases}. \tag{4.12}$$

Recasting this problem into a Markovian jump analysis, one can express the probability transition matrix as:

$$\mathbf{P} = \begin{bmatrix} 1-p & p \\ 1-p & p \end{bmatrix}, \tag{4.13}$$

with $p_{ij} = \mathbf{Pr}(\mathcal{L}[k+1] = \mathbf{L}_q^j | \mathcal{L}[k] = \mathbf{L}_q^i)$ in which $\mathcal{L}$ is a random vector that takes values from the sample space $\mathcal{S} = \{\mathbf{L}_q, \mathbf{0}\}$. Applying Theorem 1, one can specify how tolerant the velocity observers are against faulty force measurements. This leads to the calculation of p_{cr} (namely critical probability), which is defined as the maximum allowable probability of faulty measurements occurring such that the velocity observer remains MSS.

Remark 5 *In the case of measurement drop with $p < p_{cr}$, the system is no longer observable. However, since the unobservable modes are MSS, the system is stochastically detectable [83]. Figure 4.9 illustrates the value of the critical probability p_{cr} for different values of the wheel speed for the longitudinal and lateral velocity estimators. For probabilities larger than the p_{cr}, the system is not MSS.*

Figure 4.10 depicts the value of the spectral radius ρ for the longitudinal and lateral velocity estimators and different wheel speeds. This information can provide a sense of the stability margin of such systems [63].

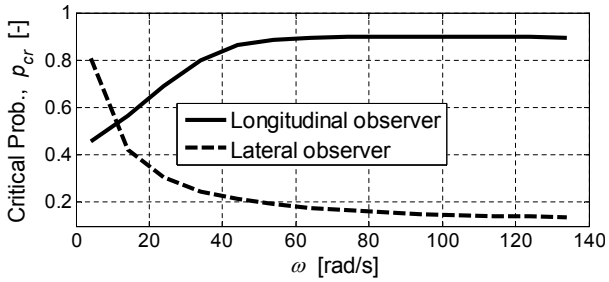

Figure 4.9: Critical probabilities for the velocity observers.

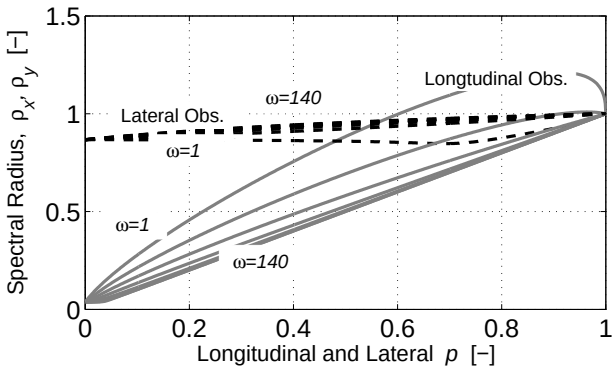

Figure 4.10: Spectral radius vs. failure probability for various ω.

In the following example, the stability and robustness of the system is studied in a case where the measurement signal drops with a certain probability. The values used in Example 3 are chosen to compare the conservativeness of the stability margin of the stochastic and arbitrary switching scenarios, and the value of p is not obtained from road experiment.

Example 3 *Given the case where the measurement signal is dropped with* $p = 0.2$ *and reaches the estimator with probability* $1 - p = 0.8$ *(i.e.* $\mathbf{L}_x = \mathbf{0}$ *with* $p = 0.2$ *and* $\mathbf{L}_x = [1.18 \quad 387]^T$ *with* $1 - p = 0.8$*), the MSS is investigated. Applying Theorem 1 in this case leads to a mean square stable system with the spectral radius* $\rho = 0.9026$*. Alternatively, if the measurement signal loss happens arbitrarily, based on the arbitrary switching discussed in section 4.2, the system becomes marginally stable, i.e.* $\rho = 1$*.*

Therefore, investigating the faulty measurement cases with the Markovian jump model

provides a less conservative criterion for the mean square stability of the estimators.

4.4 Summary

The performance and robustness of the corner-based vehicle velocity estimator, presented in Chapter 3, were analyzed in this chapter using system theoretic tools. More specifically, stability of the observer error dynamics, as a linear-time-varying system, was proven based on Lyapunov analysis, and a bound on the estimation error, as a function of road condition and measurements uncertainties, was derived. Other than this analytical bound, some numerical upper bounds on the estimation error dynamics were presented, which were based on an input-output approach to the observer error dynamics and their $\mathcal{H}_\infty$ performance, and it was shown that the observer error dynamics is a non-expansive system (i.e., it does not propagate the disturbances to the estimation error). As a real-time observer gain switching is inevitable in experiments, to change the reliance of the estimator to measurements in different instances, the stability of the velocity estimator in the presence of estimation gain switchings was also studied for two cases of arbitrary and stochastic gain switching scenarios. At the end, the sensitivity of the performance of the designed velocity estimator to tire parameter variations was investigated. These analyses were referred to as an *offline reliability assessment of the velocity observer* in this thesis.

Chapter 5

On-line Reliability Measures

In the previous chapter, several criteria for assessing the performance of the vehicle corner-based velocity estimation were investigated and introduced. Those methods were referred to as off-line reliability measures (or metrics). It is due to the fact that those are some measures which indicate fundamental performance limitations that the designed observer faces and determines the boundaries that we can expect this observer to meet terms of performance and robustness to uncertainties. In this chapter, the on-line reliability analysis of the velocity observer is discussed. As it can be inferred from its name, unlike the offline case, this method can be implemented in real-time to assess the performance of the designed observer.

The on-line reliability here refers to a level of confidence that one can assign to the estimated velocities in the existence of potential uncertainties, such as uncertainties in road condition, wheel speed, tire parameters as well as imprecision in estimated tire forces. The overall reliability module and its interactions with the vehicle measurements and the estimation module is shown in Fig. 5.1. According to this figure, since the reliability module should ultimately work concurrently with the estimation module, it can only use available measurements that the estimation module uses. Considering this limitation, proposing reliability algorithms that provide independent results from the estimation and act as a supervisory level is a challenging task. In the on-line approach discussed in this chapter, vehicle kinematics together with some technical considerations are used to provide

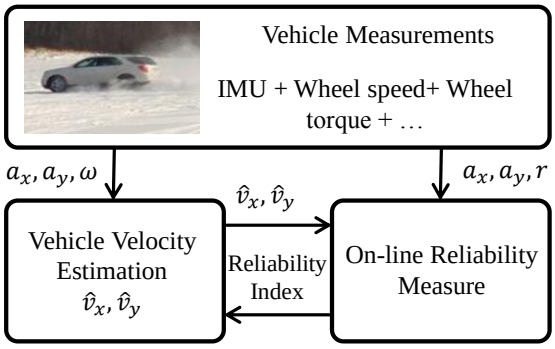

Figure 5.1: On-line reliability measure unit.

a reliability index showing the level of confidence to the estimated state, in a quantitative manner.

5.1 Procedure

The essence of the real time approach is to translate the estimated velocities (in both longitudinal and lateral directions) into a quantity that can be directly measured. Then, via vehicle kinematic relations, one can assess the correctness of the estimated quantities in a quantitative manner. More formally, the procedure is as follows. We use the following kinematic relations between longitudinal and lateral accelerations and longitudinal and lateral velocities at CG

$$a_x = \dot{v}_x - r v_y, \quad a_y = \dot{v}_y + r v_x, \tag{5.1}$$

where a_x, a_y, and r are longitudinal and lateral accelerations and yaw rate, respectively, which are measured directly from IMU. If the estimated longitudinal and lateral velocities ($\hat{v}_x$ and $\hat{v}_y$) are correct, they should satisfy (5.1). In particular, by introducing variables $\hat{a}_x = \dot{\hat{v}}_x + r\hat{v}_y$ and $\hat{a}_y = \dot{\hat{v}}_y - r\hat{v}_x$, we define the error between the estimated and measured quantities as

$$e_x = |a_x - \hat{a}_x|, \quad e_y = |a_y - \hat{a}_y|, \tag{5.2}$$

and then, by using a specific norm, we reach

$$e = e_x + e_y, \tag{5.3}$$

After finding the error signal, they are normalized to the 1-norm of the longitudinal and lateral accelerations, as

$$e_n = \frac{e_x + e_y}{|a_x| + |a_y|} = \frac{||e||_1}{||a||_1}. \tag{5.4}$$

The quantity e_n provides a sense of the unreliability of the velocity estimation and we call $1 - e_n$ the reliability index. The next step is to cluster the normalized error signal $1 - e_n$ into multiple regions, to show the level of reliability of the estimated velocities. A schematic figure of the above analysis is shown in Fig. 5.2.

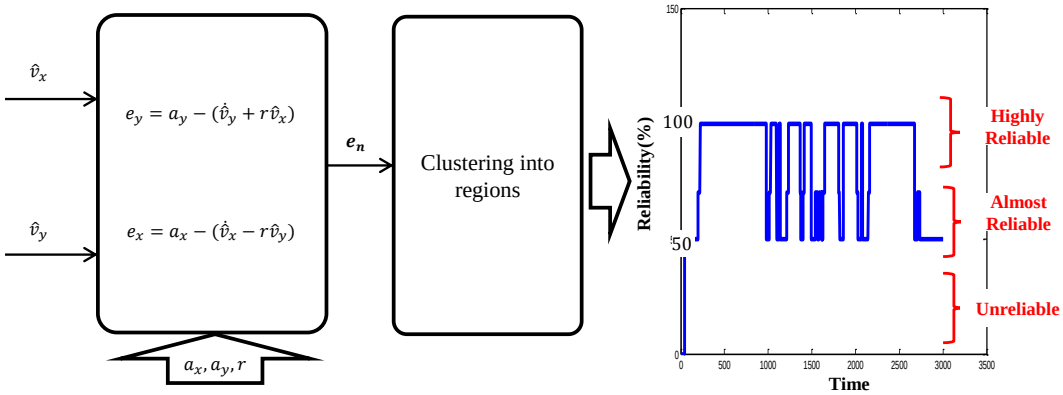

Figure 5.2: Overall scheme of the online reliability analysis.

Remark 6 ***(Technical Considerations)****: In this method, we should take care of non-smooth signals (both measurement signals and estimated states). To address this issue, we should use low pass filters to filter high frequency noises to make them appropriate for time derivation. Using such low pass filters induce some delay in the output (reliability measure) signal. However, since the delay of up to 100 ms for the reliability measure does not affect the overall result, we admit the usage of such filters.*

5.1.1 Distinguishing Measurement Faults from Estimation Faults

According to Fig. 5.2, the reliability index (measure) is a function of the longitudinal and lateral accelerations, a_x, a_y, yaw rate r and estimated longitudinal and lateral velocities,

$\hat{v}_x$ and $\hat{v}_y$, mapped onto CG. In this view, any uncertainty in either estimated velocities or IMU measurements will affect the output of the reliability index. Hence, it is important to distinguish measurement failures from estimation failures. To tackle this issue, two approaches are considered.

1. The simplest way is to use existing measurement fault diagnosis methods beside the estimation reliability module. In this approach, a fault diagnosis method such as what is studied in [84] is utilized to diagnose failures in measurements. If faults in measurement signals exist, a relay starts working and does not allow this measurement to be fed into the estimation reliability setup, as shown in Fig. 5.3.

Figure 5.3: Detecting measurement fault.

2. The other real time method to distinguish estimation fault (reliability measure) from measurement fault is to use a bank of reliability setups. In particular, one can take advantage of using all four wheels to distinguish the fault in the estimation and measurements. The main points of this method is that (i) the set of IMU measurements used for all four corners are the same, and (ii) the velocity estimation setups for four wheels operate independently. Hence, witnessing failures in the reliability index for (almost) all four estimations can be rooted back to the measurement failures. We will explain this logic more formally as follows. Let $\hat{v}_x^i$ and $\hat{v}_y^i$, where $i, j \in \{fL, fR, rL, rR\}$, be the estimated longitudinal and lateral velocities at a corner. With the same procedure as previously mentioned, we calculate the residual (error) variables as

$$\begin{aligned} e_x^i &= |a_x - \hat{a}_x^i| = |a_x - (\dot{\hat{v}}_x^i - r\hat{v}_y^i)|, \\ e_y^i &= |a_y - \hat{a}_y^i| = |a_y - (\dot{\hat{v}}_y^i + r\hat{v}_x^i)|, \end{aligned} \tag{5.5}$$

which ultimately yields $e^i = e_x^i + e_y^i$ as the residual indicator of corner i. Since each estimator in each of the four corners is run independent to the other three, the situation that all estimators fail to work simultaneously is highly improbable. On the other hand, if such an event happens, there are measurements a_x, a_y, or r which are likely to be faulty. Based on this logic, one can distinguish measurement fault from the estimation faults. The schematic structure of this approach is shown in Fig. 5.4.

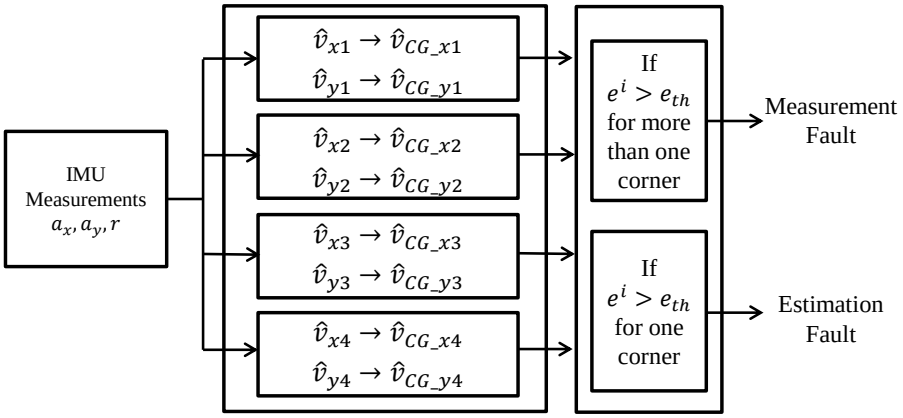

Figure 5.4: The method of bank of reliability indices.

In the end, it should be noted that the reliability index introduced in this section is designed in such a way that if both longitudinal and lateral velocities at each corner are reliable, it announces that the overal estimator is reliable. Otherwise, if one of the estimations, either longitudinal or lateral, fail to estimate properly, the reliability index will indicate that the estimator is unreliable. The following section pertains to some experimental results to show the performance of the introduced reliability measure.

5.2 Applying Reliability Indices to Modify the Estimated Velocities

In the previous section, a reliability measure for the estimated velocities at each corner was proposed. This measure can be used as an indicator to inform the control module how much it can rely on the estimated velocities. However, the estimation module itself can also take advantage of the reliability measure [85–87]. The procedure of applying such a reliability measure in enhancing the estimation is the subject of this section. Before that, some required definitions are introduced.

5.2.1 Some network definitions

An undirected graph (network) is denoted by $\mathcal{G} = \{\mathcal{V}, \mathcal{E}\}$, where $\mathcal{V} = \{v_1, v_2, \ldots, v_n\}$ is a set of nodes (or vertices) and $\mathcal{E} \subset \mathcal{V} \times \mathcal{V}$ is the set of edges. Neighbors of node $v_p \in \mathcal{V}$ are given by the set $\mathcal{N}_p = \{v_j \in \mathcal{V} \mid (v_p, v_j) \in \mathcal{E}\}$. The adjacency matrix of the graph is given by a symmetric and binary $n \times n$ matrix A, where element $A_{pj} = 1$ if $(v_p, v_j) \in \mathcal{E}$ and zero otherwise. The degree of node v_p is denoted by $d_p = \sum_{j=1}^{n} A_{pj}$. The Laplacian matrix of the graph is given by $L = D - A$, where $D = \text{diag}\{d_1, d_2, \ldots, d_n\}$.

5.2.2 Opinion Dynamics for Reliable Vehicle Estimation

The procedure of modifying the estimated corner velocities via applying the reliability measures is now introduced. The estimated velocity of each corner, denoted by $\hat{V}_i(t)$, where $i \in \{fL, fR, rL, rR\}$, is mapped into CG. The mapped value of each corner is called the opinion of that corner and is denoted by $\psi_i(t)$. In addition to this opinion, a confidence level is assigned to each corner, which is determined by the online reliability measure, mentioned in the previous section. A more reliable corner receives a larger confidence level regarding its estimated velocity. The confidence level of corner i to opinion ψ_i is denoted by $\kappa_i > 0$, as shown in Fig. 5.5. In an ideal case, all mapped velocities to CG should reach a unique value, which is the velocity of the vehicle in CG. However, this does not happen in reality

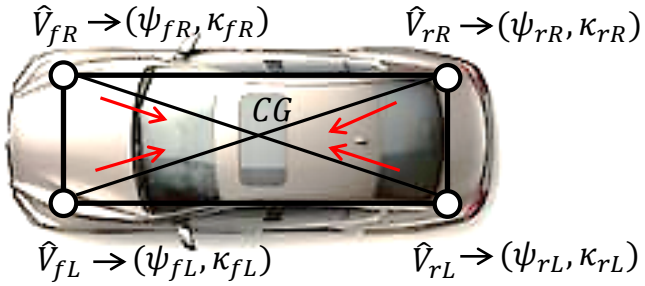

Figure 5.5: Corner opinions and their confidence level.

and there are four different values (opinions) in CG. The reason of mapping all velocities into CG is to introduce an opinion dynamics that converges to a unique equilibrium point closer to the estimated corner velocity with the highest confidence level. More formally, the proposed dynamics for each opinion is in the following form [88, 89]

$$\dot{\psi}_k(t) = \sum_{j \in \mathcal{N}_k} (\psi_k(t) - \psi_j(t)) - \kappa_j(\psi_k(t) - \psi_k(0)). \tag{5.6}$$

Aggregating the states of all opinions into a vector $\boldsymbol{\psi}(t) \in \mathbb{R}^4$, equation (5.6) yields the following opinion dynamics for longitudinal or lateral directions

$$\begin{aligned} \dot{\boldsymbol{\psi}}(t) &= -\bar{L}\boldsymbol{\psi}(t) + \boldsymbol{\mathcal{K}}\boldsymbol{\psi}(0), \\ \mathbf{y}(t) &= \boldsymbol{\psi}(t), \end{aligned} \tag{5.7}$$

in which $\mathbf{y}(t)$ is the output of interest, $\bar{L} = L + \boldsymbol{\mathcal{K}}$ where L is the Laplacian matrix [1], and confidence matrix $\boldsymbol{\mathcal{K}} = \text{diag}\{\kappa_{\text{fL}}, \kappa_{\text{fR}}, \kappa_{\text{rL}}, \kappa_{\text{rR}}\}$ indicates the level of confidence of the corners. Since each corner can communicate with other three ones, the communication graph for each direction i is a complete graph and we have

$$\bar{L} = \begin{bmatrix} 3 + \kappa_{\text{fL}} & -1 & -1 & -1 \\ -1 & 3 + \kappa_{\text{fR}} & -1 & -1 \\ -1 & -1 & 3 + \kappa_{\text{rL}} & -1 \\ -1 & -1 & -1 & 3 + \kappa_{\text{rR}} \end{bmatrix}. \tag{5.8}$$

[1] Since $\boldsymbol{\mathcal{K}}$ is a positive definite matrix, we can easily verify that $\bar{L}$ is also a positive definite matrix.

The following proposition discusses the location of the equilibrium point of the opinion dynamics.

Proposition 2 *The states in opinion dynamics* (5.7) *asymptotically converge to a convex combination of the initial opinions.*

Proof 2 *The stability of the opinion dynamics is based on the fact that matrix* $\bar{L}$ *is a Hurwitz matrix. The steady-state opinion for the longitudinal and lateral direction is*

$$\bar{\boldsymbol{\psi}} = \bar{L}^{-1}\boldsymbol{\mathcal{K}}\boldsymbol{\psi}(0). \tag{5.9}$$

We know that $L\mathbf{1} = \mathbf{0}$*, which results in* $(\bar{L} - \boldsymbol{\mathcal{K}})\mathbf{1} = \mathbf{0}$ *and it yields* $\bar{L}\mathbf{1} = \boldsymbol{\mathcal{K}}\mathbf{1}$*. Left multiplying both sides by* $\bar{L}^{-1}$*, we get* $\bar{L}^{-1}\boldsymbol{\mathcal{K}}\mathbf{1} = \mathbf{1}$*. This shows that* $\bar{L}^{-1}\boldsymbol{\mathcal{K}}$ *is a row stochastic matrix and* (5.9) *converges to some convex combinations of the elements of* $\psi(0)$*.*

As the corner with a higher confidence level has a larger feedback gain κ_i in (5.6), it pulls the steady-state opinion $\bar{\boldsymbol{\psi}}$ toward itself more than the other corners. The steady-state opinion $\bar{\boldsymbol{\psi}}$ then is remapped into each corner as a more reliable corner velocity. The overall procedure is schematically shown in Fig. 5.6.

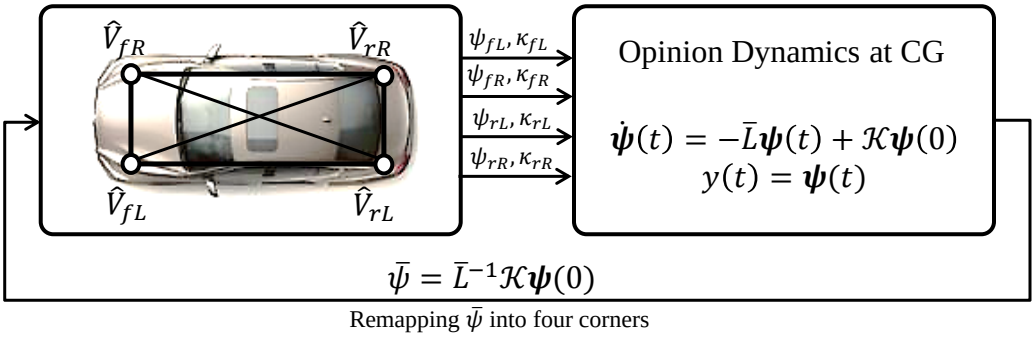

Figure 5.6: Enhancing the reliability of estimated corner velocities via opinion dynamics.

5.3 Experimental Results

In this section, some experimental results about the on-line reliability measure for the vehicle velocity estimation for different maneuvers and on various road conditions are demonstrated. In some of the tests, some additional fault is injected intentionally to the estimated values at some particular time instances (or periods) to show the performance of the on-line reliability measure. Vehicle motion characteristics are discussed and plotted for each maneuver. In the following subsection, a simple longitudinal acceleration and deceleration maneuver on a dry road is presented and will be followed by more complicated maneuvers on different road conditions, discussed subsequently. It should be noted that an experimental result showing the performance of the opinion dynamics method in enhancing the reliability of the corner velocities was demonstrated in the previous chapter. More specifically, the split μ longitudinal maneuver whose estimated velocities are shown in Fig. 3.8, uses the opinion dynamics algorithm inside its estimation module to enhance the reliability of its estimated velocity.

5.3.1 Acceleration-Deceleration on Dry Road

Here, the reliability measure (index) of the velocity estimation in a traction and brake maneuver for a four wheel drive equinox on a dry road is demonstrated. The values of longitudinal and lateral accelerations together with the steering angle are plotted in Fig. 5.7. The magnitudes of lateral acceleration a_y and steering angle δ show that the vehicle is fairly following a straight line. Moreover, the estimated longitudinal and lateral velocities as dashed lines along with the GPS measurement of these velocities as solid black lines are demonstrated. The reliability index is also depicted in Fig. 5.8.

As it is inferred from Figs. 5.7 and 5.8, the reliability index has an appropriate correspondence to the accuracy of estimated velocities (compared to those of GPS measurements). More specifically, in the time interval between $t = 6s$ to $t = 8s$, as both estimated longitudinal and lateral velocities deviate from the measured velocities, the reliability index in that time interval drops down. However, as the maneuver is a simple acceleration-brake maneuver, the performance of the reliability index is not apparent. Hence, in the following

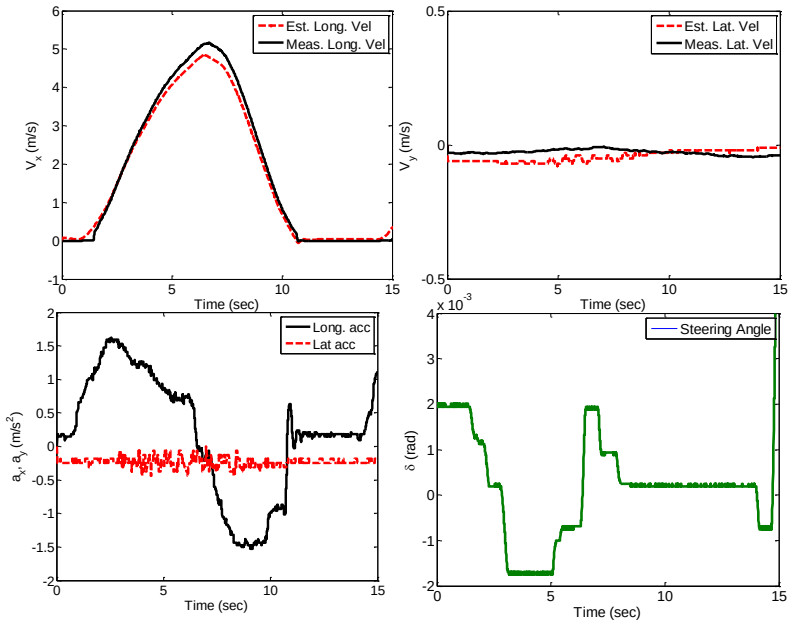

Figure 5.7: Vehicle motion characteristics for an acceleration-deceleration maneuver.

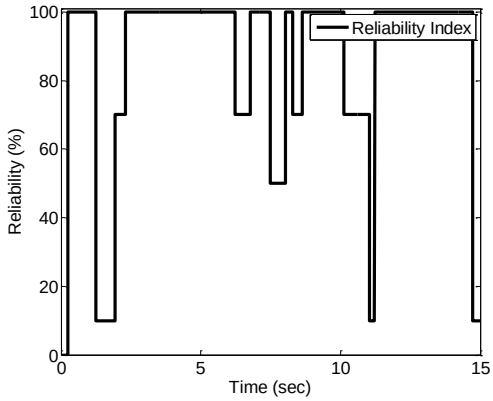

Figure 5.8: The reliability index of an acceleration-deceleration maneuver.

tests, more complicated vehicle maneuvers are discussed.

5.3.2 Steering on Dry Road

The second test belongs to a maneuver comprised of several steerings, along with both longitudinal and lateral accelerations performed by a four wheel drive equinox on a dry road, whose motion characteristics are shown in Fig. 5.9. The magnitude of the lateral acceleration a_y as well as the steering angle show that there were harsh steerings for more than 5 seconds. Moreover, the peak magnitude of lateral acceleration, which is about $8\frac{m}{s^2}$ confirms that the maneuver is on a dry road condition.[2]

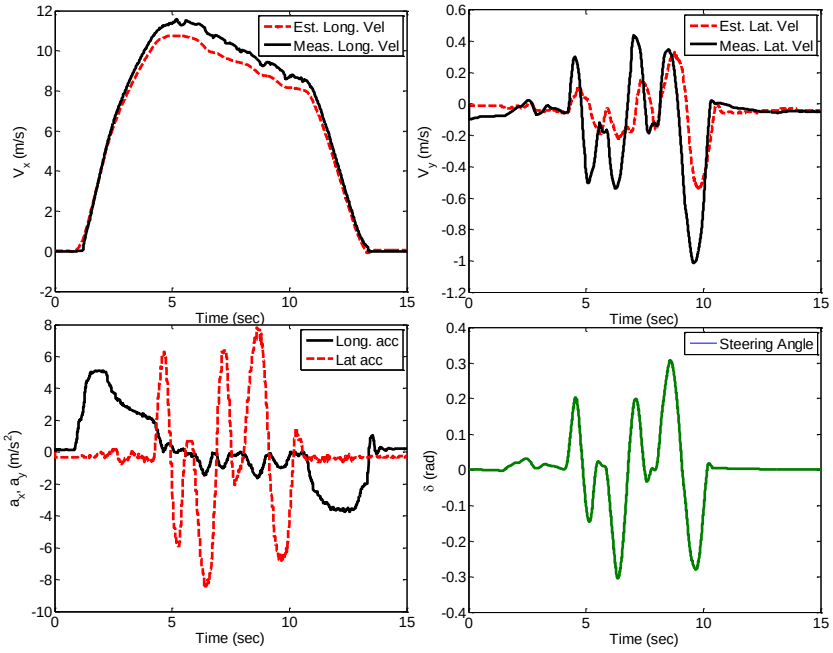

Figure 5.9: Vehicle motion characteristics for a steering maneuver on a dry road.

Based on Fig. 5.9, both longitudinal and lateral velocity estimators fail to estimate the velocity with an appropriate precision, which is confirmed via the reliability index shown in Fig. 5.10. More precisely, in a time period between $t = 5s$ and $t = 10s$, where

[2]As a rule of thumb, in the experiments, in the case of full throttle maneuvers (like the maneuvers discussed in this section) if the magnitude of longitudinal acceleration and/or lateral acceleration exceeds $6\frac{m}{s^2}$, the road is dry and it is slippery otherwise.

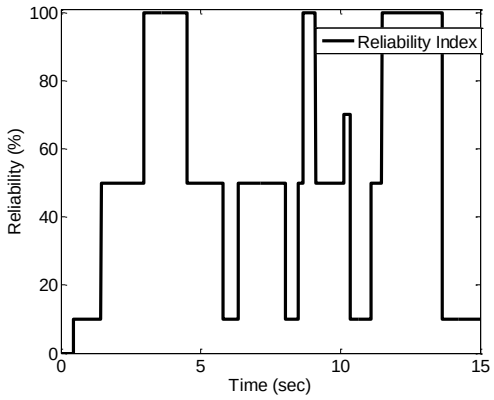

Figure 5.10: The reliability index of a steering maneuver on a dry road.

both estimated longitudinal and lateral velocities deviate from GPS measurements, the reliability index shows 50 percent (or less) reliability. However, before $t = 5s$ when both estimated longitudinal and lateral velocities are close to GPS measurements, the reliability index shows 100 percent reliability.

The following subsections belong to steering maneuvers on more slippery roads.

5.3.3 Steering on Basalt Tiles

The next maneuver is comprised of steerings with lateral accelerations on basalt tiles, with a road friction $\theta = 0.25$. As shown in Fig. 5.11, the peak magnitude the lateral acceleration is not large, which indicates that the road was slippery.

As shown in Fig. 5.11, in the beginning of the maneuver (up to $t = 4s$), the longitudinal velocity estimator has a good correspondence with the measurement; however, the lateral velocity estimation deviates considerably from the measurement. This causes a considerable signal drop in the reliability index, as shown in Fig. 5.12. Furthermore, there are some large amplitude noise signals modulated on the accelerations for both longitudinal and lateral directions. This causes some jumps in the reliability index. As shown in Figs. 5.11 and 5.12, in the tiny time interval between $t = 8s$ and $t = 9s$, the estimated velocities are close to the measured velocities, which shows the performance of the reliability

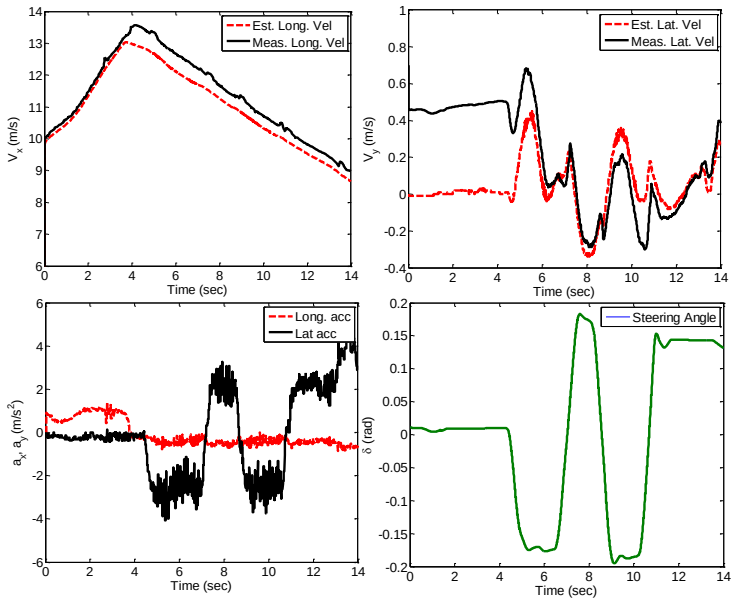

Figure 5.11: Vehicle motion characteristics for a steering maneuver on Basalt.

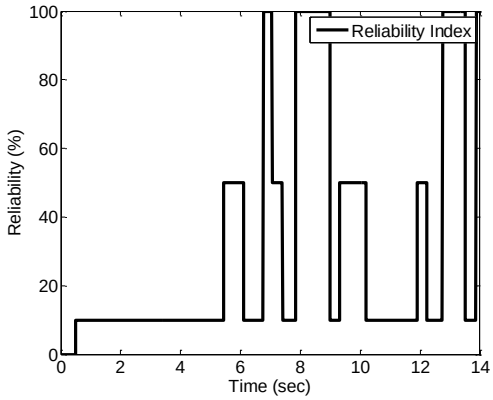

Figure 5.12: The reliability index of a steering maneuver on a Basalt.

measure.

5.3.4 Steering on a Wet Road

Another slippery road where a maneuver is performed is a wet road, with a road friction $\theta = 0.5$. The slippery road condition can also be confirmed by looking at the magnitude of the longitudinal and lateral accelerations, which are not large, as shown in Fig. 5.13.

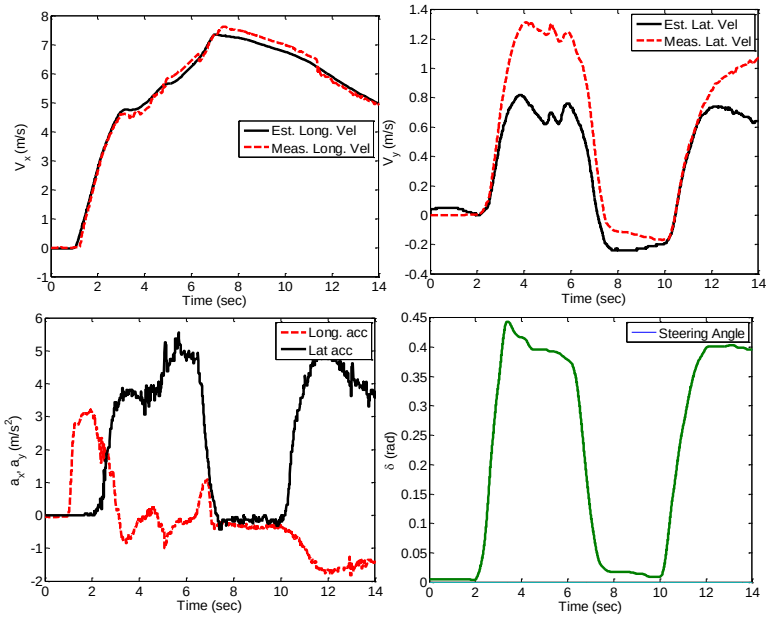

Figure 5.13: Vehicle motion characteristics for a steering maneuver on a wet road.

Based on Fig. 5.13, the estimated longitudinal velocity has an appropriate precision, in terms of agreement with GPS measurements. However, the lateral velocity, specifically between $t = 3s$ and $t = 7s$, has a significant bias with respect to the GPS measurement. From $t = 10s$ to $t = 12s$, both estimated lateral and longitudinal velocities have appropriate correspondence with the GPS measurement. Such behaviours are compatible with the reliability index shown in Fig. 5.14.

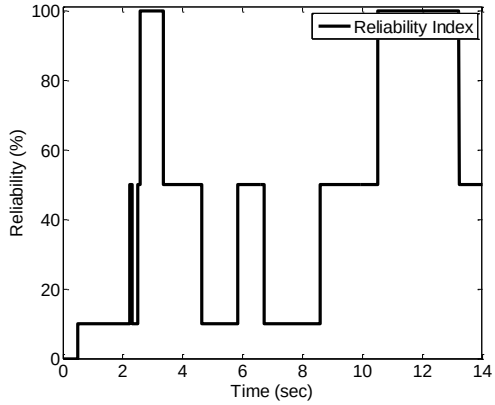

Figure 5.14: The reliability index of a steering maneuver on a wet road.

5.4 Summary

A real-time vehicle velocity estimation reliability assessment algorithm was introduced in this chapter. The algorithm was based on geometric and kinematic relations between corner velocities and the velocities in CG. Some methods to diagnose measurement fault from estimation faults and filter them in the on-line reliability measure were introduced. The proposed algorithm was tested via several experiments that comprised of different maneuvers performed on various road conditions and the performance of the reliability index was approved via comparing the estimated velocities with GPS measurements. As shown from the experimental results, the reliability index can be used in real-time scenarios to assess the level of confidence of the estimated corner longitudinal and lateral velocities. The main issue that should be addressed in this method is to make the reliability signals smooth enough, since sudden jumps in the reliability index may be interpreted as faults, which may not exist in reality. This requires more filtering on estimation and measurement signals which will eventually impose time delay to the reliability index.

Chapter 6

Road Condition Identification

As mentioned in Chapter 1, having knowledge about the road friction condition will have a great impact on the performance of the vehicle velocity estimation, and it meaningfully improves vehicle controller performance and safety; especially slip control and vehicle yaw/side slip and stability control. Much effort has been dedicated in recent years in proposing algorithms for identifying the road friction condition, which is mostly based on system identification techniques and tire model. Those approaches were introduced by detail in Chapter 2. However, there are two primary obstacles which the road condition identification faces, as described in the following:

- **Road Condition Identification in Slip-Slope Region:** As mentioned in Chapter 1, in the low slip regions, the road friction condition is very sensitive to the variations (errors) of the tire slip $\lambda = |\frac{R_e|\omega| - V_{xt}}{\max\{R_e|\omega|, V_{xt}\}}|$ which is a function of the vehicle's corner longitudinal velocity. Moreover, we know that the longitudinal velocity should be estimated (as discussed in Chapter 3) and this estimation is prone to some uncertainties. In low-slip regions, a small amount of uncertainty may yield a failure in road condition identification. Such level of sensitivity is schematically depicted in Fig. 6.1, which shows the linear region (slip - slope region) of the tire model. There, a small amount of error ($\Delta\lambda = 0.01$) in estimating slip ratio λ may cause an incorrect (icy to dry) road condition identification.

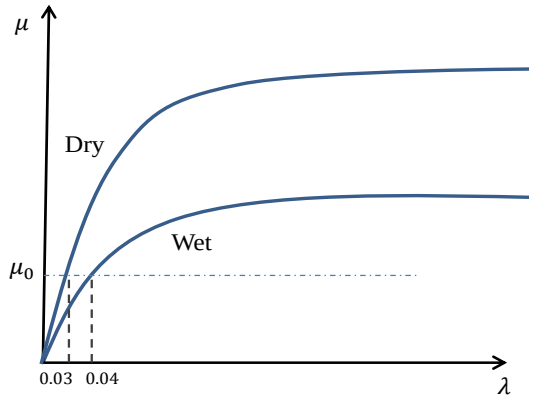

Figure 6.1: Sensitivity of the linear region of the tire model.

- **Road Condition Identification in Low Excitation Maneuvers:** A reliable road friction identification often requires that the regression vector satisfies the persistence of excitation (PE) conditions [28]. Consequently, the road friction coefficient identification approaches mentioned in Chapter 1 demand specific vehicle maneuvers or motion excitation (e.g., extensive steering action, accelerating and decelerating), which could be unrealistic/impossible in certain situations/constraints, such as constant speed cruising, surveillance, and military operations, and/or violate vehicle desired motion control and trajectory tracking objectives.

According to the presented literature review on road condition identification in Chapter 2, and the concerns that this field of study faces as mentioned above, a new look to road condition identification is proposed in this section. The approach of this study in identifying the road condition, is to use conventional vehicle sensory measurements[1] together with the vehicle lateral dynamics, and applying some post-processing techniques to come up with a less demanding road condition identification technique, compared to the former methods in terms of the required richness of the actuation signal (steering and gas pedal). Experimental tests show that the proposed method has an eminent power to address this problem in the situations where the previous methods in the literature fail to work (i.e. in law level of excitation and small tire slip regions). The theoretical foundation of this

[1] e.g., vehicle yaw rate and accelerations, wheel speed and acceleration and vehicle steering.

approach is discussed in the following section.

6.1 Vehicle Response-Based Road Condition Classification

This section presents the theoretical background of the road condition identification algorithm based on the vehicle response to lateral excitations. We begin by the linear lateral dynamics described in Chapter 2. Then we extend this analysis to the nonlinear case.

6.1.1 Linear Tire Model Case

Consider the following vehicle linear bicycle model (which was discussed in Chapter 2),

$$\begin{bmatrix} \dot{v}_y(t) \\ \dot{r}(t) \end{bmatrix} = \underbrace{\begin{bmatrix} -\frac{C_{\alpha_f}+C_{\alpha_r}}{v_x m} & -(\frac{aC_{\alpha_f}-bC_{\alpha_r}}{v_x m}+v_x) \\ -\frac{aC_{\alpha_f}-bC_{\alpha_r}}{v_x I_z} & -\frac{a^2C_{\alpha_f}+b^2C_{\alpha_r}}{v_x I_z} \end{bmatrix}}_{\mathbf{A}} \underbrace{\begin{bmatrix} v_y(t) \\ r(t) \end{bmatrix}}_{\mathbf{x}(t)} + \underbrace{\begin{bmatrix} \frac{C_{\alpha_f}}{m} \\ a\frac{C_{\alpha_f}}{I_z} \end{bmatrix}}_{\mathbf{B}} \delta, \tag{6.1}$$

where C_{α_f} and C_{α_r} are the cornering stiffness values for front and rear tracks, which are functions of the road condition θ, i.e., $C_{\alpha_f}(\theta)$, $C_{\alpha_r}(\theta)$. Here v_x is the longitudinal speed obtained from a torque and road-independent approach such as [90]. Among the two states in this dynamics, yaw rate $r(t)$ and lateral velocity $v_y(t)$, the available measurement is yaw rate and the lateral velocity must be estimated (as discussed in detail in Chapter 3). Hence, here, the yaw rate $r(t)$ is considered to be a measurable *vehicle's response* and plays a major role in the road identification algorithm. By solving (6.1) as a linear time-varying system, one can easily find the vehicle's yaw rate as

$$r(t) = \begin{bmatrix} 0 & 1 \end{bmatrix} \begin{bmatrix} v_y(t) \\ r(t) \end{bmatrix} = \begin{bmatrix} 0 & 1 \end{bmatrix} \mathbf{x}(t) = \begin{bmatrix} 0 & 1 \end{bmatrix} \left(\Phi(t,t_0)\mathbf{x}(t_0) + \int_{t_0}^{t} \Phi(t,\tau)\mathbf{B}\delta(\tau)d\tau \right), \tag{6.2}$$

where $\Phi(t,t_0)$ is the state transition matrix. According to (6.2), the value of the vehicle yaw rate is heavily dependent on the cornering stiffness (and hence, the road condition)

which appears in matrices A and B. Thus, different values of the cornering stiffness, i.e., different road conditions, result in different vehicle response (yaw rate). More formally, if we consider a value for the road condition like $\bar{\theta}$ (as the actual value of the road condition is unknown), then we have

$$r_{\bar{\theta}}(t) = [0 \quad 1] \left(\Phi(t, t_0, \bar{\theta}) \mathbf{x}(t_0) + \int_{t_0}^{t} \Phi(t, \tau, \bar{\theta}) \mathbf{B}_{\bar{\theta}} \delta(\tau) d\tau \right), \tag{6.3}$$

where $\Phi(t, t_0, \bar{\theta})$ and $B_{\bar{\theta}}$ are functions of the assumed value $\bar{\theta}$. By subtracting this value from the real (measured) value of the yaw rate $r(t)$, we get

$$\mathcal{R}_r(t) = r(t) - r_{\bar{\theta}}(t) = r(t) - [0 \quad 1] \left(\Phi(t, t_0, \bar{\theta}) \mathbf{x}(t_0) + \int_{t_0}^{t} \Phi(t, \tau, \bar{\theta}) \mathbf{B}_{\bar{\theta}} \delta(\tau) d\tau \right), \tag{6.4}$$

where $\mathcal{R}_r(t)$ is the residual signal. By changing the value of $\bar{\theta}$ from 0 (corresponding to the icy road) to 1 (corresponding to the dry road), while all of the other parameters in (6.4) are fixed, it is expected that the residual signal becomes zero at some particular value of $\bar{\theta}$. In particular, the real-time residual signal $\mathcal{R}_r(t)$ is an indicator of the difference between the actual road condition and the assumed road condition. Mathematically speaking, the true value of the road condition is obtained from

$$\theta(t) = \arg\min_{\bar{\theta}} \mathcal{R}_r(t). \tag{6.5}$$

One can improve this approach via using other vehicle states in combination with the yaw rate as indicators of the vehicle's response. To this end, other two IMU measurements, which are the vehicle's lateral and longitudinal accelerations a_x and a_y, can be used as well in order to come up with a more reliable identification algorithm. In order to use these two quantities, one should translate the states to longitudinal and lateral accelerations as $a_x = \dot{v}_x - r v_y$ and $a_y = \dot{v}_y + r v_x$. Here, longitudinal velocity v_x is obtained from the estimation and lateral velocity is obtained from the solution of the linear lateral dynamics (6.1) as

$$v_{y\bar{\theta}}(t) = [1 \quad 0] \left(\Phi(t, t_0) \mathbf{x}(t_0) + \int_{t_0}^{t} \Phi(t, \tau) \mathbf{B} \delta(\tau) d\tau \right). \tag{6.6}$$

The values of the yaw rate $r_{\bar{\theta}}(t)$ and the lateral velocity $v_{y\bar{\theta}}(t)$, derived in (6.3) and (6.6) for a presumed value $\bar{\theta}$, are used to get $a_{x\bar{\theta}} = \dot{v}_x - r_{\bar{\theta}} v_{y\bar{\theta}}$ and $a_{y\bar{\theta}} = \dot{v}_{y\bar{\theta}} + r_{\bar{\theta}} v_x$. Hence, we will find residual signals, here for longitudinal and lateral accelerations, as follows

$$\begin{aligned} \mathcal{R}_{a_x}(t) &= a_x - a_{x\bar{\theta}} = a_x - \left(\dot{v}_x - r_{\bar{\theta}} v_{y\bar{\theta}}\right), \\ \mathcal{R}_{a_y}(t) &= a_y - a_{y\bar{\theta}} = a_y - \left(\dot{v}_{y\bar{\theta}} + r_{\bar{\theta}} v_x\right). \end{aligned} \tag{6.7}$$

In order to get better results, one can combine the three residual signals obtained form (6.4) and (6.7) with some predefined weights to obtain a more reliable metric

$$\mathcal{R}(t) = \kappa_1 \mathcal{R}_r(t) + \kappa_2 \mathcal{R}_{a_x}(t) + \kappa_3 \mathcal{R}_{a_y}(t), \tag{6.8}$$

for some $\kappa_1, \kappa_2, \kappa_3 > 0$. The true road condition will be obtained from

$$\theta(t) = \arg\min_{\bar{\theta}} \mathcal{R}(t). \tag{6.9}$$

There are two important remarks regarding the implementation of this method and the sensitivity of this approach to vehicle/tire uncertainties.

Remark 7 *For the implementation of the proposed road condition identification algorithm, one way is to set the initial conditions to zero, i.e.,* $[v(0),\ r(0)]^T = [0,\ 0]^T$. *However, during the evolution of the dynamics* (6.1) *in time, a small amount of uncertainty or disturbances in the model (which usually exists) will propagate and cause the states to deviate from their actual values. Hence, it is required to update (re-initialize) the states of the system after some time interval with fresh data, which are obtained from the estimated lateral velocity* $\hat{v}_y(t)$ *(from Chapter 3) and measured yaw rate* $r(t)$. *Moreover, as the longitudinal velocity is used in the algorithm (as a parameter), it should be estimated in real-time and fed into the algorithm, i.e., dynamics* (6.1).

Remark 8 *Since in the residual values defined in* (6.4) *and* (6.7) *the only changing parameter is* $\bar{\theta}$ *and all other vehicle/tire parameters are fixed, and as the model* (6.1) *is linear with respect to the vehicle parameters, uncertainties in vehicle/tire parameters do not affect the final result* (6.9). *This is due to the fact that the method is a comparison-based algorithm (comparing the vehicle response for an assumed road condition with the real vehicle*

responses) and the effect of vehicle uncertainties in the residual signals will be eliminated. This introduces a level of flexibility of the method toward parameter uncertainties. From this view, the input signal $\delta(t)$ also does not have an effect in determining the road condition in this approach.

6.1.2 Nonlinear Tire Model Case

In order to consider the nonlinearities and saturation of the tire in the road condition identification algorithm (which happens in most cases during vehicle maneuvers), we must use the nonlinear vehicle lateral dynamics, discussed in Chapter 2. In this case, instead of linear state-space form (6.1), we have

$$\begin{bmatrix} \dot{v}_y(t) \\ \dot{r}(t) \end{bmatrix} = \begin{bmatrix} \frac{-g}{l}(bk_f + ak_r) & -(\frac{abg}{l}(k_f - k_r) + v_x) \\ \frac{mabg}{I_z l}(k_r - k_f) & -\frac{mabg}{I_z l}(bk_r + ak_f) \end{bmatrix} \begin{bmatrix} v_y(t) \\ r(t) \end{bmatrix} + \begin{bmatrix} \frac{bg}{l}k_f v_x \\ \frac{mabg}{I_z l}k_f v_x \end{bmatrix} \delta(t) + \begin{bmatrix} \frac{gv_x}{l}(b\phi_f\alpha_f + a\phi_r\alpha_r) \\ \frac{mabgv_x}{I_z l}(\phi_f\alpha_f - \phi_r\alpha_r) \end{bmatrix} \tag{6.10}$$

where parameters $k_f, k_r, \phi_f, \phi_r, \alpha_f, \alpha_r$ were defined in Chapter 2. The solution for the yaw rate $r(t)$ is not as straightforward as the linear case. However, in the discrete time version of (6.10), which is used in the implementation[2], the value of the yaw rate can be obtained in real time and hence, the residual signal $\mathcal{R}_r(t)$ can be computed in real time. Similarly, the other residual signals $\mathcal{R}_{a_x}(t)$ and $\mathcal{R}_{a_y}(t)$ can be calculated, which ultimately results in the calculation of $\mathcal{R}(t)$ and the road condition is obtained by (6.9).

The above-mentioned approach for the road condition identification based on vehicle responses to lateral excitations, for the linear and nonlinear vehicle lateral dynamics, is schematically shown in Fig. 6.2.

[2]Discretization of the nonlinear system (6.10) is done via the well-known Taylor method and the zero-order hold (ZOH) assumption [91].

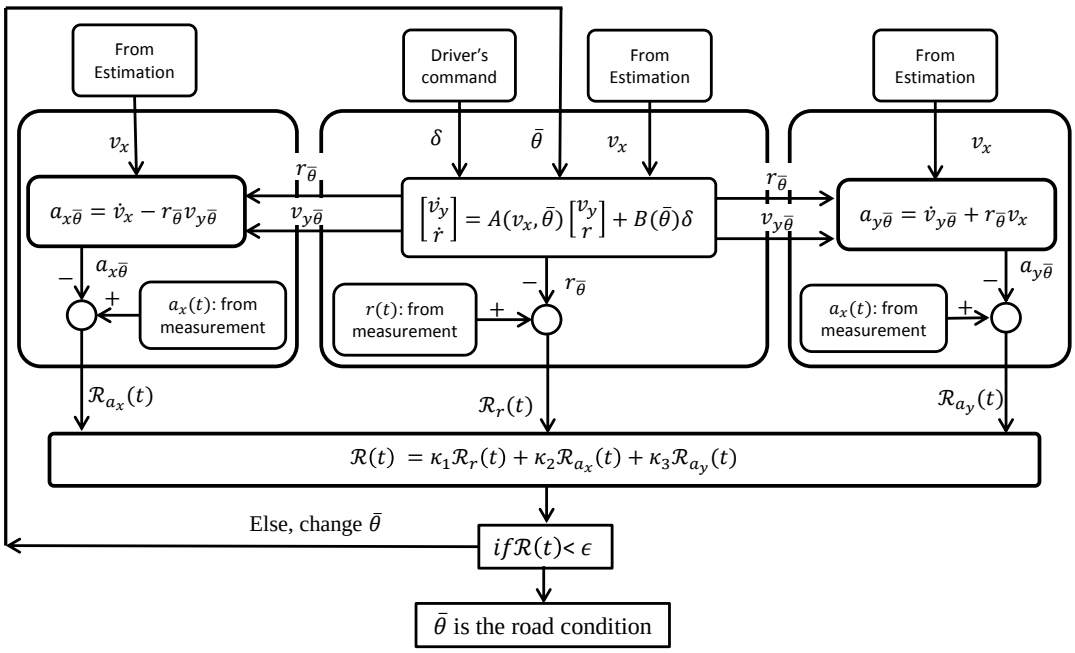

Figure 6.2: Road condition identification procedure.

6.2 Experimental Results

In this section, some experimental results will be demonstrated to show the effectiveness of the proposed response-based road condition identification algorithm. In these experiments, we will show the performance of the road condition identification algorithm using both linear lateral dynamics (6.1) and nonlinear lateral dynamics (6.10).

6.2.1 Slaloms on Dry (Using Linear Tire Model)

For the first experimental test, a harsh slalom maneuver, viz., a maneuver comprised of several steerings, is performed on a dry road. The level of lateral excitation can be understood from the magnitude of the lateral acceleration, which is more than $6\frac{m}{s^2}$, as shown in Fig. 6.3, on the left. The road identification residual signal $\mathcal{R}_r(t)$ introduced in (6.4), via using the linear lateral dynamics (6.1), is depicted in Fig. 6.3, on the right. As

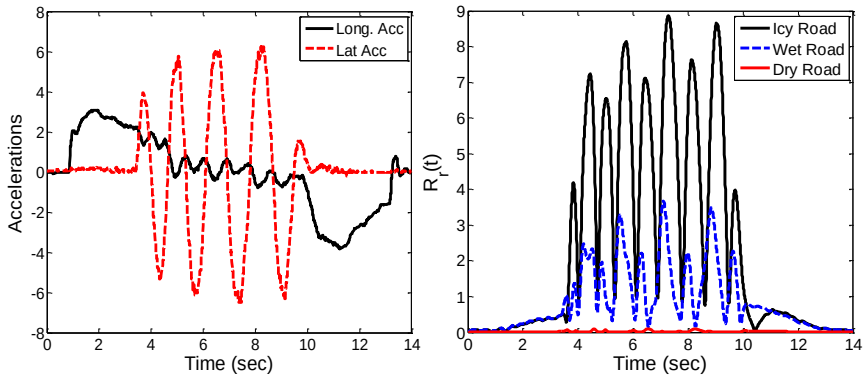

Figure 6.3: Vehicle accelerations (left), and road identification residual $\mathcal{R}_r(t)$ (right) for a harsh steering on a dry road.

it is inferred from the figure, the road condition identification works perfectly in detecting the dry road, whose error is minimum (red line). It should be noted that before the time $t = 4s$ and after time $t = 12s$, since there is no steering, the response-based road detection algorithm is unable to detect the road condition.

Another test, a mild slalom maneuver, again on a dry road, is performed. The level of lateral excitation can be inferred from the magnitude of the lateral acceleration, which is about $3\frac{m}{s^2}$, as shown in Fig. 6.4, on the left. The yaw rate residual signal $\mathcal{R}_r(t)$ is depicted

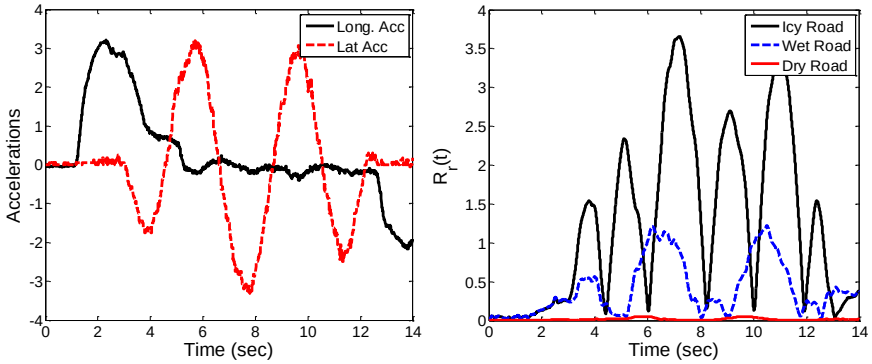

Figure 6.4: Vehicle accelerations (left), and road identification residual $\mathcal{R}_r(t)$ (right) for a mild steering on a dry road.

with respect to time in Fig. 6.4, right, which again uses the linear lateral dynamics (6.1). Despite the fact that the level of lateral excitation is not high in this maneuver, the road condition identification algorithm manages to detect the dry road with good accuracy. Here we should note that in the above two tests, harsh and mild lateral maneuvers on a dry road, the stronger residual signal $\mathcal{R}(t)$, defined in (6.8) that uses a_x and a_y in addition to the yaw rate, is not used and the yaw rate residual signal $\mathcal{R}_r(t)$ alone detects the road condition. Moreover, the linear lateral dynamics was used for road condition detection. In the following tests, it is no longer possible to detect the road condition via using the linear lateral dynamics (6.1) and the nonlinear model (6.10) should be applied. Moreover, the residual signal $\mathcal{R}(t)$, defined in (6.8), should be used to increase the precision of the road condition identification.

6.2.2 Maneuvers with Nonlinear Excitations

In this subsection, some other experimental tests are presented. The main differences between the following tests from the tests mentioned in the previous subsection are, (i) the nonlinear lateral dynamics are used as the tire goes to the saturation region, and (ii) the general residual signal $\mathcal{R}(t)$ in (6.8) that utilized lateral and longitudinal accelerations as extra measurements, is used in order to increase the accuracy of the resulting road condition identification.

The maneuver whose characteristics are shown in Fig. 6.5 is a step steer maneuver on a dry road. This maneuver comprised of a single steering, which can be inferred from the lateral acceleration shown in the figure. In this maneuver, both longitudinal and lateral accelerations are so high that the tire enters the saturation region. Hence, the nonlinear lateral dynamics should be used here. The yaw rate residual signal is shown in Fig. 6.5, at the top. Moreover, the general residual signal $\mathcal{R}(t)$ is shown in the middle, which yields a more precise road condition identification than that of $\mathcal{R}_r(t)$.

The other maneuver is a steering on a snow road. Again, the yaw rate residual signal $\mathcal{R}_r(t)$, general residual signal $\mathcal{R}(t)$ and the values of longitudinal and lateral accelerations are shown in Fig. 6.6.

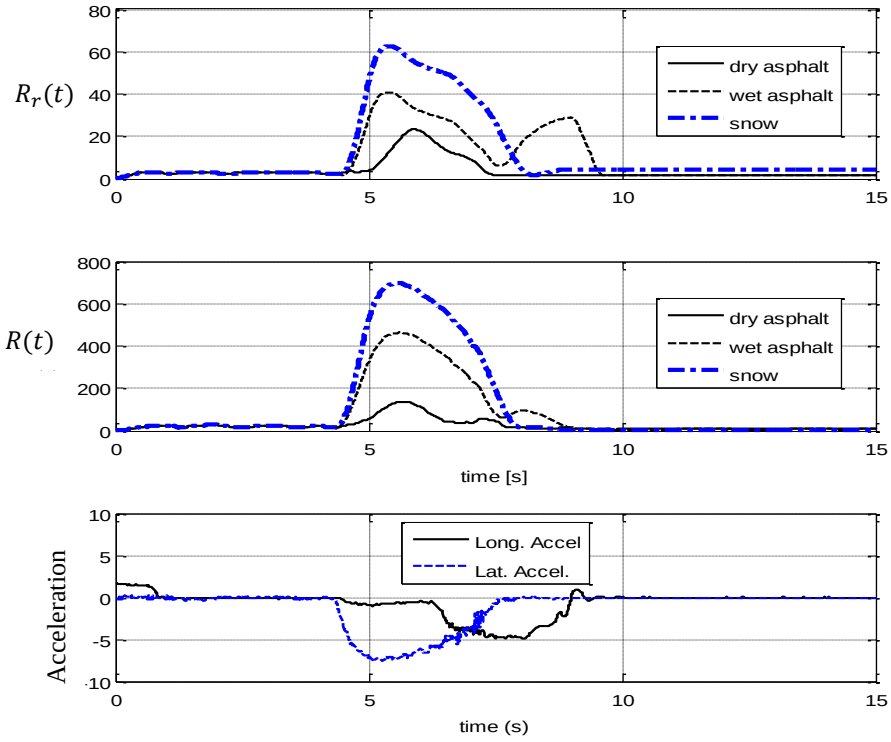

Figure 6.5: Yaw rate residual $\mathcal{R}_r(t)$ (top), general residual $\mathcal{R}(t)$ (middle) and vehicle accelerations (bottom) for a Step steering on a dry road.

The maneuver whose characteristics are shown in Fig. 6.7 demonstrates the essential advantage of using the general residual signal $\mathcal{R}(t)$ compared to the yaw rate residual $\mathcal{R}_r(t)$. This experiment includes several consecutive full turns on dry and wet roads, as shown in Fig. 6.7, on the right. The strength of the proposed road condition identification method is clearly depicted in this test. In particular, during each vehicle turn to the dry or the wet road, the residual signals, Fig. 6.7 middle, change their locations, as shown with dashed circles. Such accuracy is not detected via only using the yaw rate residual signal $\mathcal{R}_r(t)$, as shown in Fig. 6.7, at the top. This can be seen by considering the time interval between $t = 4s$ and $t = 8s$, where the road has changed but it is not detected by $\mathcal{R}_r(t)$.

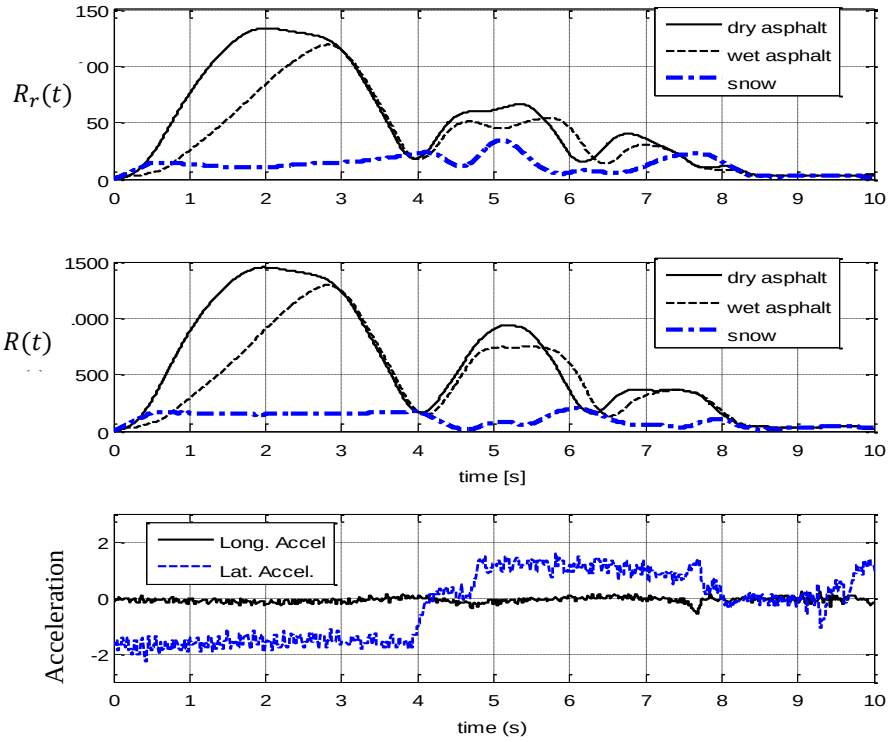

Figure 6.6: Yaw rate residual $\mathcal{R}_r(t)$ (top), general residual $\mathcal{R}(t)$ (middle) and vehicle accelerations (bottom) for a steering on snow.

6.3 Summary

An algorithm to identify (classify) the road friction condition was proposed in this chapter. The proposed road friction identification algorithm is based on vehicle responses, vehicle lateral dynamics, and appropriate tire models. This algorithm takes advantage of receiving information from the road-independent velocity estimation module to enhance its accuracy and performance. The performance of this algorithm was verified via various experiments on different road conditions and for different maneuvers. The resilience of the proposed algorithm to tire and vehicle parameter uncertainties was also discussed.

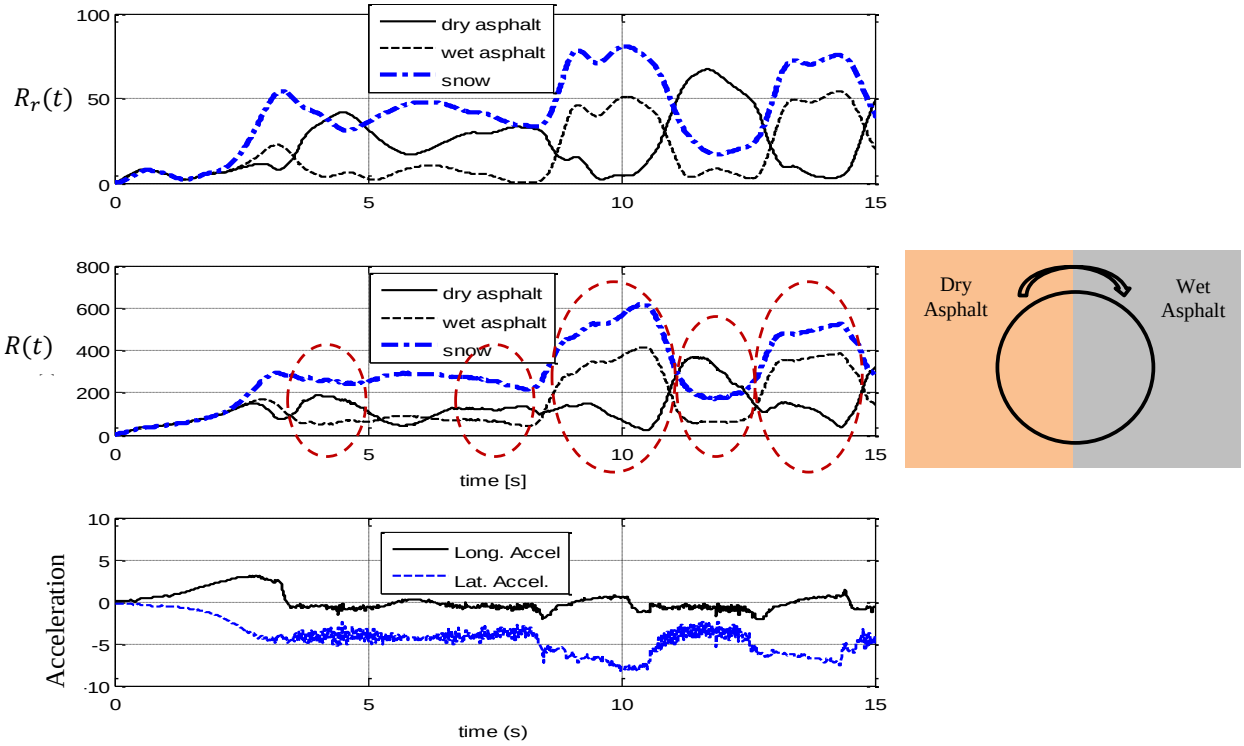

Figure 6.7: Yaw rate residual $\mathcal{R}_r(t)$ (top), general residual $\mathcal{R}(t)$ (middle) and vehicle accelerations (bottom) for several turns on dry and wet roads.

Chapter 7

Conclusion and Future Works

7.1 Summary and Conclusions

In this thesis, a reliable and resilient corner-based vehicle velocity estimation algorithm was proposed. This estimator was in the form of a combination of vehicle kinematics and LuGre tire model. The passivity of the LuGre tire model could help the velocity estimator improve its performance compared to the previous kinematic based methods. The designed vehicle velocity estimation algorithm is proven to be resilient to the time-varying tire parameters, the road friction condition, as well as sensor measurements uncertainties. The observability of the dynamics as a linear time-varying system, due to the time-varying wheel speed, was analytically studied prior to designing the observer. One of the featured advantages of the proposed velocity estimator is that it does not require knowledge about the road friction condition. Considering the fact that identifying the road condition is hard in most of the cases, as discussed in Chapter 6, finding a velocity estimation algorithm that operates independent of the road condition is invaluable. In order to further increase the performance of the designed velocity estimation algorithm, the effect of the suspension compliance and the resulting extra degree of freedom was directly added to the estimated vehicle corner velocity. The performance of the proposed velocity estimation algorithm was verified via several experimental tests, which were comprised of various standard vehicle maneuvers performed on different road conditions, and the results showed appropriate

correspondence with measurements.

The stability, performance, and robustness of the proposed corner-based vehicle velocity estimator, from a system theoretic viewpoint, were investigated in this thesis. More particularly, stability of the observer error dynamics, as a linear-time-varying system, was proven based on Lyapunov analysis, and a bound on the estimation error, as a function of road condition and measurements uncertainties, was derived. Other than this analytical bound, some numerical upper bounds on the estimation error dynamics were presented, which were based on an input-output approach to the observer error dynamics and their $\mathcal{H}_\infty$ performance, and it was shown that the observer error dynamics is a non-expansive system (i.e., it does not propagate the disturbances to the estimation error). Since real-time observer gain switching is inevitable in experiments, to change the reliance of the estimator to measurements in different instances, the stability of the velocity estimator in the presence of estimation gain switchings was also studied for two cases of arbitrary and stochastic gain switching scenarios. At the end, the sensitivity of the performance of the designed velocity estimator to tire parameter variations was investigated. These analyses were referred to as the *offline reliability assessment of the velocity observer* in this thesis.

Other than the off-line methods which were investigated as fundamental characteristics of the designed observer, a real-time reliability measure for the observer was also introduced. The proposed on-line reliability measure is considered to be a milestone that the observer should reach before its output (estimated states) is used in the control module. It was based on vehicle kinematics that translate the estimated states (longitudinal and lateral velocities at each corner) to longitudinal and lateral accelerations, which can be directly measured in conventional vehicles. After some error clustering, a reliability index was introduced which showed a level of confidence that one can assign to the estimated velocities. The proposed on-line reliability measure is tested via several experiments comprised of different maneuvers on various road conditions which proved the ability of the reliability index to diagnose failures in the estimated velocities.

The other main contribution of this thesis was to introduce a road condition identification technique. The significance of the proposed method was its simplicity in terms of implementation as well as its preliminary requirements, compared to the existing methods in the literature. The proposed road friction identification algorithm was based on

vehicle responses to lateral excitations via application of vehicle lateral dynamics and an appropriate tire model. Both linear and nonlinear (LuGre) tire models were applied to the vehicle's lateral dynamics and used in the road condition identification algorithm. One of the unique features of the proposed road condition identification algorithm is that it can take advantage of receiving information from the road-independent velocity estimation module and torque-independent speed estimator [90] to enhance its accuracy and performance. The performance of this algorithm was verified via various experiments on different road conditions and for different maneuvers. The resilience of the proposed algorithm to tire and vehicle parameter uncertainties was also discussed.

7.2 Future Work

This section provides suggestions on the direction of research required to continue the work done in this thesis. These avenues of research are presented in two parts: (i) improving single vehicle estimation, and (ii) taking advantage of networks of vehicles to improve the estimation. In other words, in this section, some new vistas that should be seriously considered in estimation and control of future generation of intelligent transportation systems are introduced. The following subsection pertains to possible future directions in a single vehicle state estimation as an extension of the work done in this thesis.

7.2.1 Improving Estimation for a Single Vehicle

As a continuation of the work done in this thesis, the following directions are introduced:

1. **Improving Corner-Based Velocity Estimation:** There are some avenues for enhancing the performacne of the proposed corner-based vehicle velocity estimation. One such direction is to use the known road condition inside the velocity estimation algorithm. As discussed in Chapter 3, the velocity estimation algorithm works properly despite the fact that the road friction condition is unknown. However, more knowledge about the road condition results in a less demanding velocity estiamtor in terms of robustness, which improves the performance of the estimator. To this

end, one can use the road condition identification algorithm, presented in Chapter 6 in order to enhance the performance of the velocity estimation. This is shown schematically with a left-to-right arrow in Fig. 7.1.

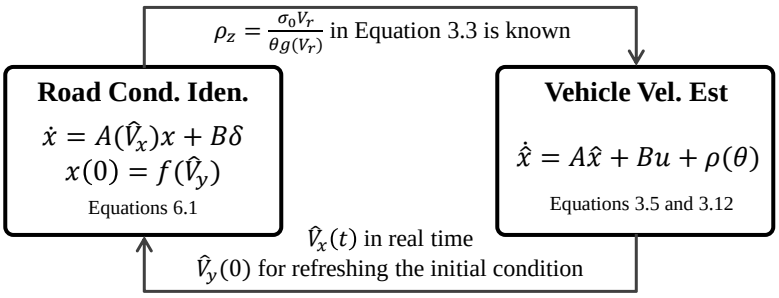

Figure 7.1: Reciprocity between vehicle velocity estimation and road condition identification.

2. **Using Temporal Redundancy for Offline Reliability Measure:** As discussed in Chapter 1, there are two different sets of redundancies which are considered and used to assess the reliability of systems. One was physical redundancy, which is based on using multiple sets of infrastructures. The other one is to look at the history of the system and use its operation throughout the time as a particular form of redundancy. One can use such an approach in analyzing the performance of the velocity estimator over time and design a reliability index based on what is witnessed during the operation of the estimator in a particular time interval. It is also possible to use the stochastic approach (Markov jump), presented in Chapter 4, as a probability distribution of fault occurrence to come up with a Bayesian approach to the behaviour of the estimator throughout the time.

3. **Enhancing the Performance of On-line Reliability Measure:** The current reliability index has proven to work properly in different situations; however, there are some issues needed to be addressed in order to improve its performance. The main issue is that the reliability index is less sensitive to signal error bias compared to noises. It is due to the fact that the derivative terms in (5.1) play major roles in

detecting faults. Hence, it is imperative to modify the designed reliability measure to be able to detect small signal error biases.

4. **Improving Road Condition Identification Algorithm:** There exists a reciprocity between the vehicle velocity estimation and the road condition identification algorithms. Such reciprocity is schematically depicted in Fig. 7.1. According to this figure, specifically, the right-to-left arrow, one can use the velocity estimation module, which operates independent of the road condition, in order to enhance the performance of the road condition identification algorithm. More specifically, as the estimated longitudinal velocity is fed directly to the road condition identification algorithm and the estimated lateral velocity should also be used after some time interval to refresh the initial condition of the algorithm, more precise values of the longitudinal and lateral velocities can definitely improve the performance of the road condition identification module.

7.2.2 Application of Vehicle Networks to Vehicle State Estimation

The emergence of new generation of communication technologies have brought new avenues to traditional studies in vehicle estimation and control. The concept of *Internet of vehicles*, as a tangible representation of *Internet of things*, has significantly changed the shape of the urban transportation. In this direction, one can use the inherent potential in the inter-vehicle communication to enhance the quality of each individual vehicle estimation and control strategies. One way is to use information of other vehicles, e.g., their positions, velocities and accelerations together with algorithms to relate these quantities to the states of each individual vehicle and find (possible) failures that occur in the velocity estimation of the vehicle. One such algorithm is schematically shown in Fig. 7.2. As shown in this figure, vehicle v_i gathers information from vehicle v_j (in a distributed manner) and then uses this information to calculate an error function e_i^j,

$$e_i^j = \kappa_1 \left(u_{ij} - \int a_{ij} dt \right) + \kappa_2 \left(u_{ij} - \frac{d(p_{ij})}{dt} \right) \tag{7.1}$$

where $\kappa_1, \kappa_2 > 0$ are some design constants and $p_{ij} = p_i(t) - p_j(t)$, $u_{ij} = u_i(t) - u_j(t)$ and $a_{ij}(t) = a_i(t) - a_j(t)$ are relative distance, velocity and acceleration of vehicles v_i and v_j, which are calculated distributedly. The magnitude of e_i^j shows the existence of velocity estimation fault in the vehicle. The detailed procedure and algorithm description can be found in [87]. This algorithm and similar distributed vehicle estimation fault diagnostics algorithms inform the existence of a rich avenue for future research in the field of vehicle estimation and control.

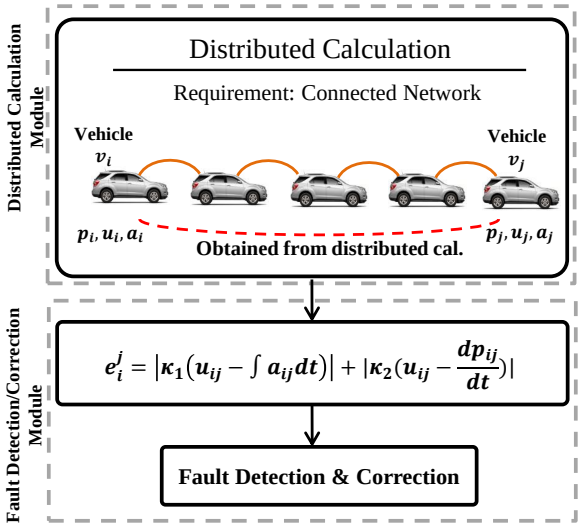

Figure 7.2: Distributed vehicle velocity fault diagnostics procedure.

References

[1] D. Schramm, M. Hiller, and R. Bardini, "Modellbildung und simulation der dynamik von kraftfahrzeugen," *Springer*, 2010.

[2] N. Patel, C. Edwards, and S. Spurgeon, "Tyre-road friction estimationa comparative study," *Proceedings of the Institution of Mechanical Engineers, Part D: Journal of Automobile Engineering*, vol. 222, no. 12, pp. 2337–2351, 2008.

[3] G. Baffet, A. Charara, and D. Lechner, "Estimation of vehicle sideslip, tire force and wheel cornering stiffness," *Control Engineering Practice*, vol. 17, no. 11, pp. 1255–1264, 2009.

[4] R. Rajamani, G. Phanomchoeng, D. Piyabongkarn, and J. Lew, "Algorithms for Real-Time Estimation of Individual Wheel Tire-Road Friction Coefficients," *IEEE/ASME Transactions on Mechatronics*, vol. 17, no. 6, pp. 1183–1195, 2012.

[5] M. Doumiati, A. Victorino, D. Lechner, G. Baffet, and A. Charara, "Observers for vehicle tyre/road forces estimation: experimental validation," *Vehicle System Dynamics*, vol. 48, no. 11, pp. 1345–1378, 2010.

[6] W. Cho, J. Yoon, S. Yim, B. Koo, and K. Yi, "Estimation of tire forces for application to vehicle stability control," *IEEE Transactions on Vehicular Technology*, vol. 59, no. 2, pp. 638–649, 2010.

[7] E. Hashemi, A. Kasaeizadeh, A. Khajepour, N. Mushchuk, and S.-K. Chen, "Robust Estimation and Experimental Evaluation of Longitudinal Friction Forces in

Ground Vehicles," in *ASME International Mechanical Engineering Congress Exposition*, 2014.

[8] S. Mammar, S. Glaser, and M. Netto, "Vehicle lateral dynamics estimation using unknown input proportional-integral observers," in *In Proc. American Control Conference*, 2006, pp. 1260–1266.

[9] Y. Wang, D. M. Bevly, and S. K. Chen, "Longitudinal Tire Force Estimation with Unknown Input Observer," in *In Proc. ASME Dynamic Systems and Control Conference*, 2012.

[10] Y. Wang, D. M. Bevly, and S.-k. Chen, "Lateral tire force estimation with unknown input observer," in *In Proc. ASME 5th Annual Dynamic Systems and Control Conference*. American Society of Mechanical Engineers, 2012, pp. 531–538.

[11] Y. H. J. Hsu, "Estimation and control of lateral tire forces using steering torque," Ph.D. dissertation, Stanford University, 2009.

[12] J. Ryu, "State and parameter estimation for vehicle dynamics control using GPS," Ph.D. dissertation, Stanford University, 2004.

[13] J. Ryu and J. C. Gerdes, "Integrating inertial sensors with global positioning system (GPS) for vehicle dynamics control," *ASME Journal of Dynamic Systems, Measurement, and Control*, vol. 126, no. 2, pp. 243–254, 2004.

[14] L. Imsland, T. A. Johansen, T. I. Fossen, H. F. Grip, J. C. Kalkkuhl, and A. Suissa, "Vehicle velocity estimation using nonlinear observers," *Automatica*, vol. 42, no. 12, pp. 2091–2103, 2006.

[15] J. A. Farrell, H.-S. Tan, and Y. Yang, "Carrier phase GPS-aided INS-based vehicle lateral control," *ASME Journal of Dynamic Systems, Measurement, and Control*, vol. 125, no. 3, pp. 339–353, 2003.

[16] D. M. Bevly, "Global positioning system (GPS): A low-cost velocity sensor for correcting inertial sensor errors on ground vehicles," *ASME Journal of Dynamic Systems, Measurement, and Control*, vol. 126, no. 2, pp. 255–264, 2004.

[17] D. M. Bevly, J. Ryu, and J. C. Gerde, "Integrating INS sensors with GPS measurements for continuous estimation of vehicle sideslip, roll, and tire cornering stiffness," *IEEE Transactions on Intelligent Transportation Systems*, vol. 7, no. 4, pp. 483–493, 2006.

[18] J.-H. Yoon and H. Peng, "A cost-effective sideslip estimation method using velocity measurements from two GPS receivers," *IEEE Transactions on Vehicular Technology*, vol. 63, no. 6, pp. 2589–2599, 2014.

[19] A. Nishio, K. Tozu, H. Yamaguchi, and K. Asano, "Development of vehicle stability control system based on vehicle sideslip angle estimation," *SAE Technical Paper*, 2001.

[20] Y. Fukada, "Slip-angle estimation for vehicle stability control," *Vehicle System Dynamics*, pp. 375–388, 1999.

[21] Y.-H. J. Hsu, S. M. Laws, and J. C. Gerdes, "Estimation of tire slip angle and friction limits using steering torque," *IEEE Transactions on Control Systems Technology*, vol. 18, no. 4, pp. 896–907, 2010.

[22] K. Nam, H. Fujimoto, and Y. Hori, "Lateral stability control of in-wheel-motor-driven electric vehicles based on sideslip angle estimation using lateral tire force sensors," *IEEE Transactions on Vehicular Technology*, vol. 61, no. 5, pp. 1972–1985, 2012.

[23] C. Ahn, H. Peng, and H. E. Tseng, "Estimation of road friction for enhanced active safety systems: algebraic approach," *in Proc. Amer. Control Conf*, pp. 1104–1109, 2009.

[24] J. Chihoon, S. Hwang, and H. Kim, "Clamping-force control for electromechanical brake," *IEEE Transactions on Vehicular Technology*, vol. 59, no. 7, pp. 3205–3212, 2010.

[25] J. Wang and R. G. Longoria, "Coordinated and reconfigurable vehicle dynamics control," *IEEE Transactions on Control Systems Technology*, 2009.

[26] C. Lee, K. Hedrick, and K. S. Yi, "Real-time slip estimation and maximum tireroad friction coefficient," *IEEE Transactions on Vehicular Technology*, vol. 9, pp. 454–458, 2004.

[27] J. O. Hahn, R. Rajamani, and L. Alexander, "GPS-based real-time identification of tireroad friction coefficient," *IEEE Trans. Control Syst. Technology*, vol. 10, pp. 331–343, 2002.

[28] Y. Chen and J. Wang, "Adaptive vehicle speed control with input injections for longitudinal motion independent road frictional condition estimation," *IEEE Transactions on Vehicular Technology*, vol. 60, pp. 839–848, 2011.

[29] H. F. Grip, L. Imsland, T. A. Johansen, T. I. Fossen, J. C. Kalkkuhl, and A. Suissa, "Nonlinear vehicle side-slip estimation with friction adaptation," *Automatica*, vol. 44, no. 3, pp. 611–622, 2008.

[30] H. Faer Grip, L. Imsland, T. A. Johansen, J. C. Kalkkuhl, and A. Suissa, "Vehicle sideslip estimation: Design, implementation, and experimental validation," *IEEE Control Systems*, vol. 29, no. 5, pp. 36–52, 2009.

[31] S.-H. You, J.-O. Hahn, and H. Lee, "New adaptive approaches to real-time estimation of vehicle sideslip angle," *Control Engineering Practice*, vol. 17, no. 12, pp. 1367–1379, 2009.

[32] G. Magallan, C. H. D. Angelo, and G. O. García, "Maximization of the traction forces in a 2WD electric vehicle," *IEEE Transactions on Vehicular Technology*, vol. 60, no. 2, pp. 369–380, 2011.

[33] C. C. Wit and P. Tsiotras, "Dynamic Tire Friction Models for Vehicle Traction Control," in *In Proc. 38th Conference on Decision & Control*, 1999, pp. 3746–3751.

[34] X. Zhang, Y. Xu, M. Pan, and F. Ren, "A vehicle ABS adaptive sliding-mode control algorithm based on the vehicle velocity estimation and tyre/road friction coefficient estimations," *Vehicle System Dynamics*, vol. 52, no. 4, pp. 475–503, 2014.

[35] F. Sun, X. Huang, J. Rudolph, and K. Lolenko, "Vehicle state estimation for anti-lock control with nonlinear observer," *Control Engineering Practice*, vol. 43, pp. 69–84, 2015.

[36] S. Antonov, A. Fehn, and A. Kugi, "Unscented kalman filter for vehicle state estimation," *Vehicle System Dynamics*, vol. 49, no. 9, pp. 1497–1520, 2011.

[37] M. Gadola, D. Chindamo, M. Romano, and F. Padula, "Development and validation of a kalman filter-based model for vehicle slip angle estimation," *Vehicle System Dynamics*, vol. 52, no. 1, pp. 68–84, 2014.

[38] H. B. Pacejka and R. S. Sharp, "Shear Force Development by Pneumatic Tyres in Steady State Conditions: A Review of Modelling Aspects," *Vehicle System Dynamics*, vol. 20, no. 3-4, pp. 121–175, 1991.

[39] R. T. Uil, "Tyre Models for Steady-State Vehicle Handling Analysis," Ph.D. dissertation, Eindhoven University of Technology, 2007.

[40] J. Deur, J. Asgari, and D. Hrovat, "A 3D Brush-Type Dynamic Tire Friction Model," *Vehicle System Dynamics*, vol. 42, no. 3, pp. 133–173, 2004.

[41] W. Liang, J. Medanic, and R. Ruhl, "Analytical Dynamic Tire Model," *Vehicle System Dynamics*, vol. 46, pp. 197–227, 2008.

[42] C. C. Wit and R. Horowitz, "Observer for Tire/Road Contact Friction Using Only Wheel Angular Velocity Information," in *In Proc. 38th Conference on Decision & Control*, 1999, pp. 3932–3937.

[43] C. Wit, P. Tsiotras, E. Velenis, M. Gissinger, and G. Gissinger, "Dynamic Friction Models for Road/Tire Longitudinal Interaction," *Vehicle System Dynamics*, vol. 39, pp. 189–226, 2003.

[44] P. Tsiotras, E. Velenis, and M. Sorine, "A LuGre Tire Friction Model With Exact Aggregate Dynamics," *Vehicle System Dynamics*, vol. 42, pp. 195–210, 2004.

[45] C. C. Wit, H. Olsson, K. J. Astrom, and P. Lischinsky, "A New Model for Control of Systems with Friction," *IEEE Transactions on Automatic Control*, vol. 40, 1995.

[46] K. J. Astrom and C. C. Wit, "Revisiting the LuGre Model," *IEEE Control System Magazine*, vol. 6, pp. 101–114, 2008.

[47] E. Hashemi, M. Pirani, A. Khajepour, and A. Kasaiezadeh, "A comprehensive study on the stability analysis of vehicle dynamics with pure/combined-slip tyre models," *Vehicle System Dynamics*, vol. 54, no. 12, pp. 1736–1761, 2016.

[48] C. Ahn, H. Peng, and H. Tseng, "Robust Estimation of Road Friction Coefficient," in *In Proc. American Control Conference*, no. 3, 2011, pp. 3948–3953.

[49] W. Cho, J. Yoon, S. Yim, B. Koo, and K. Yi, "Estimation of tire forces for application to vehicle stability control," *IEEE Transactions on Vehicular Technology*, vol. 59, no. 2, pp. 638–649, 2010.

[50] E. Hashemi, M. Pirani, A. Khajepour, B. Fidan, A. Kasaiezadeh, S. Chen, and B. Litkouhi, "Integrated estimation structure for the tire friction forces in ground vehicles," in *In Proc. IEEE Conference on Advanced Intelligent Mechatronics.* IEEE, 2016.

[51] H. J. LeBlanc, H. Zhang, X. Koutsoukos, and S. Sundaram, "Resilient asymptotic consensus in robust networks," *IEEE Journal on Selected Areas in Communications*, vol. 31, pp. 766–781, 2013.

[52] K. Stouffer, J. Falco, and K. Scarfone., "Guide to industrial control systems security," *National Institute of Standards and Technology*, 2008.

[53] A. Cardenas, S. Amin, , and S. S. Sastry, "Research challenges for security of control systems," *3rd USENIX Workshop on Hot Topics in Security*, 2008.

[54] R. Isermann, "Supervision, fault-detection and fault-diagnosis methods an introduction," *Control Engineering Practice*, vol. 5, pp. 639–652, 1997.

[55] J. von Neumann, "Probabilistic logics and the synthesis of reliable organisms from unreliable components," *Princeton University Press*, 1956.

[56] E. Y. Chow and A. S. Willsky, "Analytical redundancy and the design of robust failure detection systems," *IEEE Transactions on Automatic Control*, pp. 603–614, 1984.

[57] M. Blanke, M. Kinnaert, J. Lunze, and M. Staroswiecki, "Diagnosis and fault- tolerant control," *Springer*, 2006.

[58] R. Isermann, "Model-based fault detection and diagnosis: status and applications," *16th IFAC Symposium on Automatic Control in Aerospace*, pp. 71–85, 2004.

[59] H. K. Khalil and J. W. Grizzle, "Nonlinear systems," *Prentice hall*, 1996.

[60] K. Zhou, J. C. Doyle, and K. Glover, "Robust and optimal control," *Prentice Hall*, 1996.

[61] D. Liberzon, "Switching in systems and control," *Springer*, 2012.

[62] H. Lin and P. J. Antsaklis, "Stability and stabilizability of switched linear systems: a survey of recent results," *IEEE Transactions on Automatic Control*, pp. 308–322, 2009.

[63] O. L. V. Costa, M. D. Fragoso, and R. P. Marques, "Discrete time markovian jump linear systems," *Springer-Verlag*, 2005.

[64] ——, "Continuous time markovian jump linear systems," *Springer-Verlag*, 2005.

[65] M. Karan, P. Shi, and C. Y. Kaya, "Transition probability bounds for the stochastic stability robustness of continuous- and discrete-time markovian jump linear systems," *Automatica*, p. 21592168, 2006.

[66] J. L. Xiong, J. Lam, H. J. Gao, and W. C. Daniel, "On robust stabilization of markovian jump systems with uncertain switching probabilities," *Automatica*, vol. 41, pp. 897–903, 2005.

[67] R. Krtolica, U. Ozguner, H. Chan, H. Goktas, J. Winkelman, and M. Liubakka, "Stability of linear feedback systems with random communication delays," *Int. J. Control*, vol. 54, pp. 925–953, 1994.

[68] P. Seiler and R. Sengupta, "Analysis of communication losses in vehicle control problems," *In Proc. American Control Conference*, pp. 1491–1496, 2001.

[69] L. Zhang and E. Boukas, "Stability and stabilization of markovian jump linear systems with partly unknown transition probabilities," *Automatica*, vol. 45, pp. 463–468, 2009.

[70] M. Pirani, E. Hashemi, A. Khajepour, B. Fidan, A. Kasaiezadeh, S. Chen, and B. Litkouhi, "Resilient corner based vehicle velocity estimation," *IEEE Transactions on Control Systems Technology*, 2017.

[71] E. Hashemi, M. Pirani, A. Khajepour, A. Kasaiezadeh, S.-K. Chen, and B. Litkouhi, "Corner-based estimation of tire forces and vehicle velocities robust to road conditions," *Control Engineering Practice*, vol. 61, pp. 28–40, 2017.

[72] E. Hashemi, "Full Vehicle State Estimation Using a Holistic Corner-based Approach," Ph.D. dissertation, University of Waterloo, 2017.

[73] E. Hashemi, S. Khosravani, A. Khajepour, A. Kasaiezadeh, S.-K. Chen, and B. Litkouhi, "Longitudinal vehicle state estimation using nonlinear and parameter-varying observers," *Mechatronics*, vol. 43, pp. 28–39, 2017.

[74] R. Toth, *Modeling and Identification of Linear Parameter-Varying Systems*. Springer, 2010.

[75] E. Hashemi, R. Zarringhalam, A. Khajepour, W. Melek, A. Kasaiezadeh, and S.-K. Chen, "Real-time estimation of the road bank and grade angles with unknown input observers," *Vehicle System Dynamics*, vol. 55, no. 5, pp. 648–667, 2017.

[76] J. E. Slotine and W. Li, "Applied nonlinear control," *Prentice Hall*, 1991.

[77] A. Czornik, A. Nawrat, M. Niezabitowski, and A. Szyda, "On the lyapunov and bohl exponent of time-varying discrete linear system," *In Proc. 20th Mediterranean Conference on Control and Automation (MED)*, pp. 194–197, 2012.

[78] T. Berger, "Bohl exponent for time-varying linear differential-algebraic equations," *Int. J. Control*, vol. 85, pp. 1433–1451, 2012.

[79] H. Lin and P. J. Antsaklis, "Stability and stabilizability of switched linear systems: a survey of recent results," *IEEE Transactions on Automatic control*, vol. 54, no. 2, pp. 308–322, 2009.

[80] D. Liberzon, *Switching in systems and control*. Boston, MA, USA: Birkhuser, 2003.

[81] T. B. Hoang, W. P. Lepine, A. D. Bernardinis, and M. Netto, "Extended braking stiffness estimation based on a switched observer, with an application to wheel-acceleration control," *IEEE Transactions on Control Systems Technology*, vol. 22, no. 6, pp. 2384 – 2392, 2014.

[82] V. Gupta, R. M. Murray, and B. Hassibi, "On the control of jump linear markov systems with markov state estimation," *In Proc. American Control Conference*, pp. 2893 – 2898, 2003.

[83] V. Dragan and T. Morozan, "Observability and detectability of a class of discrete-time stochastic linear systems," *IMA Journal of Mathematical Control and Information*, vol. 23, pp. 371–394, 2006.

[84] R. Zarringhalam, A. Rezaeian, A. Khajepour, and W. Melek, "Vehicle sensor failure detection and fault-tolerant estimation of states," *Symposium on Advanced Intelligent Systems*, 2012.

[85] M. Pirani and S. Sundaram, "On the smallest eigenvalue of grounded Laplacian matrices," *IEEE Transactions on Automatic Control*, vol. 61, no. 2, pp. 509–514, 2016.

[86] M. Pirani, E. M. Shahrivar, B. Fidan, and S. Sundaram, "Robustness of leader - follower networked dynamical systems," *arXiv:1604.08651v1*, 2016.

[87] M. Pirani, E. Hashemi, A. Khajepour, B. Fidan, B. Litkouhi, and S. K. Chen, "Cooperative vehicle speed fault diagnostics and correction," *arXiv:1706.09447*, 2017.

[88] E. Hashemi, M. Pirani, B. Fidan, A. Khajepour, and S. C. A. Kasaiezadeh, "Distributed robust vehicle state estimation," *IEEE Intelligent Vehicles Symposium*, pp. 693–698, 2017.

[89] E. Hashemi, M. Pirani, A. Khajepour, B. Fidan, and S. C. A. Kasaiezadeh, "Opinion dynamics based vehicle velocity estimation and diagnosis," *IEEE Transaction on Intelligent Transportation Systems, submitted*, 2017.

[90] A. Kasaiezadeh, E. Hashemi, A. Khajepour, B. Litkouhi, and S.-K. Chen, "Corner-based longitudinal speed estimation," 2016, uS Pending Patent.

[91] N. Kazantzis and C. Kravaris, "Time-discretization of nonlinear control systems via taylor methods," *Computers and Chemical Engineering*, vol. 23, pp. 763–784, 1999.

[92] U. Kiencke, "Real-Time Estimation of Adhesion Characteristic Between Tires and Road," in *In Proc. of IFAC World Congress*, 1993.

[93] U. W. Kiencke and A. Daiss, "Estimation of Tyre Friction for Enhanced ABS-Systems," in *In Proc. of International Symposium on Advanced Vehicle Control*, 1994.

[94] Y. H. Judy and J. C. Gerdes, "The predictive nature of pneumatic trail: Tire slip angle and peak force estimation using steering torque," in *AVEC08*, 2008.

[95] F. Garofalo, G. Celentano, and L. Glielmo, "Stability Robustness of Interval Matrices Via Lyapunov Quadratic Forms," *IEEE Transactions on Automatic Control*, vol. 38, no. 2, pp. 281–284, 1993.

[96] P. Gahinet, P. Apkarian, and M. Chilali, "Affine Parameter-Dependent Lyapunov Functions and Real Parametric Uncertainty," *IEEE Transactions on Automatic Control*, vol. 41, no. 3, pp. 436–442, 1996.

[97] C. Ahn, H. Peng, and H. E. Tseng, "Estimation of road friction for enhanced active safety systems: Dynamic approach," *in Proc. Amer. Control Conf*, pp. 1110–1115, 2009.

[98] P. A. Bliman, T. Bonald, and M. Sorine, "Hysteresis operators and tire friction models: Application to vehicle dynamic simulations," *Proc. of the International Council for Industrial and Applied Mathematics*, 1995.

[99] A. V. Zanten, R. Erhardt, and G. Pfaff, "The vehicle dynamics control system of bosch," *SAE Technical Paper-950759*, 1995.

[100] A. V. Zanten, "Evolution of electronic control systems for improving the vehicle dynamic behavior," *International Symposium on Advanced Vehicle Control,*, 2002.

[101] D. Gebre-Egziabher, R. C. Hayward, and J. D. Powell, "A low-cost GPS/inertial attitude heading reference system (AHRS) for general aviation applications," *Position location and navigation symposium*, 1998.

[102] A. Hac and M. Simpson, "Estimation of vehicle side slip angle and yaw rate," *SAE Technical Paper*, 2000.

[103] K. Kobayashi, K. Watanabe, and C. Science, "Estimation of absolute vehicle speed using fuzzy logic rule-based kalman filter," *In Proc. American Control Conference*, 1995.

[104] C. Canudas-De-Wit, M. L. Petersen, and A. Shiriaev, "A new nonlinear observer for tire/road distributed contact friction," *In Proc. 42nd IEEE Conference on Decision and Control*, 2003.

[105] M. Hiemer, A. V. Vietinghoff, U. Kiencke, and T. Matsunaga, "Determination of the vehicle body side slip angle with non-linear observer strategies," *SAE Technical Paper*, 2005.

[106] L. Imsland, T. A. Johansen, T. I. Fossen, J. C. Kalkkuhl, and A. Suissa, "Vehicle velocity estimation using modular nonlinear observers," *Proc. 44th IEEE Conference on Decision and Control*, 2005.

[107] R. Wang and J. Wang, "Tire–road friction coefficient and tire cornering stiffness estimation based on longitudinal tire force difference generation," *Control Engineering Practice*, vol. 21, no. 1, pp. 65–75, 2013.

[108] Y. Chen and J. Wang, "Adaptive vehicle speed control with input injections for longitudinal motion independent road frictional condition estimation," *IEEE Transactions on Vehicular Technology*, vol. 60, no. 3, pp. 839–848, 2011.

[109] M. Choi, J. J. Oh, and S. B. Choi, "Linearized recursive least squares methods for real-time identification of tire–road friction coefficient," *IEEE Transactions on Vehicular Technology*, vol. 62, no. 7, pp. 2906–2918, 2013.

[110] J. Rath, K. Veluvolu, and M. Defoort, "Simultaneous estimation of road profile and tyre road friction for automotive vehicle," *IEEE Transactions on Vehicular Technology*, vol. 64, no. 10, pp. 4461–4471, 2014.

[111] M. Doumiati, A. Victorino, A. Charara, and D. Lechner, "Lateral load transfer and normal forces estimation for vehicle safety: experimental test," *Vehicle System Dynamics*, vol. 47, no. 12, pp. 1511–1533, 2009.

[112] K. Nam, S. Oh, H. Fujimoto, and Y. Hori, "Estimation of sideslip and roll angles of electric vehicles using lateral tire force sensors through rls and kalman filter approaches," *IEEE Transactions on Industrial Electronics*, vol. 60, no. 3, pp. 988–1000, 2013.

[113] E. Kayacan, E. Kayacan, H. Ramon, and W. Saeys, "Distributed nonlinear model predictive control of an autonomous tractor–trailer system," *Mechatronics*, vol. 24, no. 8, pp. 926–933, 2014.

[114] B. Li, H. Du, W. Li, and Y. Zhang, "Side-slip angle estimation based lateral dynamics control for omni-directional vehicles with optimal steering angle and traction/brake torque distribution," *Mechatronics*, 2014.

[115] H. Dugoff, P. Fancher, and L. Segel, "An analysis of tire traction properties and their influence on vehicle dynamic performance," SAE Technical Paper, Tech. Rep., 1970.

[116] H. Zhang, X. Huang, J. Wang, and H. R. Karimi, "Robust energy-to-peak sideslip angle estimation with applications to ground vehicles," *Mechatronics*, 2014.

[117] F. Sun, K. Lolenko, and J. Rudolph, "Nonlinear observer design for state estimation during antilock braking," *Proceedings of the Institution of Mechanical Engineers, Part I: Journal of Systems and Control Engineering*, vol. 228, no. 2, pp. 78–86, 2014.

[118] L. Imsland, T. Johansen, T. Fossen, J. Kalkkuhl, and A. Suissa, "Vehicle Velocity Estimation using Modular Nonlinear Observers," in *In Proc. 44th IEEE Conference on Decision and Control*, 2005, pp. 6728–6733.